Novel roles of the central cell death pathway and cell corpse engulfment pathways in *C. elegans*

Dissertation der Fakultät für Biologie
der Ludwig-Maximilians-Universität
München

Sayantan Chakraborty

26th November 2015

Declaration

I declare that I have authored this thesis independently and without any unauthorized aid. The research described here has not been published anywhere else apart from those mentioned in the section "Publications and manuscripts originating from this thesis". This dissertation or parts of it, has not been submitted/presented to any another examination board and neither have I been subjected to a previous doctoral examination.

Munich, the 26th of November, 2015

Sayantan Chakraborty

Acknowledgements

I want to express my deepest appreciation to my mentor Prof. Dr. Barbara Conradt, who has an excellent scientific temperament and a gift of high intellect. Through the ups and downs of my doctoral research, she has continually conveyed a spirit of scientific adventure. Her guidance and excitement have tremendously helped me in the completion of this dissertation. Thank you for keeping your office door open and being available for all the times when I needed it.

Special thanks to Dr. Tamara Mikeladze-Dvali, who offered me guidance whenever possible. I have learnt a lot from her too. Genetics has been really cool to work with. My gratitude towards Dr. Heinke Holzkamp for advising me through some really interesting genetics is endless. It has been awesome to work with PD Dr. Eric J. Lambie, discussions with whom have always been interesting and insightful. My boundless gratefulness also goes towards Dr. Samik Bindu whose timely appointment in our lab resulted in the creation of a tool that significantly accelerated our discoveries. I have had great insightful interactions with Prof. Dr. Heinrich Leonhardt. Thank you, for all those nice conversations.

I have always enjoyed my life in the lab. Fabs, also known as Fabio - the fish guy, has been the center of my attention since the dawn of time. Finally, we met in Munich! The office B02.061, I must say is a great place to relax. I have joked with Anna time and again. But, her confidence in facing my jokes is colossal! Thank you bro, for all the fun times! Thank you, Sriyash, Fabian, Jeffrey (JZ), Simon and Nikhil for spicing up the dissertation text. The immense efforts of Fabs, Nikhil, Hai and Sebastian to select the cover of this dissertation are irrefutable.

Whatever I say about my parents, will always be less. Their constant belief in my abilities and my passion has helped me push through thick and thin. Thank you for your blessings!

I have learnt something or the other from everyone in the lab. Thank you, everybody!

To anyone, whom I may have forgotten, I sincerely apologize. Thank you as well!

Publications and manuscripts originating from this thesis

Sayantan Chakraborty, Eric J. Lambie, Samik Bindu, Tamara Mikeladze-Dvali and Barbara Conradt. (2015). Engulfment pathways promote programmed cell death by enhancing the unequal segregation of apoptotic potential. **Accepted for publication in *Nature Communications*.**

Sayantan Chakraborty, Tamara Mikeladze-Dvali and Barbara Conradt. Novel functions of *C. elegans ced-3* caspase in centrosome asymmetry and segregation. **Manuscript in preparation.**

CONTENTS

Contents

SUMMARY

Programmed cell death or apoptosis is an evolutionarily conserved process of cell elimination. In *C. elegans*, *egl-1* BH3-only, *ced-9* Bcl-2, *ced-4* Apaf-1 and *ced-3* caspase constitute the central cell death pathway. Cells undergoing apoptosis form corpses and are subsequently engulfed by phagocytes. Two evolutionarily conserved cell corpse engulfment pathways constitute the engulfment machinery. It has been reported that in *C. elegans*, components of the conserved engulfment pathways also promote programmed cell death via an unknown mechanism. The NSM neuroblast (NSMnb) divides asymmetrically along the dorsal-ventral axis during *C. elegans* embryonic development to give rise to a ventrally positioned large NSM which is programmed to survive, and a dorsally positioned small NSM sister cell (NSMsc) which is programmed to die. Using the NSM lineage as a model, I have obtained evidence that CED-1 mEGF10 which is the phagocytic receptor in *C. elegans* and is essential for corpse engulfment, becomes enriched selectively on plasma membrane of neighboring cells apposing the dorsal side of the NSMnb, which later forms the NSMsc. Furthermore, I have determined that CED-1 mEGF10 plays an essential role in generating a dorsal-ventral gradient of CED-3 caspase activity within the NSMnb. My observations also suggest that the components of the two evolutionarily conserved cell corpse engulfment pathways promote apoptosis by participating in the generation of this gradient of apoptotic potential in mothers of cells programmed to die. This gradient then facilitates the preferential segregation of apoptotic potential into the daughter fated to undergo programmed cell death. The fate of the NSMsc is hence predetermined in the NSMnb.

Asymmetry in the NSM lineage is not restricted to the asymmetric daughters born from the NSMnb. I found that centrosomes, the microtubule organizing centers of a cell, can be asymmetrically segregated with respect to the amount of pericentriolar material (PCM)

associated with each centrosome. Interestingly, both 'centrosome size' in the NSMnb and the segregation of 'large' and 'small' centrosomes are dependent on the components of the central cell death pathway. Furthermore, I have evidence that CED-3 dependent cleavage of the PCM component TAC-1 may contribute to centrosome asymmetry and segregation in the NSM lineage. Finally, I have discovered an invariant phenomenon of centrosome asymmetry and segregation that exists across lineages in a developing *C. elegans* embryo.

Within the context of apoptosis, the central cell death pathway and the cell corpse engulfment pathways have previously been thought to act specifically in apoptotic cells and within the engulfing cells, respectively. I have ascertained that the central cell death pathway and the cell corpse engulfment pathways are already active in the mother of the cell programmed to die and the neighboring cells, respectively. Further, I have evidence on how the components of the engulfment pathways promote programmed cell death. They do so by polarizing the NSMnb and hence facilitating the asymmetric segregation of factors that mediate NSMsc apoptosis. It is in fact a signaling function of the conserved engulfment pathways and not the process of engulfment *per se* that promotes apoptosis. Therefore, I have been able to shed light on how apoptosis is modulated in the NSM lineage during *C. elegans* development.

INTRODUCTION

1. Programmed cell death

Programmed cell death or apoptosis refers to the regulated killing of a cell and is an important aspect of animal development. Apoptosis, which was first observed during amphibian metamorphosis, has indispensable roles in animals (Figure 1) (Vogt, 1842; Jacobson et al., 1997; Fuchs and Steller, 2011). These roles of programmed cell death have been associated with but are not limited to elimination of cells between the developing digits in higher vertebrates, removal of physiological structures which are no longer necessary for an animal during its development: such as deletion of Müllerian ducts in developing males and Wolfian ducts in developing females, maintaining a balance between the overproduction of cells with the physiological numbers required and eliminating injured or abnormal cells during a host damage response. Aberrant apoptosis can inadvertently affect an organism and subsequently cause diseases. For example, excess cell death leads to neurological diseases like Alzheimer's and insufficient cell death has been linked to cancers (Kerr et al., 1972; Minn et al., 1995; Raffo et al., 1995; Chan et al., 1999; Allen et al., 2001; Fulda et al., 2002; Gastard et al., 2003; Cribbs et al., 2004; Cotman et al., 2005; Goolsby et al., 2005; Miquel et al., 2005; Ayala-Grosso et al., 2006; Avery-Kiejda et al., 2011).
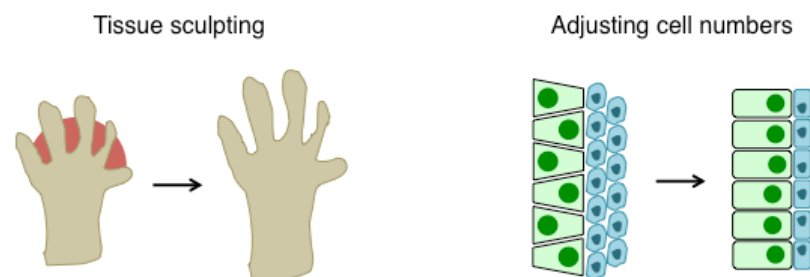
Figure 1. Examples of developmental aspects of programmed cell death during animal development.
Apoptosis or programmed cell death helps in shaping animal organs and also maintaining the physiological homeostasis of cell numbers.

2. *Caenorhabditis elegans* – an excellent model to study programmed cell death

C. elegans is a nematode often found in large populations in rotting plant materials (Felix and Duveau, 2012). Compared to other metazoan model organisms, it has a short life cycle. The life cycle of the nematode is less than 3 days (Figure 2). Apart from its short life cycle, the 1 mm long worm is easy and inexpensive to culture on agar plates with *E. coli* as a food source. *C. elegans* has two sexes: hermaphrodites (XX) and males (XO) (Figure 2). Male worms occur at a low frequency naturally (~0.2%), since they are generated only when there is a spontaneous non-disjunction of the X-chromosome at meiosis (Zarkower, 2006).

The haploid genome of *C. elegans* consists of six chromosomes and is arranged as linkage groups (LG). LG I to LG V constitute the autosomes and LG X the sex chromosome. The *C. elegans* genome is 97 Mb in size and consists of ~21,000 genes (Consortium, 1998). 38% of these genes have orthologs in mammals (Shaye and Greenwald, 2011).

C. elegans is transparent throughout its life cycle and hence its distinct anatomical structures can be visualized using differential interference contrast (DIC) microscopy (Figure 2). Due to the ease of observing developing embryos, larvae and adults, the complete somatic cell lineage has been determined (Sulston, 1976; Sulston and Horvitz, 1977; Sulston et al., 1983). This cell lineage is essentially invariant between animals. Given the power of this invariant cell lineage in *C. elegans*, not only is the fate of each cell is known but also when and which cells die. Further, the morphological characteristics and refractile nature of dying cells make it easy to identify them in live animals using DIC microscopy.

a

Hermaphrodite (XX)   Male (XO)

b
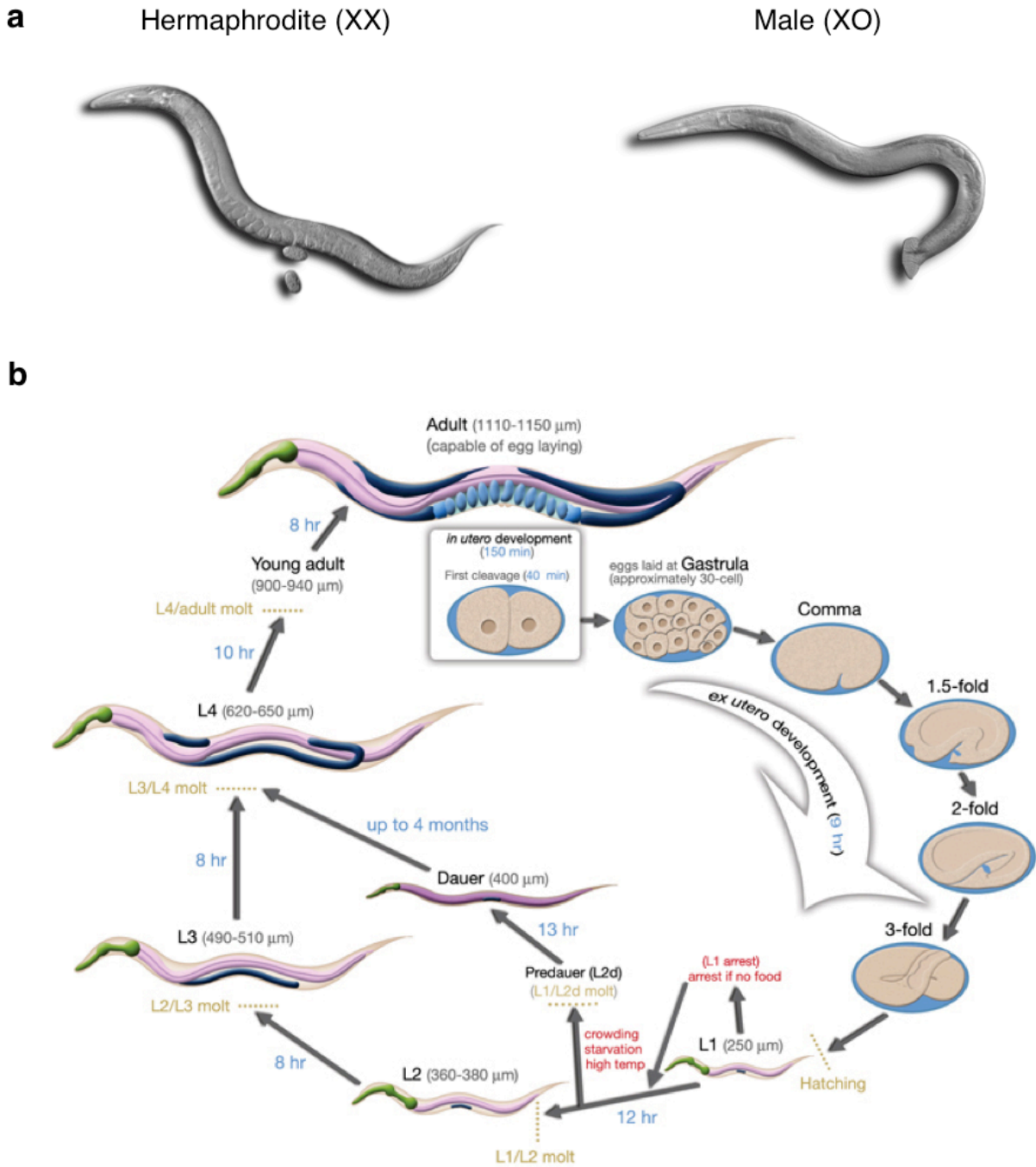
Figure 2. *C. elegans* **is an excellent model organism.**
a. DIC micrograph of a representative wild-type hermaphrodite (XX) and male (XO) *C. elegans*. (Image courtesy of Sebastian Lühr). **b.** Life cycle of *C. elegans* at 22°C. (Schematics adapted from wormbook.org).

3. The evolutionarily conserved central cell death pathway

Exactly 1090 and 1179 somatic cells are born during hermaphrodite or male *C. elegans* development, respectively. Of those, 131 or 148 cells, respectively, reproducibly undergo programmed cell death (Sulston and Horvitz, 1977; Kimble and Hirsh, 1979; Sulston et al., 1983). Extensive genetic analyses have helped discover the genes that constitute the central cell death pathway. This pathway consists of four genes *egl-1*, *ced-9*, *ced-4* and *ced-3* (EGL, Egg-laying defective; CED, Cell death abnormal) (Figure 3). *egl-1* negatively regulates *ced-9* which in turn negatively regulates *ced-4*; *ced-4* positively regulates *ced-3* (Ellis and Horvitz, 1986; Hengartner et al., 1992; Conradt and Horvitz, 1998). Based on their functions, *egl-1*, *ced-4* and *ced-3* are described as pro-apoptotic genes while *ced-9* is described as an anti-apoptotic gene. BH3-only, Bcl-2, Apaf-1 and Caspase are the mammalian homologs of EGL-1, CED-9, CED-4 and CED-3, respectively (Figure 3) (Yuan and Horvitz, 1992; Yuan et al., 1993; Hengartner and Horvitz, 1994; Conradt and Horvitz, 1998).

CED-9 protects cells from undergoing apoptosis (Hengartner et al., 1992; Hengartner and Horvitz, 1994). CED-9 is bound to the outer mitochondrial membrane and further interacts with a dimer of the pro-apoptotic protein CED-4, thereby inhibiting CED-4 activity and hence causing cell survival (Chen et al., 2000; Yan et al., 2005). In response to apoptotic stimuli, interaction of EGL-1 with CED-9 initiates programmed cell death (Conradt and Horvitz, 1998; del Peso et al., 1998; del Peso et al., 2000; Yan et al., 2004). EGL-1 binds to CED-9 thereby causing a conformational change in CED-9 and hence resulting in the release of the CED-4 dimer (Chinnaiyan et al., 1997; James et al., 1997; Spector et al., 1997; Wu et al., 1997; Chen et al., 2000; Yan et al., 2004; Yan et al., 2005). Once the CED-4 dimer is

released, it oligomerises to form an octamer called 'Apoptosome' (Yan et al., 2005). This apoptosome now facilitates the autocatalytic conversion of inactive pro-CED-3 to active CED-3 caspase (Yuan and Horvitz, 1992; Chinnaiyan et al., 1997; Irmler et al., 1997; Seshagiri and Miller, 1997; Yang et al., 1998; Huang et al., 2013). Formation of active-CED-3 further initiates downstream events that bring about the death of the cell. Once a cell undergoes apoptosis in *C. elegans*, it has a distinct 'button-shaped' refractile morphology and hence can be identified using DIC microscopy (Sulston, 1976; Sulston and Horvitz, 1977; Sulston et al., 1983).
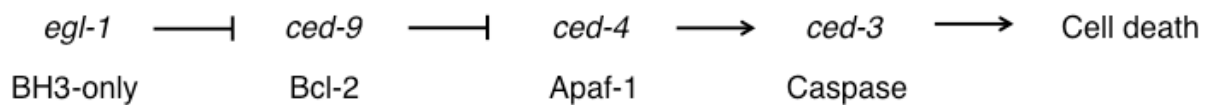
Figure 3. The evolutionarily conserved central cell death pathway.
C. elegans genes involved in programmed cell death are indicated. Also indicated are the mammalian homologs of these genes.

4. The evolutionarily conserved cell corpse engulfment pathways

In *C. elegans*, cell corpses are rapidly engulfed (Sulston and Horvitz, 1977; Robertson and Thomson, 1982; Sulston et al., 1983). Studies on the removal of cell corpses in *C. elegans* have helped elucidate two evolutionarily conserved partially redundant pathways that mediate cell corpse engulfment. The two pathways act in phagocytes and are the CED-1 mEGF-10, CED-6 GULP, CED-7 ABC, DYN-1 (DYN, Dynamin-related) Dyn1-dependent pathway and

the CED-2 CrkII, CED-5 Dock180, CED-10 Rac, CED-12 ELMO-dependent pathway (Figure 4) (reviewed in: Lu and Zhou, 2012; Hochreiter-Hufford and Ravichandran, 2013).

For controlled engulfment of a cell corpse, processes downstream of active CED-3 are initiated. Phosphatidylserine (PS) normally remains restricted to the inner leaflet of the plasma membrane. Exposure of PS, also termed as PS-flipping, is a hallmark of apoptosis. In mammals, Xkr8 (XKr, XK-related protein 8) mediates PS exposure by phospholipid scrambling (Suzuki et al., 2013; Suzuki et al., 2014). Xkr8 consists of six transmembrane regions and localizes to the plasma membrane. It has been shown that, a caspase dependent cleavage of Xkr8 mediates PS-exposure by phospholipid scrambling (Suzuki et al., 2013). CED-8 is the *C. elegans* ortholog of Xkr8 (Stanfield and Horvitz, 2000). Like in mammals, in *C. elegans*, active CED-3 caspase cleaves and thus activates the Xkr8-like protein CED-8, which further mediates phosphatidylserine (PS) exposure on the surface of the cell corpse (Chen et al., 2013). Once PS is exposed on the cell surface, it acts as one of several 'eat me signals'. Phagocytes expressing the mEGF-10 (Multiple epidermal growth factor-like domains protein 10)-like receptor CED-1, recognize this 'eat me signal' and initiate the engulfment process (Hedgecock et al., 1983; Ellis et al., 1991; Zhou et al., 2001; Yu et al., 2006; Venegas and Zhou, 2007; Zhou and Yu, 2008; Li et al., 2015).

CED-1 accumulates on plasma membrane regions of the phagocytic cells that are in contact with the dying cells (Zhou et al., 2001). CED-6 GULP, a phosphotyrosine-binding (PTB) domain containing protein binds to CED-1 and further mediates downstream signaling to the GTPase, DYN-1 Dynamin (Liu and Hengartner, 1998). DYN-1 Dynamin functioning downstream of CED-6 GULP, has been shown to play a role in vesicle delivery to the

extending pseudopodia to promote efficient corpse engulfment (Figure 4) (Yu et al., 2006). In the second parallel pathway, UNC-73 Trio (UNC, Uncoordinated) activates MIG-2 RhoG (MIG, Abnormal cell migration), which in turn activates the CED-5 Dock180/CED-12 Elmo complex and CED-10 downstream of this complex (Wu and Horvitz, 1998; deBakker et al., 2004; Neukomm et al., 2011). Activation of CED-10 promotes cytoskeleton rearrangement necessary for cell engulfment (Kinchen et al., 2005). CED-5 and CED-12 can also be activated by CED-2 CrkII (Figure 4) (Reddien and Horvitz, 2000; Akakura et al., 2005).
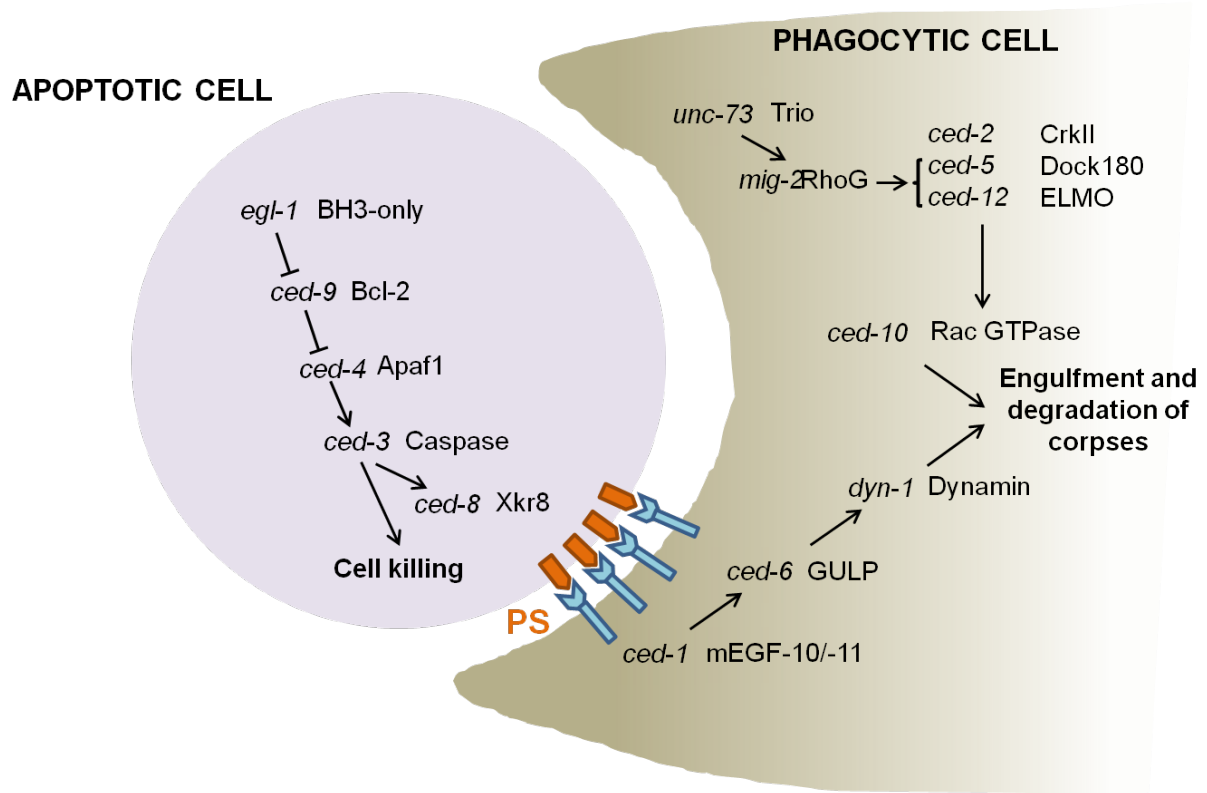
Figure 4. Crosstalk between an apoptotic cell and its phagocyte.
C. elegans genes involved in programmed cell death and the engulfment of corpses are indicated within the apoptotic cell (pink) and phagocytic cell (brown), respectively (see text for details). Also indicated are the mammalian homologs of these genes.

5. The NSM lineage as a model for *in vivo* single cell analysis

In order to dissect mechanisms that play a role in determining the fate of a cell, *in vivo* single cell analyses prove extremely useful. To that end, the NSM lineage is a good *in vivo* model to perform single cell analyses. The two NSM (neurosecretory motorneuron) neuroblasts (NSMnb), which are bilaterally symmetric, are born ~230 min post-fertilization of the *C. elegans* oocyte. 180 min later (~410 min post-fertilization), during the 11th round of embryonic cell divisions, the neuroblasts undergo an asymmetric cell division along the dorsal-ventral axis to give rise to a ventrally positioned large cell, the NSM, and a dorsally positioned small cell, the NSM sister cell (NSMsc) (Figure 5) (Sulston et al., 1983; Hatzold and Conradt, 2008). The NSMsc undergoes programmed cell death and forms a corpse ~20 min post its birth. The NSM however, survives and differentiates into a serotonergic motorneuron.
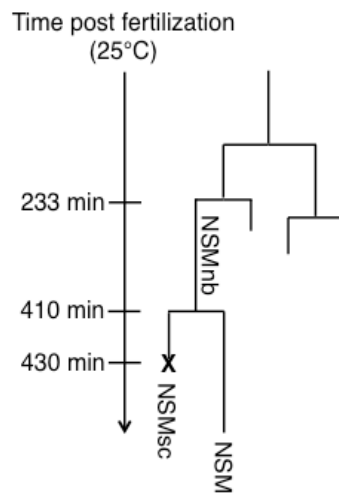
Figure 5. NSM lineage during *C. elegans* development.
Indicated are NSM neuroblast (NSMnb), NSM (Neurosecretory motorneuron) and the NSM sister cell (NSMsc) (see text for details). 'X' denotes the time point at which the NSMsc forms a corpse. Vertical lines depict individual cells and horizontal lines cell divisions.

Previous studies in the NSM lineage have shed light on how the central cell death pathway is regulated in order to bring about NSMsc apoptosis (Figure 6). *ces-2* and *ces-1* (CES, cell death specification) encode an HLF (HLF, hepatic leukemia factor)-like bZIP (bZIP, basic leucine-zipper) transcription factor and a Snail like zinc-finger transcription factor, respectively (Ellis and Horvitz, 1991; Metzstein et al., 1996; Metzstein and Horvitz, 1999). *ces-2* and *ces-1* genetically act upstream of *egl-1* (Conradt and Horvitz, 1998). Loss-of-function mutations in *ces-2* and a gain-of-function mutation in *ces-1* affect NSMnb polarity thereby causing a symmetrical NSMnb division and the inappropriate survival of the NSMsc (Figure 6). *ces-2* negatively regulates *ces-1* to cause NSMsc death (Ellis and Horvitz, 1991; Hatzold and Conradt, 2008). Cis-regulatory regions upstream of the *ces-1* transcription unit contain CES-2 binding sites. Mutations in those sites affect CES-2 binding, thereby presumably resulting in overexpression of *ces-1*, which further ensues a negative regulation of *egl-1* and hence, causes inappropriate NSMsc survival (Metzstein and Horvitz, 1999). Overexpression of *ces-1* from extrachromosomal arrays of wild-type *ces-1* also results in NSMsc survival (Metzstein and Horvitz, 1999). Further, eliminating *ces-2* function results in *ces-1* overexpression, causing a loss of NSMnb polarity and NSMsc survival (Figure 6) (Hatzold and Conradt, 2008). Snail-like family of zinc-finger DNA-binding proteins can act as transcription repressors (de Herreros et al., 2010). Snail-binding sites have been discovered in the *egl-1* locus (Thellmann et al., 2003). *In vitro* data suggest that a heterodimer of HLH-2/HLH-3 (HLH, helix loop helix) binds to these Snail-binding sites, hence activating *egl-1* transcription and causing NSMsc death *in vivo*. CES-1 can also bind to those regulatory regions to repress *egl-1* transcription. The fate of the NSM and the NSMsc is hence determined by the asymmetric segregation of CES-1 (Figure 6) (Hatzold and Conradt, 2008). It has been demonstrated that CES-1 is asymmetrically segregated to the NSM, thus repressing

13

egl-1 transcription in the NSM. Overexpressed CES-1 is segregated to both the NSM and the NSMsc (Figure 6) (Hatzold and Conradt, 2008). It has therefore been proposed that *ces-1* overexpression outcompetes HLH-2/HLH-3 for the Snail-binding sites, resulting in a transcriptional repression of *egl-1* in the inappropriately surviving NSMsc (Thellmann et al., 2003). It has also been demonstrated that CES-1 can affect cell cycle progression in the NSM lineage (Yan et al., 2013). Specifically, CES-1 acts as a transcriptional repressor of *cdc25.2*, which encodes a Cdc25 (CDC, cell division cycle related)-like phosphatase.
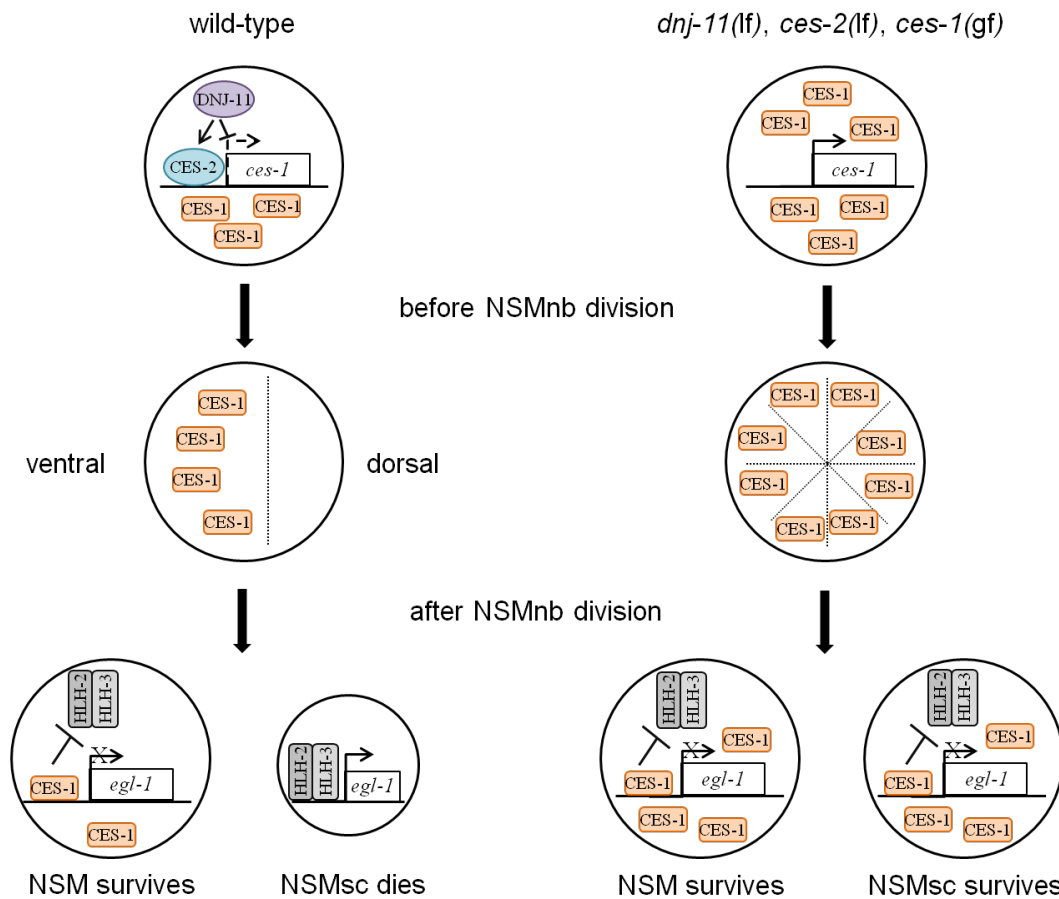
Figure 6. Molecular players involved in the asymmetric division of the NSMnb affect NSM and NSMsc fate.
Molecular models showing DNJ-11, CES-2, HLH-2/HLH-3 and CES-1 in the NSMnb, NSM and NSMsc in wild-type and *dnj-11(*lf*)*, *ces-2(*lf*)* and *ces-1(*gf*)* animals (see text for details). 'X' indicates inhibition of gene transcription.

The MIDA1-Zrf-like chaperone gene *dnj-11* (DNJ, <u>DnaJ</u> domain), which is required for *C. elegans* embryonic development, also regulates NSMnb polarity and the apoptotic death of the NSMsc (Hatzold and Conradt, 2008). It has been shown that together with *ces-2*, *dnj-11* antagonizes *ces-1* function to cause NSMsc death. Therefore, loss-of-function mutations in *dnj-11* result in the loss of *egl-1* transcription, which further results in inappropriate NSMsc survival.

The division of the NSMnb and the fate of the NSMsc can therefore be genetically altered by loss-of-function mutations in *dnj-11* and *ces-2* and a gain-of-function mutation in *ces-1*. Hence, single cell manipulations in this lineage help us answer various questions pertaining to known developmental processes, such as, ascertaining the functional significance of asymmetric cell divisions during neuronal development or stem cell like divisions. Given that the genetic pathways underlying programmed cell death and asymmetric cell division in the NSM lineage are conserved from flies to humans, novel discoveries might similarly be conserved.

METHODS

1. Strains

Mutations used in this study are listed below and have been previously described (Riddle et al., 1997): LGI: *ced-1(e1735)* (Hedgecock et al., 1983); *ces-1(n703gf)* (Metzstein and Horvitz, 1999); *ces-2(bc213)* (Hatzold and Conradt, 2008). LGII: *vieSi15* [P*spd-5gfp::spd-5*] (Cabral et al., 2013), *bcSi1* [P*mex-5gfp::tac-1*] and *bcSi4* [P*mex-5gfp::tac-1(D251A)*] (this study). LGIII: *ceh-20(ay9)* (Takacs-Vellai et al., 2007); *ced-9(n1950)* (Hengartner et al., 1992); *ced-4(n1162)* (Ellis and Horvitz, 1986; Yuan and Horvitz, 1992); *bcIs66* [P*tph-1his-24::gfp*] (Hatzold and Conradt, 2008), *ced-6(n1813)* (Ellis et al., 1991). LGIV: *ced-2(n1994)* (Ellis et al., 1991), *ced-3(n717, n718, n2427, n2433)* (Shaham et al., 1999); *dnj-11(bc212)* (Hatzold and Conradt, 2008). LGV: *egl-1(n1084n3082)* (Conradt and Horvitz, 1998); *enIs1* [P*ced-1ced-1δc::gfp*] (Zhou et al., 2001), *ltIs44* [P*pie-1mCherry::plcδph*] (Audhya et al., 2005), *smIs76* [P*hspsAnxV::gfp*] (Mapes et al., 2012). LGX: *ced-8(n1891)* (Ellis et al., 1991); *ceh-30(n3714)* (Schwartz and Horvitz, 2007). Additional transgenes used in this study were *bcIs109* [P*ced-3ced-3::gfp*] (this study), *bcIs104* [P*pie-1gfp::tac-1*] (Bellanger and Gonczy, 2003) and *ddIs6* [P*pie-1tbg-1::gfp, unc-119*(+)] (van der Voet et al., 2009). The strain N2 (Bristol) was used as wild-type. Strains were grown on NGM plates seeded with *E. coli* strain OP50 and maintained at 15°C essentially as described (Brenner, 1974).

2. P*ced-3ced-3::gfp* fosmid construction

My colleagues Samik Bindu and Eric J. Lambie generated the *ced-3::gfp* reporter using a recombineering technique (Tursun et al., 2009). The fosmid WRM0610cE07 was obtained

from Source BioScience UK Limited. It was then transformed into *E. coli* strain SW105 followed by a heat shock to induce the expression of the λ Red recombinase. The electro-competent cells containing the fosmid of interest and the recombinase were then allowed to take up a cassette containing the *gfp* sequence as well as the selectable marker *galK*, which is flanked by *frt* sites, the targets of Flp recombinase. The whole cassette was PCR amplified from pBALU1 using the primer sets o1860 (5'-CGCTCATTCAGCAAAGCTTCTGGACCAACTCAATACATATTCCATATGAGTAAAG GAGAAGAACTTTTCAC-3') and o1861 (5'-AACACGGCTTATG GTTGGTGCATCGACAAAGTTCATATCCTCTTCTTGTATAGTTCATCCATGCCATG-3'). Using this primer set the *gfp* tag was inserted at the C-terminal end of *ced-3* in exon 8. Recombinants stably maintaining the *galK* cassette were selected on a minimal medium with galactose. The second recombinase Flipase (Flp) was then induced by arabinose, which resulted in the removal of the *galK* marker. Following this, the fosmid (pBC1378) was isolated and electroporated into the *E. coli* strain EPI 300 for amplification and maintenance.

3. Germline transformation

Transgenic animals were obtained by microinjecting as described (Mello et al., 1991). The P*ced-3ced-3::gfp* fosmid (pBC1378) (0.5ng/µl) was co-injected into N2 with the plasmid pRF4 (150ng/µl), which contains the *rol-6*(*su1006dm*) allele, which causes a dominant Rol phenotype (Kramer et al., 1990). Three lines carrying extrachromosomal arrays were obtained, one of which was used to stably integrate the array into the genome by UV radiation. Three independent integrated lines were obtained. The integrated allele used for our studies was

named *bcIs109* and backcrossed twice to wild-type. *bcIs109* can restore the wild-type phenotype in a *ced-3(n717)* mutant.

4. TAC-1 biochemistry

My colleague Samik Bindu performed this experiment. *C. elegans tac-1* cDNA was cloned 3' of the ORF encoding GST by inserting it into the EcoNI site of the bacterial expression plasmid pGEX-4T-3. The resulting plasmid (pBC1385) was transformed into *E. coli* BL21 (DE3) cells for TAC-1::GST expression. Extraction of TAC-1::GST fusion protein was performed as previously described (Rolland et al., 2009). Bacteria containing pBC1385 (50 ml culture) were grown to A600/ml=0.6 and TAC-1::GST expression induced with 1mM IPTG for 2 hours at 37°C. Cells were collected, resuspended in 1ml NETN buffer [20 mM Tris-HCl pH 8.0, 0.5% NP-40, 100 mM NaCl, and a cocktail of protease inhibitor (Roche)] and lysed by sonication. Debris was sedimented by centrifugation and TAC-1::GST fusion protein was purified using 200 µl glutathione agarose beads (GE Healthcare) for 1 hour at 4°C. The beads were washed three times for 10 min with 1 ml of NETN buffer at 4°C. These beads were subsequently used for the *in vitro* cleavage assay.

CED-3 protein fused to a FLAG octapeptide at its C-terminus was obtained from pET-CED-3 plasmid (gift from H. R. Horvitz) expressed in *E. coli* BL21 (DE3) cells. CED-3 lysate was obtained as previously described (Xue et al., 1996). The bacteria containing pET-CED-3 was grown in a 50 ml log-phase culture to A600/ml=0.6 and CED-3 expression was induced with 1mM IPTG for 2 hours at RT. Cells were collected, resuspended in 1 ml of CED-3 buffer

[50 mM Tris-HC1 pH 8.0, 0.5 mM EDTA, 0.5 mM sucrose, 5% glycerol and supplementary protease inhibitors] and lysed by sonication. Debris was sedimented by centrifugation and the resulting supernatant was used for the *in vitro* cleavage assay.

For the *in vitro* TAC-1::GST cleavage assay, 20 µl of TAC-1::GST bound glutathione agarose beads (see above) were incubated with 10 µl of CED-3 lysate (see above) and 10 µl of CED-3 buffer (final reaction volume of 40 µl). In parallel, two control reactions were set up, one without CED-3 lysate and one with CED-3 lysate in which the activity of CED-3 had been inhibited. To inhibit the catalytic activity of CED-3, 10 µl of the CED-3 lysate was pre-incubated for 20 min at 37°C with 5 mM of an inhibitor (Iodoacetic acid) as described(Xue et al., 1996). The cleavage reaction was carried out for 1 hour at 37°C and the reaction was terminated by adding an equal volume of 2x Laemmli buffer. To analyse the cleavage reaction, a western blot was performed using CeTAC-1 (Hadwiger et al., 2010) as a primary antibody (1:100) and the HRP conjugated anti- mouse secondary antibody (1:1000) (Bio-Rad). The blot was developed using a Chemiluminescence (Amersham) kit and detected using ChemiDoc XRS+ (BioRad).

5. GFP::TAC-1 and GFP::TAC-1(D251A) strain construction

gfp::tac-1 was PCR amplified from *bcIs104,* stitched between the *mex-5* promoter and the *tbb-2* 3'UTR, and cloned into pCFJ350 to generate plasmid pBC1476 [P*mex-5gfp::tac-1*]. To generate a plasmid that expresses CED-3 cleavage resistant GFP::TAC-1 protein, the codon for aspartate at position 251 of the TAC-1 protein (GAT) was mutated to code for

alanine (GCT) and subsequently cloned into pCFJ350 as described above (plasmid pBC1477). Both plasmids were injected separately into *C. elegans* strain EG6699 [*ttTi5605 II; unc-119(ed3) III; oxEx1578*] using the protocol outlined in Wormbuilder (http://www.wormbuilder.org/test-page/protocol/) and integrated into chromosome II (Frokjaer-Jensen et al., 2012). For each plasmid, two independent MosSCI insertions were obtained and named *bcSi1* and *bcSi2* for GFP::TAC-1(+) and *bcSi3* and *bcSi4* for GFP::TAC-1(D215A). *bcSi1* and *bcSi4* were used for analyses.

6. Microscopy

6.1. NSMsc survival. NSM sister cell survival was scored in L4 larvae or young adults carrying *bcIs66* [P$_{tph-1}$*his-24::gfp*] using a Zeiss Axioskop 2 equipped with epifluorescence as previously described (Thellmann et al., 2003).

6.2. Imaging of ABprppapa, ABprppapp, ABprpppaa, ABprpppap, ABprpppapa, ABplpappa and ABplpappaa divisions. Prior to the experiments, all strains were grown at 25°C overnight. The lineage of the individual cells were first determined using 4D-microscopy and lineage analysis was performed using a Zeiss Imager microscope and SIMIBioCell software (Simi Reality Motion Systems GmbH, Unterschleissheim, Germany) as described before (Schnabel et al., 1997) . Once the lineage was established, confocal microscopy was performed as described hereafter. Adult worms were dissected to obtain 4 cell stage embryos. These embryos were mounted on a 2% agar pad and covered with a glass cover slip that was sealed with petroleum jelly to avoid drying of the embryos. The slides were incubated at 25°C

for 135 minutes. The embryos were then imaged using a Leica TCS SP5 II confocal microscope. A Z-stack volume of 12-15 μm with a step size of 1 μm was set up. The recording was performed for 2 hours in order to accommodate all divisions in one image sequence. Following imaging, a noise reduction step was performed in the Leica Application Suite (LAS) to remove cytoplasmic noise.

6.3. Imaging of NSMnb [CED-3::GFP; CED-1ΔC::GFP; sAnxV::GFP and GFP::TAC-1]. Prior to the experiments, all strains were grown at 25°C overnight. Adults were dissected to obtain mixed stage embryos. These embryos were mounted on a 2% agar pad and covered with a glass cover slip that was sealed with petroleum jelly to avoid drying of the embryos. The slides were incubated at 25°C until the embryos reached the comma stage of development. To induce sAnxV::GFP expression from the heat shock promoter, embryos were incubated at 33°C for 45 min and subsequently allowed to recover for 2 hours as previously described (Mapes et al., 2012). Imaging was performed using a Leica TCS SP5 II confocal microscope. For all reporters, a Z-stack volume of 7-10 μm with a step size of 0.5 μm was set up. The recording was initiated before the NSMnb divided and continued until at least 25-30 min post NSMnb cytokinesis for CED-3::GFP, CED-1ΔC::GFP and sAnxV::GFP embryos and at least 10 min post NSMnb cytokinesis for GFP::TAC-1 embryos. Following imaging, a noise reduction step was performed using the Leica Application Suite (LAS) to remove cytoplasmic noise.

6.4. Fluorescence quantifications. For all reporters, the ventral NSM and dorsal NSMsc were identified by following the division of the NSMnb in each recording.

6.4A. CED-3::GFP analysis. Following confocal acquisition of CED-3::GFP embryos (as described above), for every Z-slice in which a distinct cell boundary (visualized with mCherry::PLCΔPH) for either the NSM or NSMsc could be seen, the number of CED-3::GFP pixels within the cell boundary was determined by drawing a region of interest on the cell boundary. The CED-3::GFP pixels obtained from different Z-slices of a particular cell were summed up to obtain the total CED-3::GFP pixels of that cell. Using the same regions of interest, the volumes of the cells were determined by summing up the areas of the cross sections of each cell. The total number of CED-3::GFP pixels obtained per cell was then divided by the volume of the respective cell and thus the 'CED-3::GFP pixels/cell volume' or 'CED-3::GFP concentration' was obtained. This procedure was repeated for all time points analyzed in this study. CED-3::GFP concentrations were normalized against the mean CED-3::GFP concentration of the NSM or NSMsc at t=0 min.

6.4B. CED-1ΔC::GFP analysis ([Figure 7](#)). Following confocal acquisition of CED-1ΔC::GFP embryos (as described above), the center plane of the NSMnb (at metaphase or 5 min prior to metaphase), the NSM or the NSMsc (both ~20 min post cytokinesis) was identified and used for analysis. The cell boundaries of NSMnb, NSM and NSMsc were visualized with mCherry::PLCΔPH. The dorsal ('d') and ventral ('v') side of the NSMnb was marked based on the position of the NSMnb daughters post cytokinesis. 'CED-1ΔC::GFP pixels/length' apposing the dorsal or ventral side of the NSMnb was determined by summing up the pixels apposing either side of the cell and dividing it by the length of the respective cell boundary. Post NSMnb cytokinesis (~20 min post cytokinesis), 'CED-1ΔC::GFP pixels/length' was

obtained by summing up the pixels surrounding the cell boundary of either daughter cell and dividing it by its circumference.

6.4C. GFP::TAC-1 analysis (Figure 8). Following confocal acquisition of GFP::TAC-1 embryos (as described above), a region of interest with a constant area for all slices of a Z-stack was drawn around the 'dorsal' or 'ventral' PCM in the NSMnb at metaphase. The total number of GFP::TAC-1 pixels associated with either PCM through the entire Z-stack was determined by summing up the number of GFP::TAC-1 pixels obtained from the different slices. The mean GFP::TAC-1 pixels of 'ventral' and 'dorsal' PCM in wild-type were normalized to 1. Each of the ventral and dorsal GFP::TAC-1 pixels obtained for *ces-2(bc213)*, *ced-3(n717)* and *ced-3(n718)* embryo were normalized against this value of 1. The time of GFP::TAC-1 dissociation (TOD) in the NSMsc was obtained by following the GFP::TAC-1 signal associated with the PCM inherited by the NSMsc from the onset of anaphase (the first image frame at which the centrosomes move away from their metaphase position) until no GFP::TAC-1 signal associated with the PCM was detected anymore. The same procedure was used for the ABprppapa, ABprppapp, ABprpppaa, ABprpppap, ABprpppapa, ABplpappa and ABplpappaa divisions. In the case of *ces-1(n703*gf*)* and *ces-2(bc213)*, the identity of the NSM and the NSMsc were determined by their wild type position post-cytokinesis. When the axis was random, the cell that was closest to the wild-type NSM position was designated 'NSM'.

7. NSM, NSMsc, ABprppapa, ABprppapp, ABprpppaa, ABprpppap, ABprpppapa, ABplpappa and ABplpappaa volume analysis. The cell boundaries were visualized with mCherry::PLCΔPH. For every Z-slice for which the distinct cellular boundaries of the NSM

and the NSMsc could be seen, a region of interest (ROI) was drawn. Using these ROIs, the NSM and the NSMsc volumes were obtained by summing up the cross section area of each cell. For volumetric analysis of ABprppapa, ABprppapp, ABprpppaa, ABprpppap, ABprpppapa, ABplpappa and ABplpappaa daughter cells post-cytokinesis, a region of interest was drawn over the cell boundary of the daughter cells and the cross section area of each cell per Z slice was summed up to obtain the total cellular volume. In case of CED-3::GFP embryos, this procedure was repeated for all time points analyzed in this study and the cell volumes were normalized against the mean CED-3::GFP concentration of the NSM or NSMsc at t=0 min.

Figure 7. Schematic description of CED-1ΔC::GFP analysis.

Following image acquisition of NSMnb, dorsal ('d') and ventral ('v') sides were marked based on the division of the cell. CED-1ΔC::GFP pixels/length were obtained by drawing on the dorsal and ventral sides using mCherry::PLCΔPH (*ltIs44*) as a reference and subsequent analysis was performed. For NSM and NSMsc, the same process was used but the complete cell boundary was taken into account.
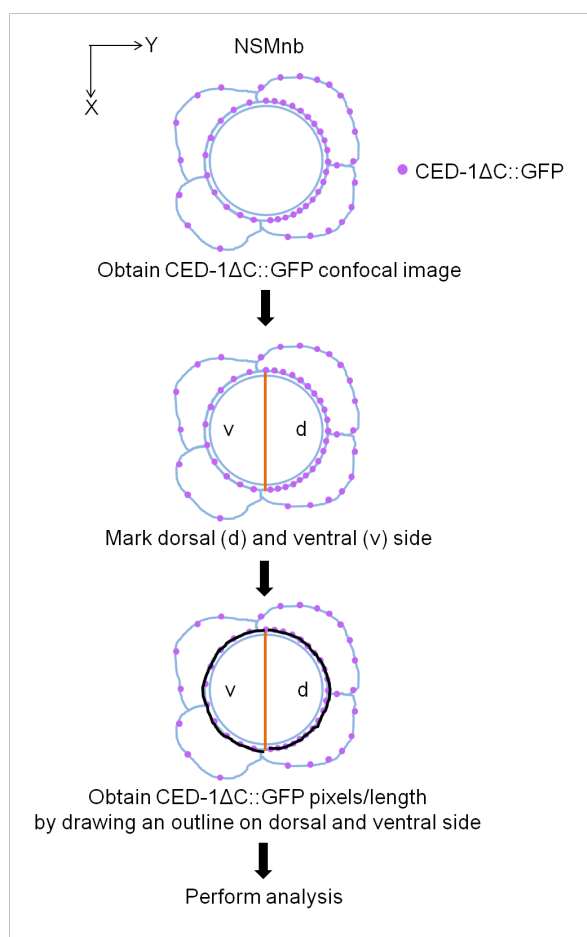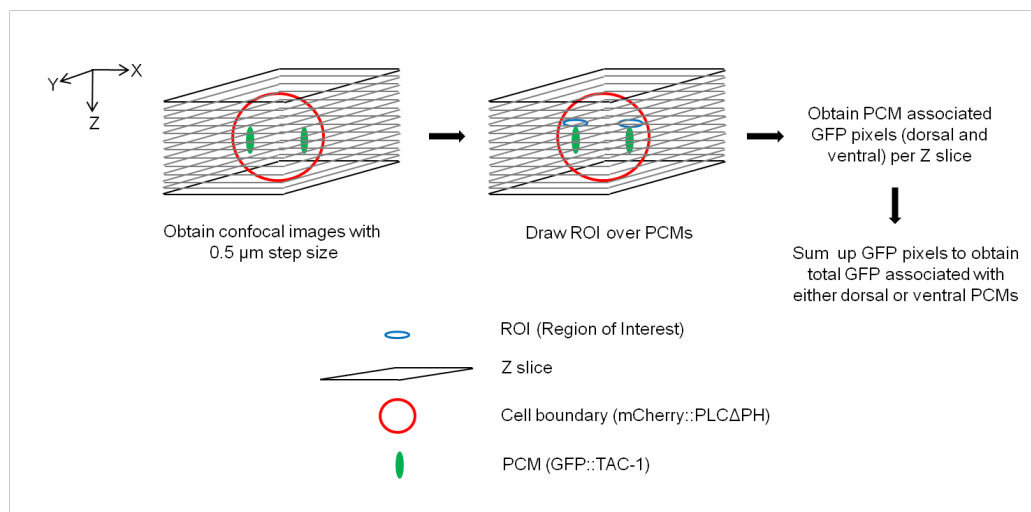
Figure 8. Schematic description of the quantification of GFP::TAC-1 associated with dorsal and ventral PCM.

A region of interest (ROI) was drawn around the dorsal and ventral PCM in the NSMnb [mCherry::PLCΔPH (*ltIs44*) was used to visualize NSMnb cell boundary], and the total GFP::TAC-1 pixels per PCM was obtained by adding up the numbers of GFP::TAC-1 pixels obtained for the individual Z slices as shown.

RESULTS

1. Components of the engulfment pathways promote programmed cell death in *C. elegans*

Due to the transparent nature of *C. elegans* and the invariancy in its cell lineage, mutations that block programmed cell death can be characterized by counting the number of inappropriately surviving cells in the anterior pharynx of the animal (Ellis and Horvitz, 1986; Schwartz, 2007). In the anterior pharynx of a wild-type animal, 16 cells undergo programmed cell death (Sulston et al., 1983). The nuclei of the inappropriately surviving cells in animals defective for cell death are visible using DIC microscopy. The penetrance of different cell death mutations can be assayed by counting the number of extra nuclei in the anterior pharynx of those animals.

Animals homozygous for strong loss-of-function mutations in *ced-3* caspase, such as *n717* and *n718*, harbor approximately 12 extra cells in the anterior pharynx (Shaham et al., 1999). Weak loss-of-function mutations in *ced-3*, such as *n2427*, result in the survival of approximately 1 extra cell in the anterior pharynx. A similar observation can be made for weak loss-of-function mutations in *egl-1* and *ced-4* (4 extra cells and 2 extra cells, respectively) (Reddien et al., 2001). On the contrary, loss-of-function mutations in the genes of the two engulfment pathways do not cause inappropriate cell survival in the developing *C. elegans* embryo. Therefore, no extra cells in the anterior pharynx can be detected in such mutant animals. Interestingly, it has previously been reported that animals that are mutant for any of the components of the two engulfment pathways as well as for either *egl-1*, *ced-4* or *ced-3* weak loss-of-function alleles, harbor a significantly higher number of inappropriately surviving cells in the anterior pharynx (5, 5 and 6 extra cells, respectively) (Hoeppner et al.,

2001; Reddien et al., 2001). In other words, the loss of components of the engulfment pathways enhances the general cell death defect of weak *egl-1*, *ced-4* or *ced-3* loss-of-function alleles. Therefore, it has been proposed that the engulfment genes promote the killing of cells programmed to die.

The promotion of the killing of cells programmed to die is not restricted to the cells in the anterior pharynx. In the ventral cord of *C. elegans* larvae, loss of *ced-1* enhances the inappropriate survival of cells in *ced-3(n2427)* animals. Hypodermal cells engulf the dying cells of the ventral cord. It has been demonstrated that rescuing *ced-1* function specifically in the hypodermis can rescue this enhancement of cell survival in the ventral cord conferred by *ced-1(e1735)* in *ced-3(n2427)* animals. It has therefore been proposed that the engulfment pathways act in the engulfing cells to perform this killing function (Reddien et al., 2001). It has also been shown that the engulfment pathways affect a process that is downstream of *ced-9* and independent of *ced-8*. The mechanism of this pro-apoptotic function of the components of the engulfment pathways however, remains to be elucidated.

Using the apoptotic death of the NSMsc as a paradigm, I have been able to shed light on how engulfment pathways promote the death of the NSMsc. I present evidence which demonstrate that the components of the cell engulfment pathways contribute to NSMsc death by playing a role in the polar localization of apoptotic factors (including CED-3 caspase activity) within the NSMnb and by further enhancing the unequal segregation of this potential into the NSMsc and NSM.

1.1. *ced-1* **promotes NSMsc apoptosis**

Differentiated NSMs express the gene *tph-1* which encodes the enzyme tryptophan hydroxylase (Sze et al., 2000). This enzyme catalyzes the rate-limiting first step in serotonin biosynthesis in *C. elegans*. Therefore, serotonergic neurons including the NSMs can be visualized using a P*tph-1his-24::gfp* reporter (Sze et al., 2000). Since NSMsc undergo apoptosis, they do not express this reporter. Mutations that result in the inappropriate survival of the NSMsc, cause the NSMsc to adopt the fate of its surviving sister. Therefore, the surviving NSMsc also express the P*tph-1his-24::gfp* reporter (Thellmann et al., 2003).

A strong loss-of-function mutation in the *ced-3* caspase gene *n717*, results in 100% NSM survival (Figure 9). The weak allele *n2427* causes NSMsc survival in 13% of NSM lineages. I found, that a strong *ced-1* loss-of-function mutation *e1735*, which does not cause NSMsc survival, significantly enhanced the NSMsc survival phenotype in animals that are homozygous for *ced-3(n2427)* (from 13% to 55%; Figure 9). Therefore, I propose that *ced-1* also promotes the programmed cell death of NSMsc.

Genotype	% NSMsc survival
+/+	0
ced-1(e1735)	0
ced-3(n717)	100
ced-3(n2427)	13
ced-1(e1735); ced-3(n2427)	55

Figure 9. *ced-1* **promotes NSMsc apoptosis.**
Percent (%) NSMsc survival scored in various genetic backgrounds (n=60-110). All strains analyzed were homozygous for P*tph-1his-24::gfp* (*bcIs66*).

1.2. *ced-1* plays a role in increasing the level of CED-3 caspase in the NSMsc

The ability of the engulfment pathways to promote cell killing has been shown to act downstream of *ced-9* (Reddien et al., 2001). Therefore, *ced-1* might affect *ced-3* in the NSM lineage. In order to visualize CED-3 *in vivo*, my colleagues Samik Bindu and Eric J. Lambie generated a fosmid-based *ced-3* reporter (P$_{ced-3}$*ced-3::gfp*) (Figure 10a). Since *ced-3* is first expressed as the zymogen proCED-3, which further autocatalyzes to generate active CED-3, the C-terminally GFP tagged CED-3 (CED-3::GFP) labels both forms of CED-3 (proCED-3::GFP and active CED-3:GFP). Therefore using this reporter, the levels of pro- and active forms of CED-3 caspase cannot be distinguished. To further determine whether CED-3::GFP retains its pro-apoptotic function, the multi-copy transgenic allele (*bcIs109*) obtained after integrating the reporter into the *C. elegans* genome, was introduced into *ced-3(n717)* animals. The reporter rescued the general cell-death defect of *ced-3(n717)* in the anterior pharynx of these animals, which demonstrates that CED-3 expressed from this transgene is functional (Figure 10b).

Using this fosmid-based *ced-3* reporter, I analyzed the expression pattern of CED-3::GFP in the NSM lineage of wild-type embryos. I observed CED-3::GFP in the NSMnb in metaphase, i.e. before it underwent division to form the NSM and the NSMsc (Figure 11a). This observation suggests that CED-3 is already present in the NSMnb, the mother of a dying cell. A similar observation was previously made in animals expressing a truncated CED-3 reporter (Maurer et al., 2007). Specifically, truncated CED-3::GFP was observed in cells that were not destined to die and also in mothers of dying cells.
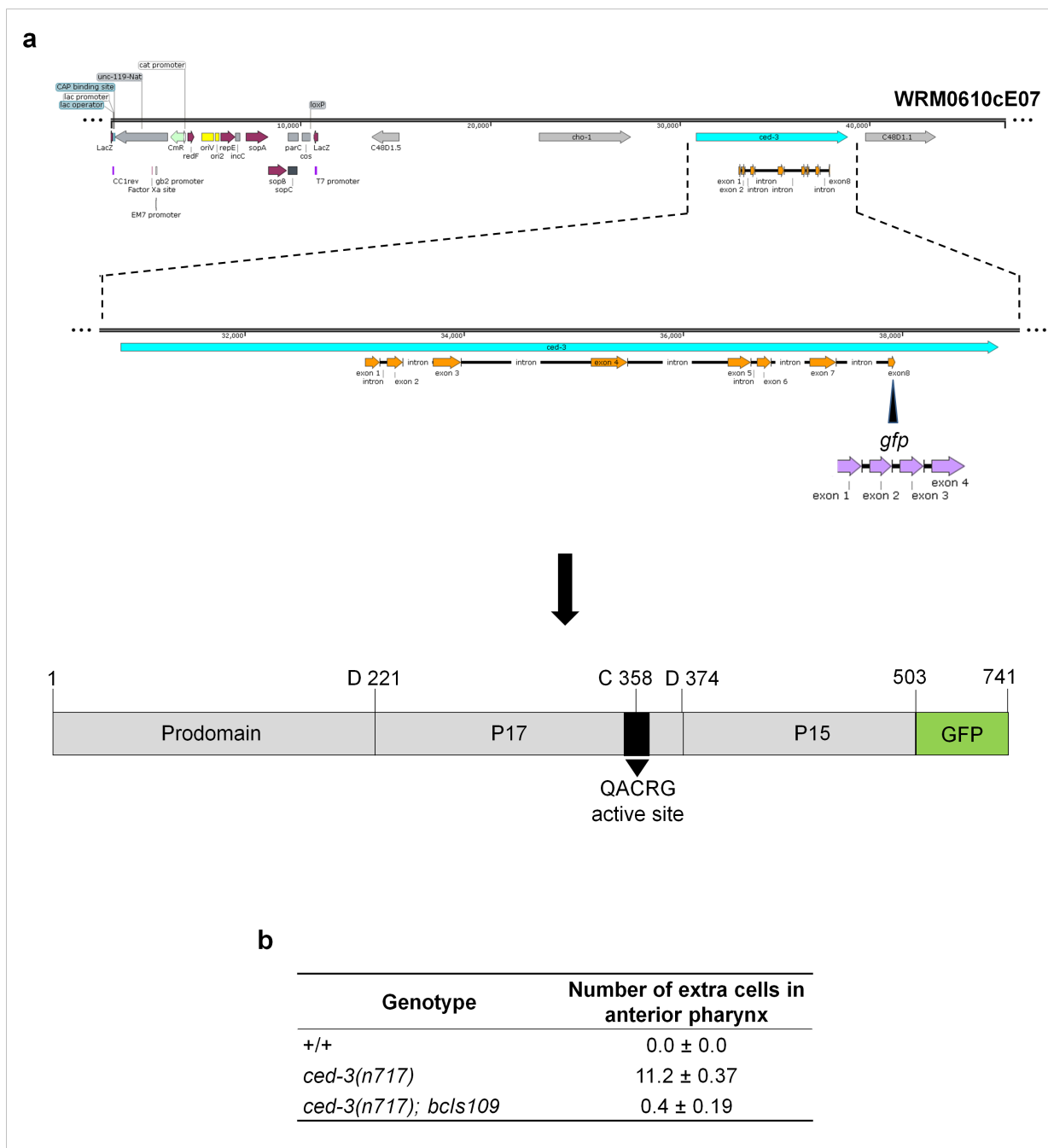
Figure 10. A fosmid based P$_{ced-3}$ced-3::gfp reporter complements *ced-3(n717)*.
a. Top: Fosmid map of WRM0610cE07 with *ced-3* transcription unit. The complete fosmid map with the gene annotations was obtained from the *C. elegans* TransgeneOme project

(https://transgeneome.mpi-cbg.de/transgeneomics/index.html) Middle. Exon-intron structure of *ced-3* transcription unit. The open reading frame of *gfp* was inserted in frame at the 5' end of exon eight to generate P$_{ced-3}$*ced-3::gfp* (pBC1378). Upon expression of this construct, both proCED-3 and active CED-3[*] protein are fused to GFP and can be visualized *in vivo*. Bottom: Schematic of proCED-3::GFP fusion protein. The prodomain, p17 and p15 domain as well as the active site are indicated. Numbers above bar represent amino acid positions. **b.** Number of extra cells in the anterior pharynx for the given genotypes. A stable, integrated transgene of P$_{ced-3}$*ced-3::gfp* (*bcIs109*) rescues the general cell-death (Ced) defect of *ced-3(n717)* animals. Data are means ± standard error of the mean (n=12-15).
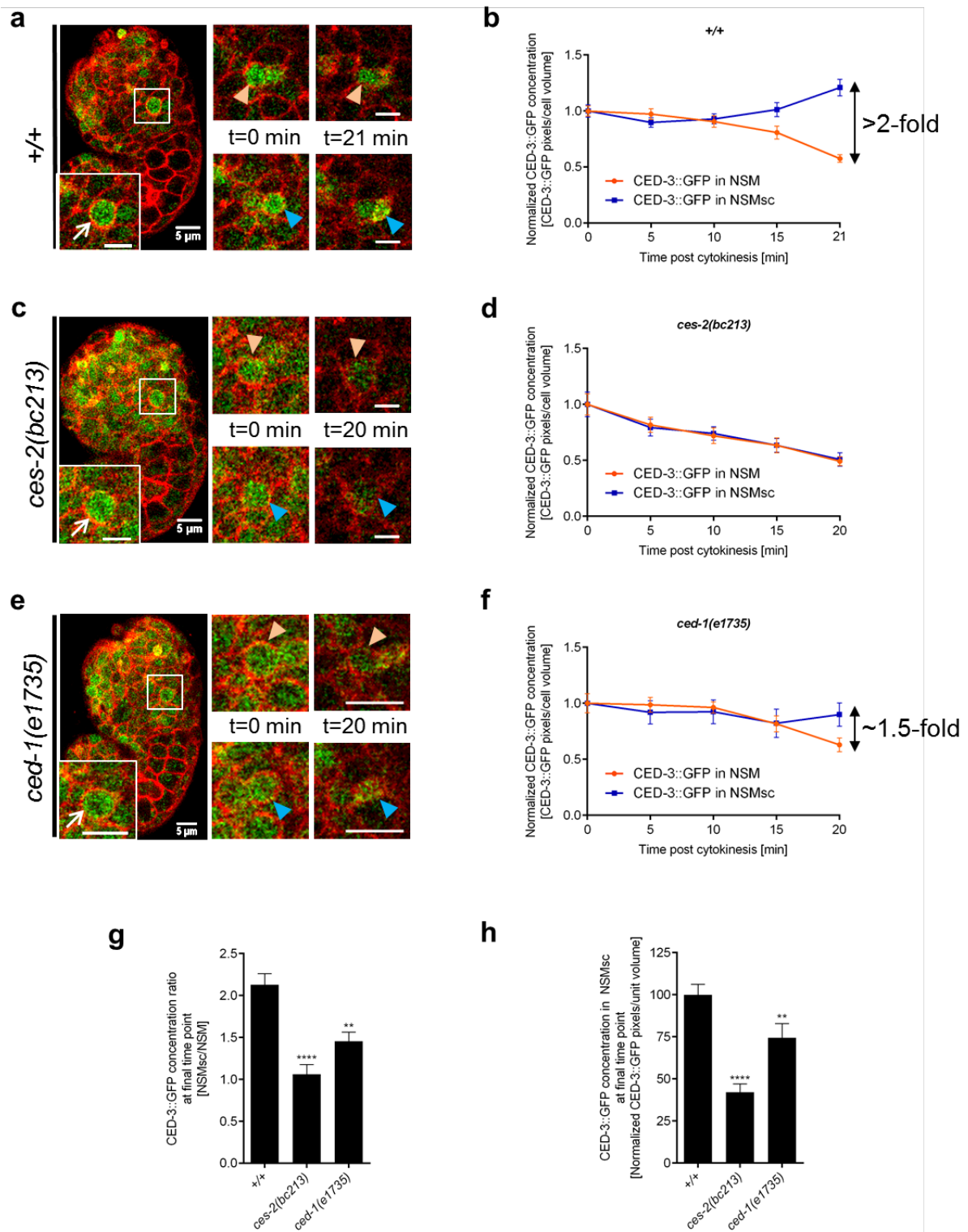
Figure 11. CED-3::GFP dynamics in the NSM lineage

a. c. e. Left images: Two channel overlay projections of single plane confocal images of representative wild-type (+/+), *ces-2(bc213)* and *ced-1(e1735)* embryos at metaphase expressing P*ced-3ced-3::gfp* (*bcIs109*) and P*pie-1mCherry::plcδph* (*ltIs44*). Insets represent

enlarged images of NSMnb (scale bar = 5 µm) at metaphase. White arrows point to NSMnb. Right images: Single plane confocal images of NSMnb daughter cells at cytokinesis (t=0 min) and at the time point at which the NSMsc corpse became visible in +/+ and *ced-1(e1735)* with the help of mCherry::PLCΔPH (t=21 min post-cytokinesis for +/+ and t=20 min post-cytokinesis for *ced-1(e1735)*; in *ces-2(bc213)* t=20 min was analyzed as NSMsc does not form a corpse). Blue arrowheads point to the NSMsc and orange arrowheads point to the NSM. **b. d. f.** Normalized means of CED-3::GFP concentration [CED-3::GFP pixels/cell volume] at various time points post-cytokinesis [min] in NSMsc (blue) and NSM (orange) in wild-type (+/+), *ces-2(bc213)* or *ced-1(e1735),* respectively (n=8). **g.** Ratios of CED-3::GFP concentrations in the NSMsc and in the NSM at final time point. **h.** Comparison of CED-3::GFP concentrations in the NSMsc at final time point. Statistics were performed using Student's t-test by comparing the respective means to wild-type (**p≤0.01 and ****p≤0.0001). Error bars denote the standard error of the mean.

To further analyze whether CED-3::GFP behaves differently in the daughter cells post NSMnb cytokinesis, I performed a time course analysis. I found that both the NSM and the NSMsc inherit equal concentration of CED-3::GFP (Figure 11a; t=0 min). Further, starting 10 min post-cytokinesis, CED-3::GFP concentration in the NSMsc gradually increased and reached its maximum at ~21 min post-cytokinesis, the time at which the NSMsc had adopted the morphology typical of a cell corpse (Figure 11a, b; t=21 min). Contrary to this, in the NSM, starting 10 min post-cytokinesis, CED-3::GFP concentration gradually decreased (Figure 11b). Upon comparing the final CED-3::GFP concentrations in the NSMsc and the NSM at 21 min post-cytokinesis, I found that CED-3::GFP concentration in the NSMsc was more than 2-fold higher than that in the NSM (Figure 11b, g).

Since the division of the NSMnb can be genetically manipulated by a loss-of-function mutation of *ces-2*, I analyzed CED-3::GFP in *ces-2(bc213)* animals. *bc213* is a putative null allele of *ces-2* and therefore disrupts NSMnb polarity, which further results in the birth of equally sized NSM and NSMsc (Figure 6, 12) (Hatzold and Conradt, 2008). I observed CED-

3::GFP in the NSMnb of *ces-2(bc213)* embryos (Figure 11c). Upon further quantifying the dynamics of CED-3::GFP concentration in the daughter cells, I found that CED-3::GFP concentration did not increase in the NSMsc post-cytokinesis; instead, the concentration gradually decreased in both the NSM and NSMsc. At 20 min post cytokinesis, both the NSM and the NSMsc had similar CED-3::GFP concentrations (Figure 11d, g). This observation suggests that since in *ces-2(bc213)* animals, both the NSMnb daughters survive and have a similar fate, CED-3::GFP levels may also behave similarly in those cells. Therefore, the NSMsc-specific increase in CED-3::GFP concentration observed after cytokinesis is dependent on *ces-2* and hence, most likely on the polarity of the NSMnb and its ability to divide asymmetrically.

To determine whether *ced-1* influences CED-3::GFP in the NSM lineage, I analyzed CED-3::GFP dynamics in *ced-1(e1735)* animals. In these animals, the division of the NSMnb is comparable to that of wild-type (Figure 12). Consistent with wild-type and *ces-2(bc213)* animals, I observed CED-3::GFP in the NSMnb at metaphase. Interestingly, I found that post-cytokinesis, the increase of CED-3::GFP concentration in the NSMsc was delayed with respect to wild-type, but there was no change in the decrease of CED-3::GFP concentration in the NSM (Figure 11e, f). In *ced-1(e1735)* animals, the NSMsc undergoes apoptosis approximately at the same time point as that of wild type NSMsc, i.e. ~20 min post-cytokinesis. At this time point, CED-3::GFP concentration in the NSMsc was significantly lower compared to wild-type (Figure 11f). The concentration of CED-3::GFP in the NSMsc was only 1.5-fold higher than that in the NSM (Figure 11g, h).

To rule out that the temporal changes in CED-3::GFP concentrations in the NSM and NSMsc were due to changes in NSM and NSMsc volume, I quantified the changes in the

daughter cells' volume in all genetic backgrounds analyzed. The changes in NSM and NSMsc

volumes post-cytokinesis were similar in all genotypes, suggesting that the changes in CED-

3::GFP concentration in the NSMsc were not caused by differences in cell volume and that the

increase in CED-3::GFP concentration observed in the NSMsc in wild-type embryos depicts

an increase in the amount of CED-3::GFP (Figure 13). Taken together, I conclude that *ced-1*

promotes the increase in the level of CED-3 caspase specifically in the NSMsc.
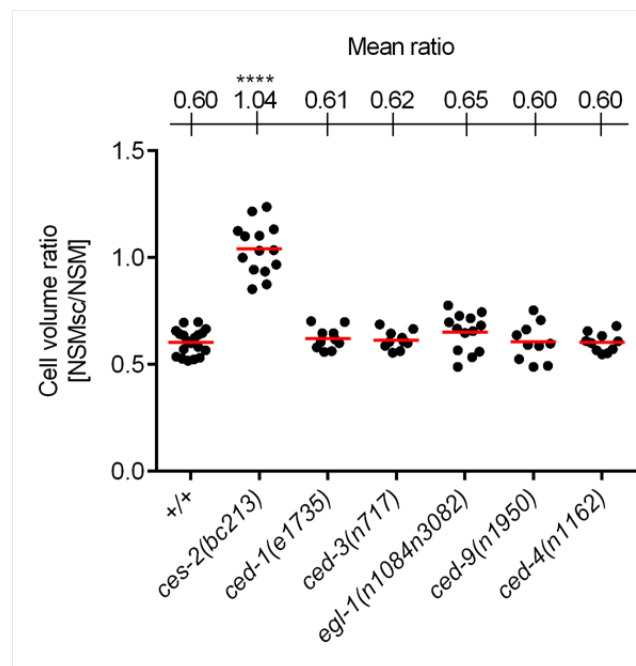
Figure 12. NSMsc to NSM cell volume ratios.
Ratio of the NSMsc cell volume to the NSM cell volume post cytokinesis of individual NSMnb divisions in different genetic backgrounds (wild-type (+/+), *ces-2(bc213)*, *ced-1(e1735)*, *ced-3(n717)*, *egl-1(n1084n3082)*, *ced-9(n1950)*, *ced-4(n1162)*) expressing P$_{pie-1}$*gfp::tac-1* (*bcIs104*) and P$_{pie-1}$*mCherry::plcδph* (*ltIs44*) (n=10-19). Mean ratios are indicated on top. All statistical analyses (Student's t-test) were done in comparison to wild-type (+/+) (****p≤0.0001).
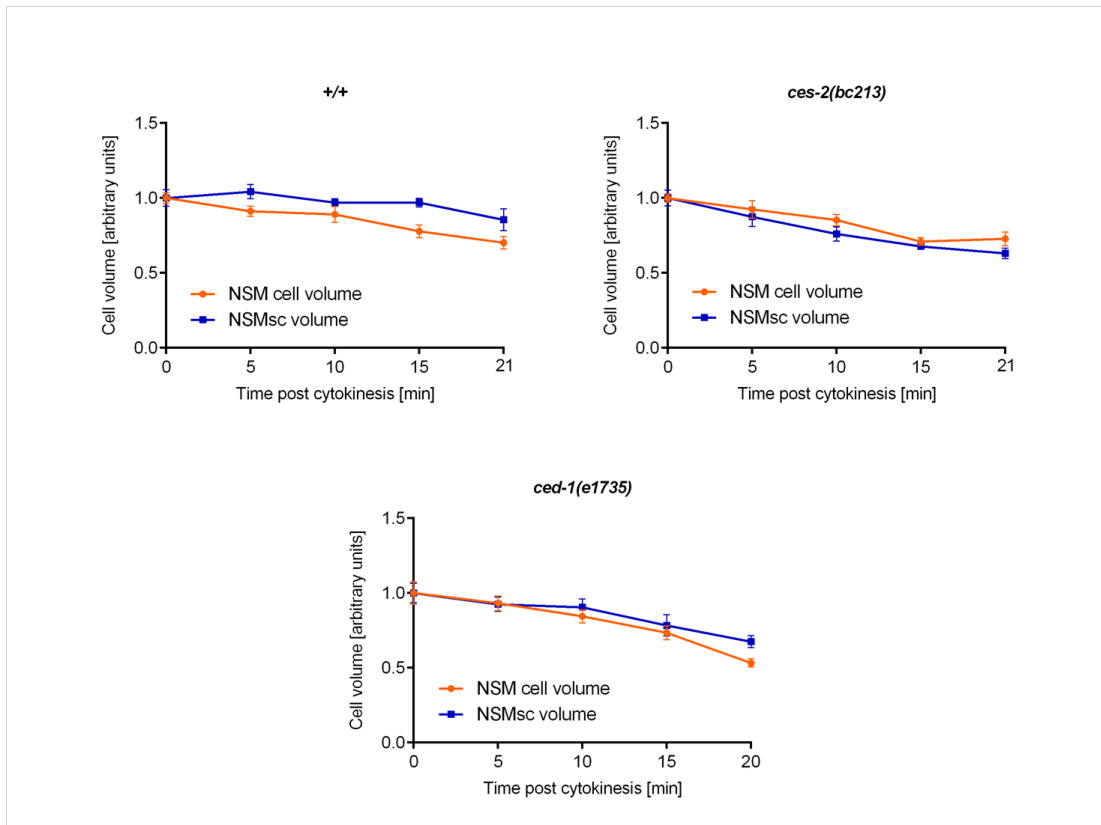
Figure 13. Changes in NSM and NSMsc volume post NSMnb cytokinesis are similar across mutants.
Cell volume analysis of NSM and NSMsc post NSMnb cytokinesis in embryos at different time points expressing P*ced-3ced-3::gfp* (*bcIs109*) and P*pie-1mCherry::plcδph* (*ltIs44*) in the given genetic backgrounds (wild-type (*+/+*), *ces-2(bc213)* and *ced-1(e1735)*) (n=8). All cell volumes obtained for NSM or NSMsc at the various time points were normalized against the cell volume obtained at t=0 min for the respective cell.

1.3. *ced-3* is required for asymmetric CED-1 enrichment around the NSMnb

Since, it has been proposed that the components of the engulfment pathways promote programmed cell death in a non cell-autonomous manner (Reddien et al., 2001), I used a CED-1::GFP fusion reporter (CED-1ΔC::GFP) (Zhou et al., 2001) to elucidate the temporal and spatial distribution of CED-1 receptor in the neighbors of the NSM lineage. The NSMnb divides along the dorsal-ventral axis, whereby the dorsal side of the NSMnb forms the NSMsc, which is programmed to die, and the ventral side forms the NSM, which is programmed to survive (Figure 14a). The cell that engulfs the NSMsc corpse is also present on the dorsal side to the NSMnb. It has previously been shown that CED-1 enrichment occurs on plasma membrane regions of the phagocytes that engulf a cell corpse (Zhou et al., 2001). Similarly, I observed CED-1 enrichment on the plasma membrane regions of the engulfing cell that apposes the NSMsc corpse (2.5-fold enrichment compared to plasma membrane regions of cells surrounding the NSM; Figure 14). Since in *ced-3(n717)* animals the NSMsc survive and are not engulfed, I did not observe any CED-1 enrichment around the inappropriately surviving NSMsc in *ced-3(n717)* animals (Figure 14b, c). Concomitant with previous reports, this observation suggests that CED-1 enrichment around the NSMsc cell corpse is also dependent on *ced-3* function.
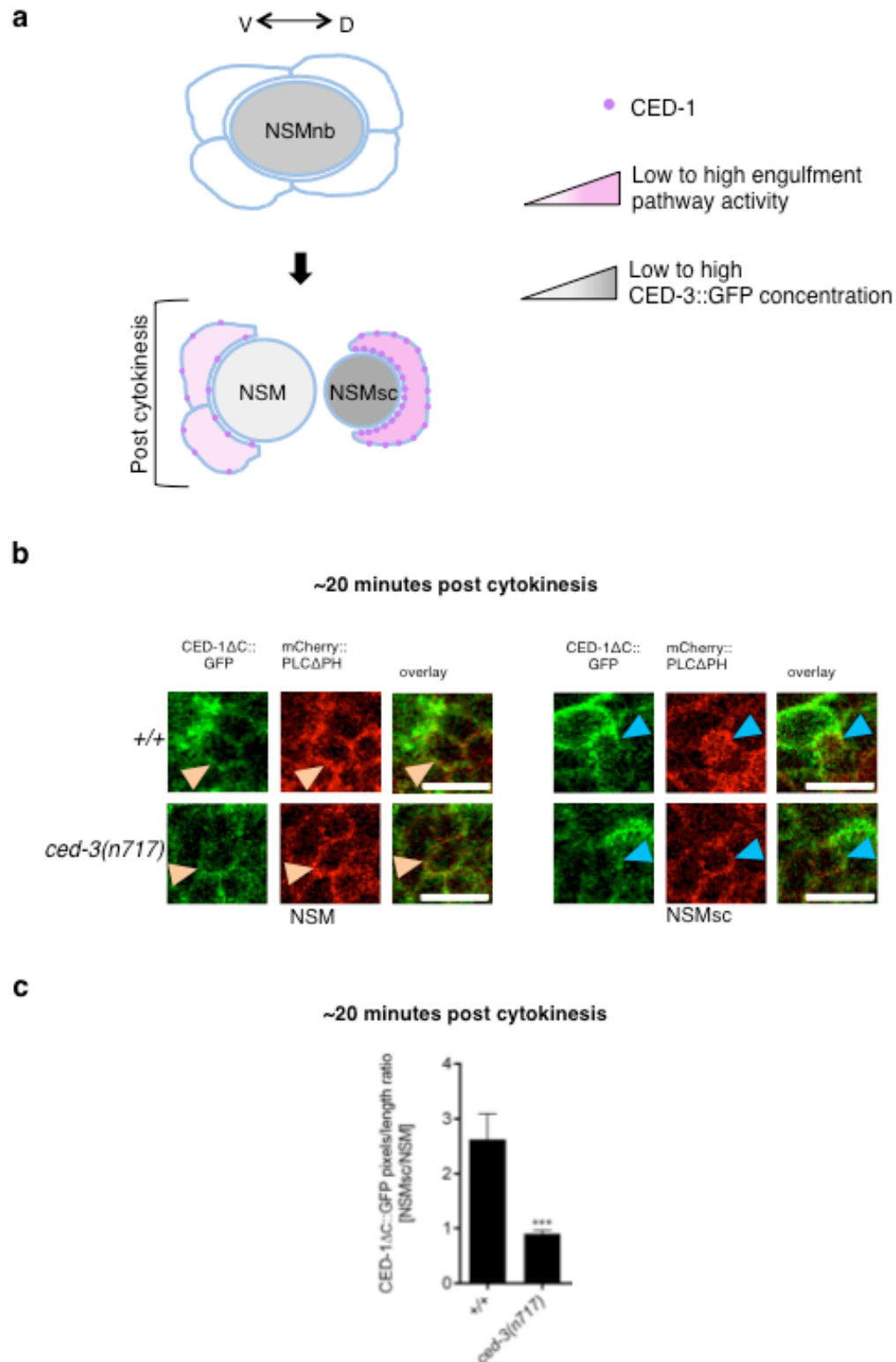
Figure 14. CED-1 clustering around the NSMsc corpse is dependent on *ced-3*.
a. The NSMnb divides along the dorsal 'd' and ventral 'v' axis to give rise to the NSM and NSMsc. CED-1 enrichment can be observed on plasma membrane regions of the engulfing cell that apposes the NSMsc corpse. **b.** Single plane and overlay confocal images of

representative NSM and NSMsc in wild-type (+/+) and *ced-3(n717)* embryos expressing P*ced-1ced-1δC::gfp* (*enIs1*) and P*pie-1mCherry::plcδph* (*ltIs44*) (scale bar = 5 μm). Orange and blue arrowheads denote the NSM and NSMsc, respectively. The red channel has been enhanced for better visualization of the cells. **c.** Ratios of CED-1ΔC::GFP pixels/length surrounding the NSMsc and the NSM ~20 min post NSMnb cytokinesis (n=4-8). Statistics were performed using Student's t-test by comparing the respective means to wild-type (*p≤0.05, **p≤0.01 and ***p≤0.001). Error bars denote the standard error of the mean.

Next, I extended my analysis to the NSMnb and its neighbors. Surprisingly, I found that at NSMnb metaphase, CED-1 was 1.3-fold enriched on plasma membrane regions of the two cells apposing the dorsal side of the NSMnb compared to the ventral side (Figure 15a, b). To further determine whether this asymmetric CED-1 localization is set up temporally or whether it exists throughout the NSMnb cell cycle, I performed a similar analysis 5 min before NSMnb entered metaphase. Interestingly, asymmetric CED-1 enrichment was not observed 5 min before NSMnb metaphase i.e. at this time point there were similar levels of CED-1 on the plasma membrane regions of the cells apposing the dorsal and ventral sides of the NSMnb (Figure 15c, d). However, I observed a higher expression of *ced-1* in the dorsal NSMnb neighbors compared to the ventral neighbors (Figure 16). Since I previously observed CED-3::GFP in the NSMnb at metaphase, hence suggesting that CED-3 is present in the cell, I analyzed CED-1 enrichment in *ced-3(n717)* animals. In these animals, CED-1 enrichment around the NSMnb was disrupted, implying that asymmetric CED-1 enrichment around the NSMnb is dependent on *ced-3* function (Figure 15a, b).

Taking together the observations made for CED-1 clustering around the NSM lineage, I conclude that CED-1 enrichment on the plasma membrane regions of the cells apposing the dorsal side of the NSMnb does not occur until NSMnb reaches metaphase (Figure 15, 17). *ced-3* activity in the NSMnb induces CED-1 enrichment on the plasma membranes of the

neighboring cells apposing the dorsal side of the NSMnb. I speculate that CED-1 enrichment and activation may occur preferentially in dorsal rather ventral neighbors since higher expression of *ced-1* is observed in the dorsal NSMnb neighbors compared to the ventral neighbors (Figure 16). As CED-1 enrichment activates the components of the engulfment pathways in phagocytes, I propose that CED-1 enrichment around the dorsal side of the NSMnb activates the components of the two engulfment pathways in the dorsal neighbors (Figure 17).
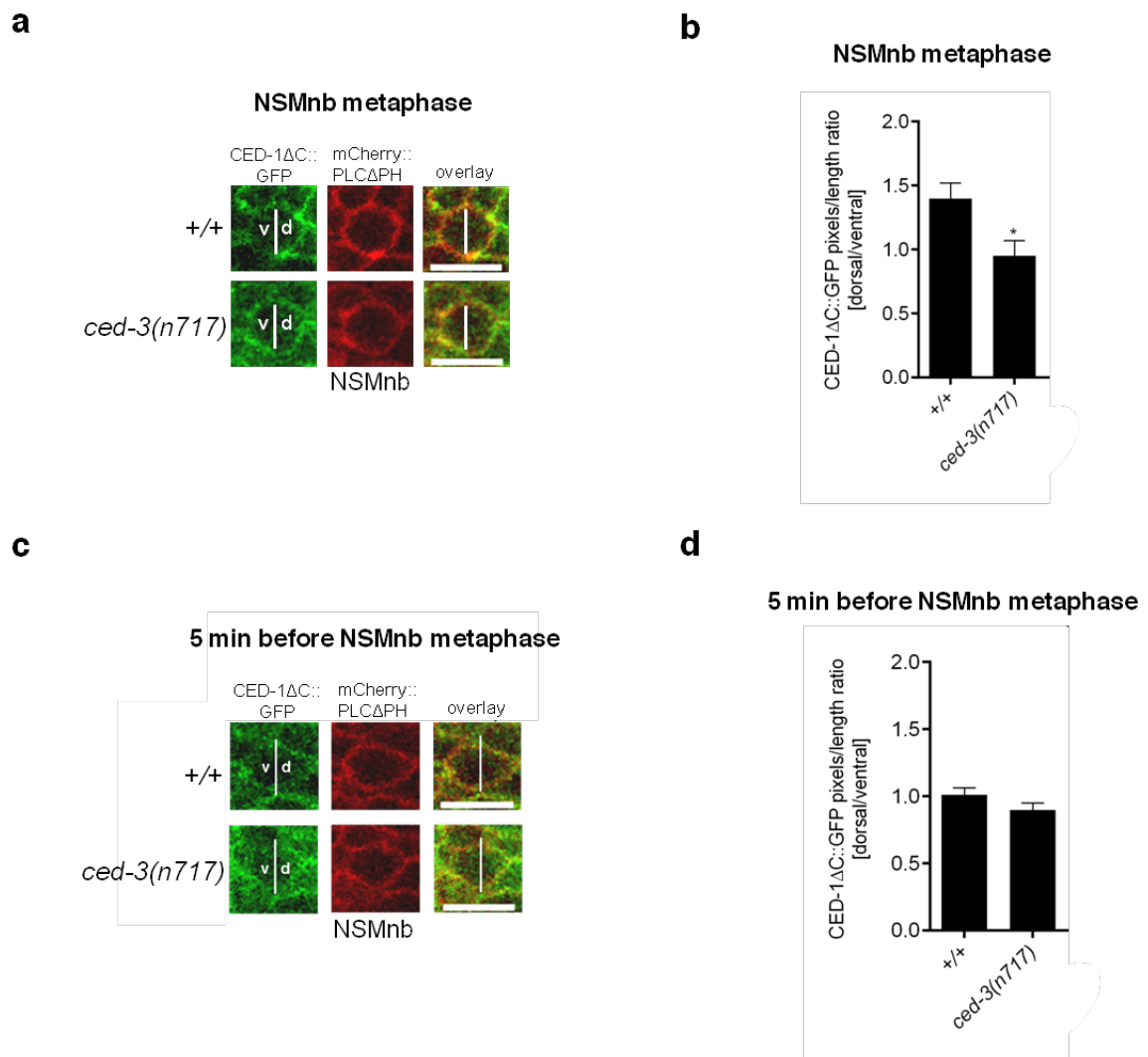
Figure 15. CED-1 becomes enriched in a *ced-3*-dependent manner on neighboring cells apposing the dorsal side of the NSMnb.

a. Single channel and overlay projections of single plane confocal images of representative NSMnb at metaphase in wild-type (+/+) and *ced-3(n717)* embryos expressing P*$_{ced-1}$ced-1δc::gfp* (*enIs1*) and P*$_{pie-1}$mCherry::plcδph* (*ltIs44*). White vertical lines indicate the border between the dorsal 'd' and ventral 'v' side of the NSMnb (scale bar = 5 μm). **b.** Ratios of CED-1ΔC::GFP pixels/length apposing the dorsal and the ventral side of the NSMnb at metaphase in various genetic backgrounds (n=8-9). **c.** Single channel and overlay projections of single plane confocal images of the NSMnb 5 min before metaphase in wild-type (+/+), *ced-3(n717)* and *ced-8(n1891)* embryos. White vertical lines indicate the border between the dorsal 'd' and ventral 'v' side of the NSMnb (scale bar = 5 μm). **d.** Ratios of CED-1ΔC::GFP pixels/length apposing the dorsal and the ventral side of the NSMnb 5 min before metaphase in various genetic backgrounds (n=8-9). Statistics were performed using Student's t-test by comparing the respective means to wild-type (*p≤0.05, **p≤0.01 and ***p≤0.001). Error bars denote the standard error of the mean.

5 min before NSMnb metaphase
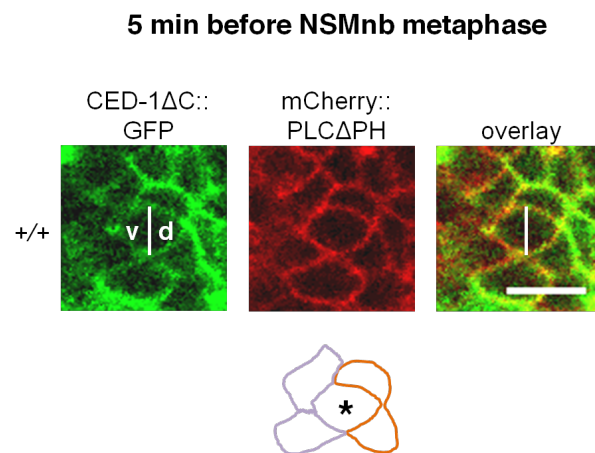
Figure 16. CED-1 expression in dorsal and ventral neighbors of the NSMnb.
Single channel and overlay projections of a single plane confocal image of the NSMnb and its neighbors 5 min before metaphase in wild-type (+/+) embryos expressing P*$_{ced-1}$ced-1δC::gfp* (*enIs1*) and P*$_{pie-1}$mCherry::plcδph* (*ltIs44*). White vertical lines indicate the border between the dorsal 'd' and ventral 'v' side of the NSMnb (scale bar = 5 μm). Black asterisk in the schematic indicates the NSMnb. Orange and purple outlines indicate the cell boundaries of the dorsal and ventral NSMnb neighbors, respectively. mCherry::PLCΔPH (*ltIs44*) was used to visualize NSMnb cell boundary.
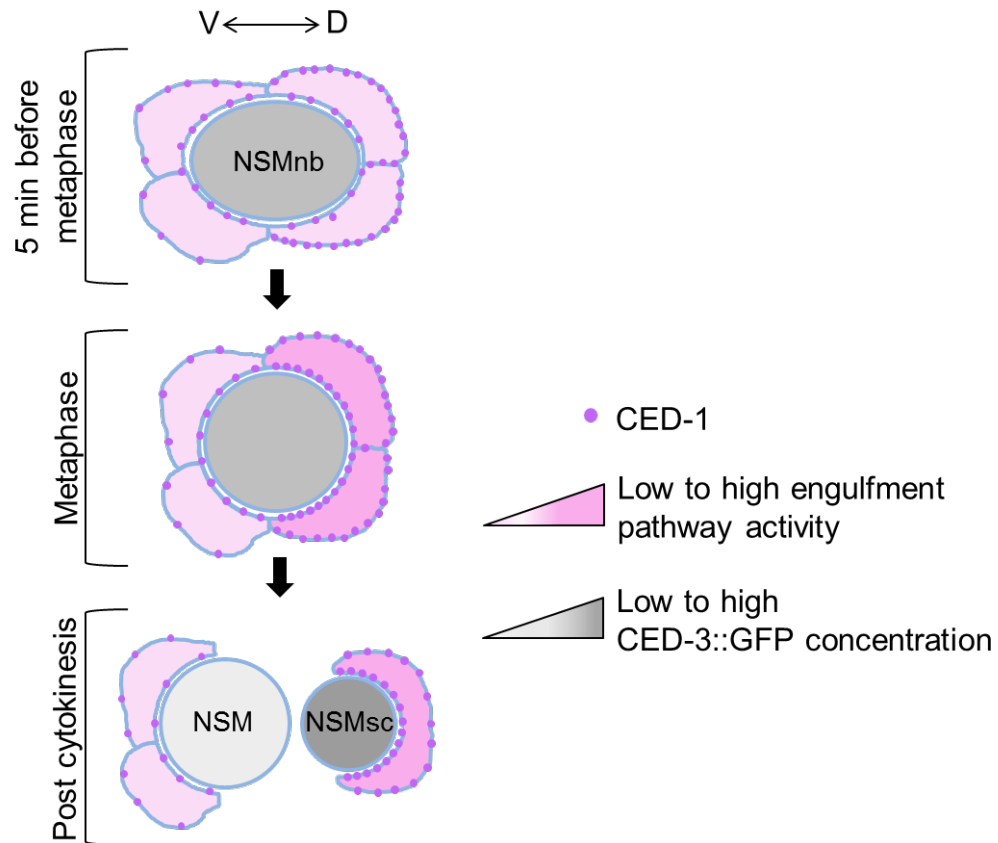
Figure 17. Molecular model depicting the process of CED-1 enrichment on the dorsal side of the NSM lineage.

ced-3 activity present in the NSMnb results in the enrichment of CED-1 on plasma membranes of neighboring cells apposing the dorsal side of the NSMnb. CED-1 enrichment on the plasma membranes of the dorsal neighbors leads to the activation of components of the two engulfment pathways in these cells. Post NSMnb cytokinesis, CED-3::GFP (grey gradient) increases in the NSMsc. At the time point of NSMsc death (~20 min post cytokinesis), CED-1 enrichment can be observed on plasma membrane regions of the engulfing cell that apposes the NSMsc corpse.

Cell corpses exhibit 'eat me signals' on their surfaces. In *C. elegans*, phosphatidylserine (PS) is the only 'eat me signal' that has been identified. It has been shown that PS exposure on the surface of a cell corpse induces CED-1 enrichment on plasma membranes of the engulfing cells apposing the cell corpse and that PS acts as a ligand for CED-1 (Venegas and Zhou, 2007; Li et al., 2015). Secreted AnnexinV can be used as a tool to identify apoptotic cells (Vermes et al., 1995). AnnexinV, initially discovered as a vascular protein and which has strong anticoagulant properties, is a calcium-dependent phospholipid-binding protein that binds to negatively charged PS (Reutelingsperger et al., 1985; Tait et al., 1989; Andree et al., 1990; Raynal and Pollard, 1994). I used a secreted AnnexinV::GFP fusion protein (sAnxV::GFP) (Mapes et al., 2012) to visualize PS exposure in the NSM lineage. I observed PS exposure on the surface of the dying NSMsc but not on the dorsal side of the NSMnb (Figure 18a). This suggests that CED-1 enrichment on the plasma membrane regions of the neighboring cells apposing the dorsal side of NSMnb is independent of PS exposure.

ced-8 encodes a Xkr8-like protein phosholipid scramblase and promotes PS exposure on the surface of cell corpses (Stanfield and Horvitz, 2000; Chen et al., 2013; Suzuki et al., 2013). A loss-of-function mutation in *ced-8*, *n1891*, disrupts this process in dying cells including the NSMsc (Figure 18b, c). When I analyzed this mutation in the NSM lineage, I observed that although CED-1 enrichment around the NSMsc was disrupted, it had no effect on CED-1 enrichment around the dorsal side of the NSMnb (Figure 18 d, e). Therefore, I conclude that CED-1 becomes enriched around the dorsal side of the NSMnb in a *ced-3* dependent but *ced-8* independent manner. Since the NSMnb does not undergo apoptosis, I propose that asymmetric CED-1 enrichment around the dorsal side of the NSMnb is dependent

on other unidentified CED-1 interacting ligands exposed on the NSMnb surface ([Figure 19](#)).

Like CED-8, these molecules may be activated by CED-3 dependent cleavage.
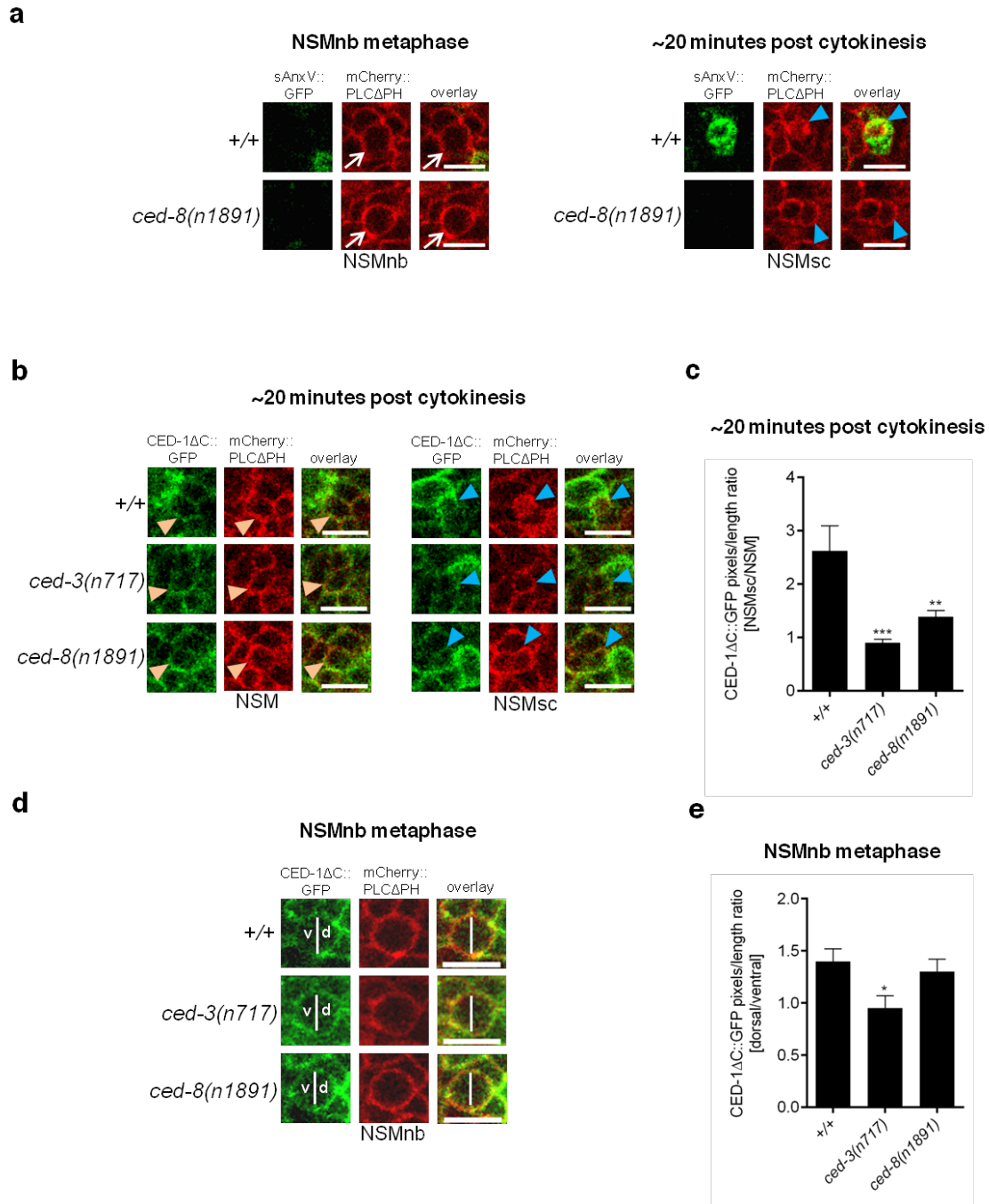
Figure 18. CED-1 clustering around the NSMnb is dependent on *ced-3* but not on *ced-8*.
a. Single channel and overlay projections of single plane confocal images of representative NSMnb (at metaphase) and NSMsc (~20 min post cytokinesis) of representative wild-type (+/+) and *ced-8(n1891)* embryos expressing P*$_{hsp}$sAnxV::gfp* (*smIs76*) and P*$_{pie-}$*

$_1mCherry::plc\delta ph$ (*ltIs44*) (scale bar = 5 µm). White arrows depict NSMnb and blue arrowheads depict NSMsc. **b.** Single plane and overlay confocal images of representative NSM and NSMsc in wild-type (+/+), *ced-3(n717)* and *ced-8(n1891)* embryos expressing $P_{ced-1}ced-1\delta C::gfp$ (*enIs1*) and $P_{pie-1}mCherry::plc\delta ph$ (*ltIs44*) (scale bar = 5 µm). Orange and blue arrowheads denote the NSM and NSMsc, respectively. The red channel has been enhanced for better visualization of the cells. **c.** Ratios of CED-1ΔC::GFP pixels/length surrounding the NSMsc and the NSM ~20 min post NSMnb cytokinesis (n=4-8). **d.** Single channel and overlay projections of single plane confocal images of representative NSMnb 5 min before metaphase in wild-type (+/+), *ced-3(n717)* and *ced-8(n1891)* embryos expressing $P_{ced-1}ced-1\delta c::gfp$ (*enIs1*) and $P_{pie-1}mCherry::plc\delta ph$ (*ltIs44*). White vertical lines indicate the border between the dorsal 'd' and ventral 'v' side of the NSMnb (scale bar = 5 µm). **e.** Ratios of CED-1ΔC::GFP pixels/length apposing the dorsal and the ventral side of the NSMnb 5 min before metaphase in various genetic backgrounds (n=8-9). Statistics were performed using Student's t-test by comparing the respective means to wild-type (*p≤0.05, **p≤0.01 and ***p≤0.001). Error bars denote the standard error of the mean.
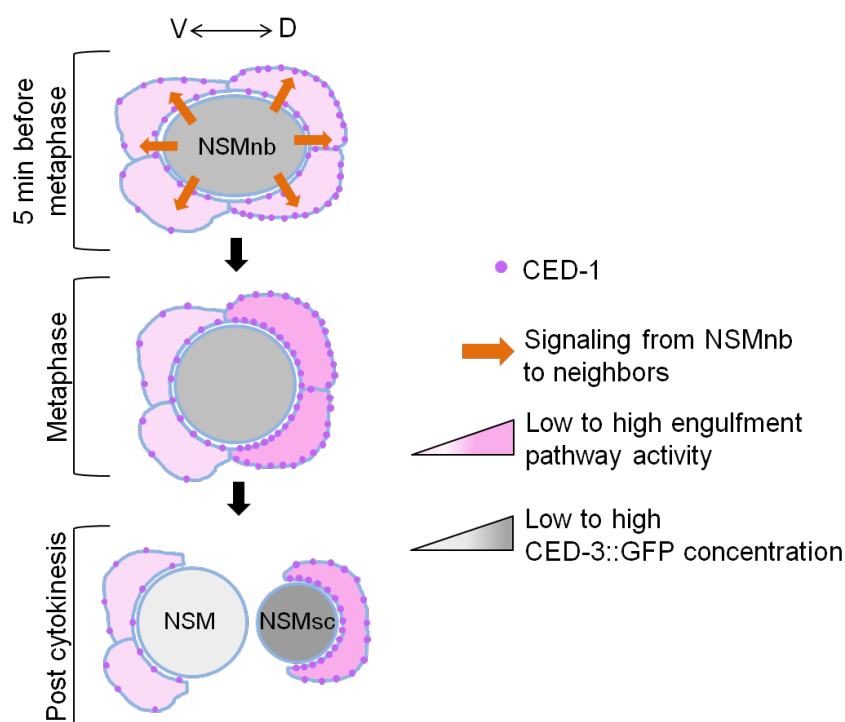
Figure 19. CED-1 enrichment around the NSMnb is dependent on *ced-3* activity and independent of PS exposure.

CED-1 enrichment on the plasma membranes regions of the neighboring cells apposing the dorsal surface of the NSMnb may be dependent on unidentified CED-1 interacting molecules exposed on the NSMnb surface. Such molecules may act downstream of *ced-3*.

1.4. Genes of the engulfment pathway mediate the establishment of a CED-3 caspase activity gradient in the NSMnb

Based on my findings I conclude that *ced-3* is expressed in the NSMnb and that *ced-3* activity is necessary for CED-1 enrichment on plasma membranes of cells apposing the dorsal side of the NSMnb. In order to determine the spatial distribution of CED-3 activity in the NSMnb, I developed an *in vivo* assay based on TAC-1, which is a component of the pericentriolar material (PCM) of centrosomes (Bellanger and Gonczy, 2003; Le Bot et al., 2003; Srayko et al., 2003). Centrosomes are the main microtubule organizing centers (MTOCs) of animal cells. A centrosome consists of a pair of centrioles that are surrounded by a proteinaceous matrix, the PCM. The centrosomes duplicate once a cell enters the S-phase of the cell cycle. At metaphase, the centrosomes are located at the opposite poles of a cell and are then inherited by the respective daughter cells. *In vitro* experiments by Samik Bindu suggested that TAC-1 (TAC, <u>TACC</u> protein family) has a caspase cleavage site and can be cleaved by active CED-3 caspase (Figure 20a). Upon expressing a GFP::TAC-1 fusion protein (expressed from a multi-copy integration of P*$_{pie-1}$gfp::tac-1* transgene) (Bellanger and Gonczy, 2003), I observed that at NSMnb metaphase, an asymmetry exists in the amount of GFP::TAC-1 associated with the PCMs of the two centrosomes. In the NSMnb at metaphase, the ventral centrosome had 1.3-fold more GFP::TAC-1 associated with it as compared to the dorsal centrosome (Figure 21a, b). *n717* and *n718* are strong loss-of-function alleles of *ced-3*. *n2433* is a mutation in the active site of CED-3, which renders the proCED-3 unable to autocatalyze itself to active CED-3. Loss of *ced-3* function in *ced-3(n717)*, *ced-3(n718)* and *ced-3(2433)* animals disrupted the asymmetry of PCM associated GFP::TAC-1 (ratios of 1.01, 1.03 and 1.13, respectively; Figure 21a, b). Specifically, there was an increase in the amount of

GFP::TAC-1 associated with the PCM of the dorsal centrosome (Figure 20b). Since *in vitro* experiments suggested that CED-3 cleaves TAC-1 after amino acid 251 (Figure 20a), I generated a non-cleavable GFP::TAC-1 protein, GFP::TAC-1(D251A). This non-cleavable reporter when introduced into a wild-type animal, should reciprocate the phenotype observed in *ced-3* mutant animals expressing the multi-copy P*pie-1gfp::tac-1* transgene. As expected, the single-copy GFP::TAC-1(D251A) reporter exhibited a ratio of 1.14 in wild-type animals (Figure 20c, d). This observation suggests the presence of lower amounts of GFP::TAC-1 on the dorsal side compared to the ventral side of the NSMnb at metaphase. Further, this asymmetry is mediated in part by CED-3 dependent cleavage of GFP::TAC-1. Since *ced-3* is expressed in the NSMnb, I propose that a dorsal-ventral gradient of CED-3 caspase activity exists in this cell, and that a higher level of this activity is present on the dorsal part of the NSMnb, which subsequently forms the NSMsc (Figure 22).

In *ces-2* mutants, the gradient of CED-3 caspase activity was also disrupted (ratio of 1.03; Figure 21a, b). A loss-of-function mutation in *dnj-11* and a gain-of-function mutation in *ces-1* similarly disrupted the gradient of CED-3 caspase activity (ratios of 0.91 and 0.98, respectively; Figure 21b). The genes *ceh-20* (CEH, <u>C. elegans</u> <u>h</u>omeobox) and *ceh-30* encode transcription factors that control cell deaths independent of the NSM lineage during *C. elegans* development (Liu et al., 2006; Peden et al., 2007; Schwartz and Horvitz, 2007). Loss-of-function mutations in these genes did not affect the gradient of CED-3 caspase activity (ratios of 1.27 and 1.28, respectively; Figure 21b). I therefore conclude that the disruption of the CED-3 caspase activity gradient due to mutations in *dnj-11*, *ces-2* and *ces-1* are due to their specific functions in the NSM lineage and not due to a general consequence of aberrant transcriptional regulation.

I further observed that the generation of the gradient of CED-3 caspase activity is dependent on the components of the central cell death pathway. Specifically, mutations in *egl-1* BH3-only, *ced-9* Bcl-2 and *ced-4* Apaf-1 also affect the caspase gradient, demonstrating that the central cell death pathway is already active to a certain degree in the NSMnb (ratios of 1.04, 1.07, and 1.08, respectively; Figure 21b). Mutations in *egl-1*, *ced-9* and *ced-4* however do not affect the asymmetric division of the NSMnb (Figure 12).

Surprisingly, loss of *ced-1* function also disrupted the gradient of CED-3 caspase activity in the NSMnb (ratio of 1.05; Figure 21a, b). Furthermore, loss of the CrkII-like adaptor gene *ced-2*, which is a component of the *ced-2, ced-5, ced-10, ced-12*-dependent engulfment pathway (Hedgecock et al., 1983; Reddien and Horvitz, 2000) or the GULP-like adaptor gene *ced-6*, another component of the *ced-1, ced-6, ced-7, dyn-1*-dependent engulfment pathway (Ellis et al., 1991; Liu and Hengartner, 1998) disrupted the gradient (ratios of 1.06 and 1.04, respectively; Figure 21a, b). I have previously demonstrated that CED-1 enrichment occurs on the plasma membrane regions of the neighboring cells apposing the dorsal side of the NSMnb and that the components of the engulfment pathways are likely to be activated in these cells. The evidence that loss of *ced-1*, *ced-2* and *ced-6* function disrupts the gradient of CED-3 caspase activity in the NSMnb further strengthens this notion. Hence, I conclude that the components of the engulfment pathways are not only activated in the neighbors of the NSMnb but also play a role in generating the dorsal-ventral gradient of CED-3 caspase activity in the NSMnb (Figure 22). This gradient however is not affected by the loss of *ced-8* (ratio of 1.24; Figure 21b). Hence, it strengthens the assumption that *ced-8* function is not necessary for CED-1 enrichment around the NSMnb.

Since loss of *ced-1* function in animals homozygous for *ced-3(n2427)* enhances the inappropriate survival of NSMsc (Figure 9), I analyzed the gradient of CED-3 caspase activity in *ced-1(e1735); ced-3(n2427)* animals. I observed that the gradient was disrupted in these animals (ratio of 1.03; Figure 21b). Since *n2427* is a weak mutant allele of *ced-3*, the gradient of CED-3 caspase activity in *ced-3(n2427)* animals was similar to wild-type (ratio of 1.27; Figure 21b). Interestingly, in all the 16 embryos of *ced-1(e1735); ced-3(n2427)* animals that were analyzed, I did not observe NSMsc undergoing apoptosis within the time frame (40 min post NSMnb cytokinesis) of live-imaging, further suggesting that NSMsc apoptosis may be significantly delayed in these animals. Taken together, my observations suggest that the enhancement of inappropriate NSMsc survival in *ced-1(e1735); ced-3(n2427)* animals may be dependent on the combined effects of the disruption of the gradient of CED-3 caspase activity in the NSMnb and the hindrance in CED-3 protein function in the NSMsc (see Discussion p.82).
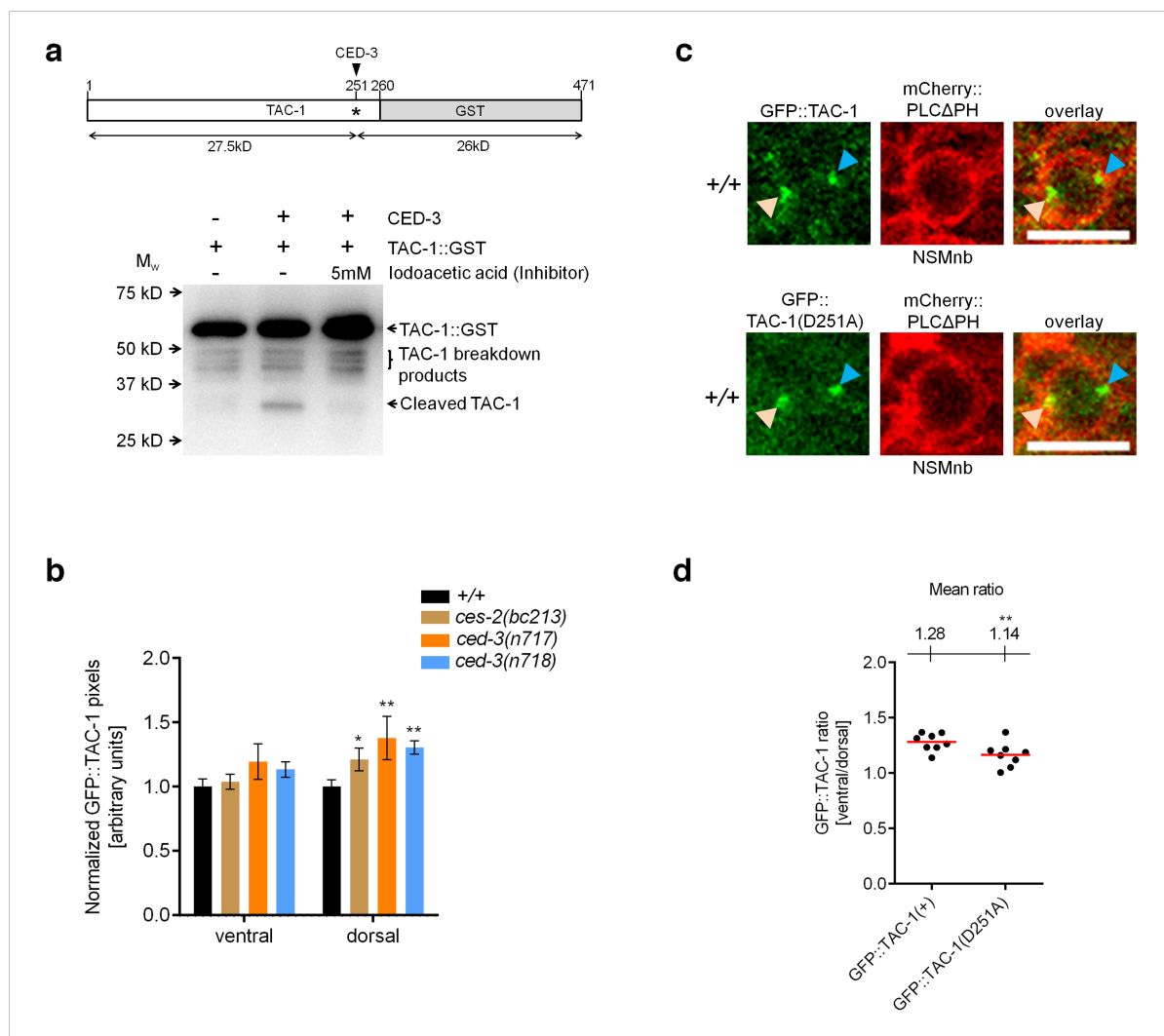
Figure 20. TAC-1 is a substrate of CED-3.
a. Top. Schematic of TAC-1::GST fusion protein, which was used for CED-3 cleavage reactions *in vitro*. The CED-3 cleavage site in TAC-1 (*) as well as the expected cleavage products is indicated. Numbers above bar represent amino acid positions. Bottom: western blot of different *in vitro* cleavage reactions. TAC-1::GST and TAC-1 were visualized using an antibody specific to *C. elegans* TAC-1. **b.** Normalized GFP::TAC-1 pixels [arbitrary units] associated with ventral or dorsal PCMs in the NSMnb at metaphase in wild-type (+/+), *ces-2(bc213), ced-3(n717)* and *ced-3(n718)* embryos expressing P*pie-1gfp::tac-1* (*bcIs104*) and P*pie-1mCherry::plcδph* (*ltIs44*) (n=5-19). The mean pixel intensities of GFP::TAC-1 associated with the ventral or dorsal PCMs in wild-type (+/+) were set to 1 and the pixel intensities in *ces-2(bc213)*, *ced-3(n717)* and *ced-3(n718)* embryos were normalized against this wild-type value of 1. **c.** Maximum intensity single channel and overlay projections of confocal images of representative NSMnb at metaphase expressing P*pie-1mCherry::plcδph* (*ltIs44*) and either single copy integrations of P*pie-1gfp::tac-1*(+) (*bcSi1*) (left) or P*pie-1gfp::tac-1(D251A)* (*bcSi4*) (right) in wild-type (+/+) embryos (scale bar = 5 μm). Orange arrowheads indicate the PCM

in the ventral part of the NSMnb and blue arrowheads indicate the PCM in the dorsal part of the NSMnb. **d.** Ratios of GFP::TAC-1 pixels associated with the ventral and dorsal PCM in individual NSMnb cells at metaphase in wild-type (+/+) embryos expressing P*pie-1gfp::tac-1(+)* (*bcSi1*) (left) or P*pie-1gfp::tac-1(D251A)* (*bcSi4*) (n=8). The mean ratio is given (top). Mean ratios were analyzed using the Student's t-test (*p≤0.05, **p≤0.01). Error bars denote the standard error of the mean.
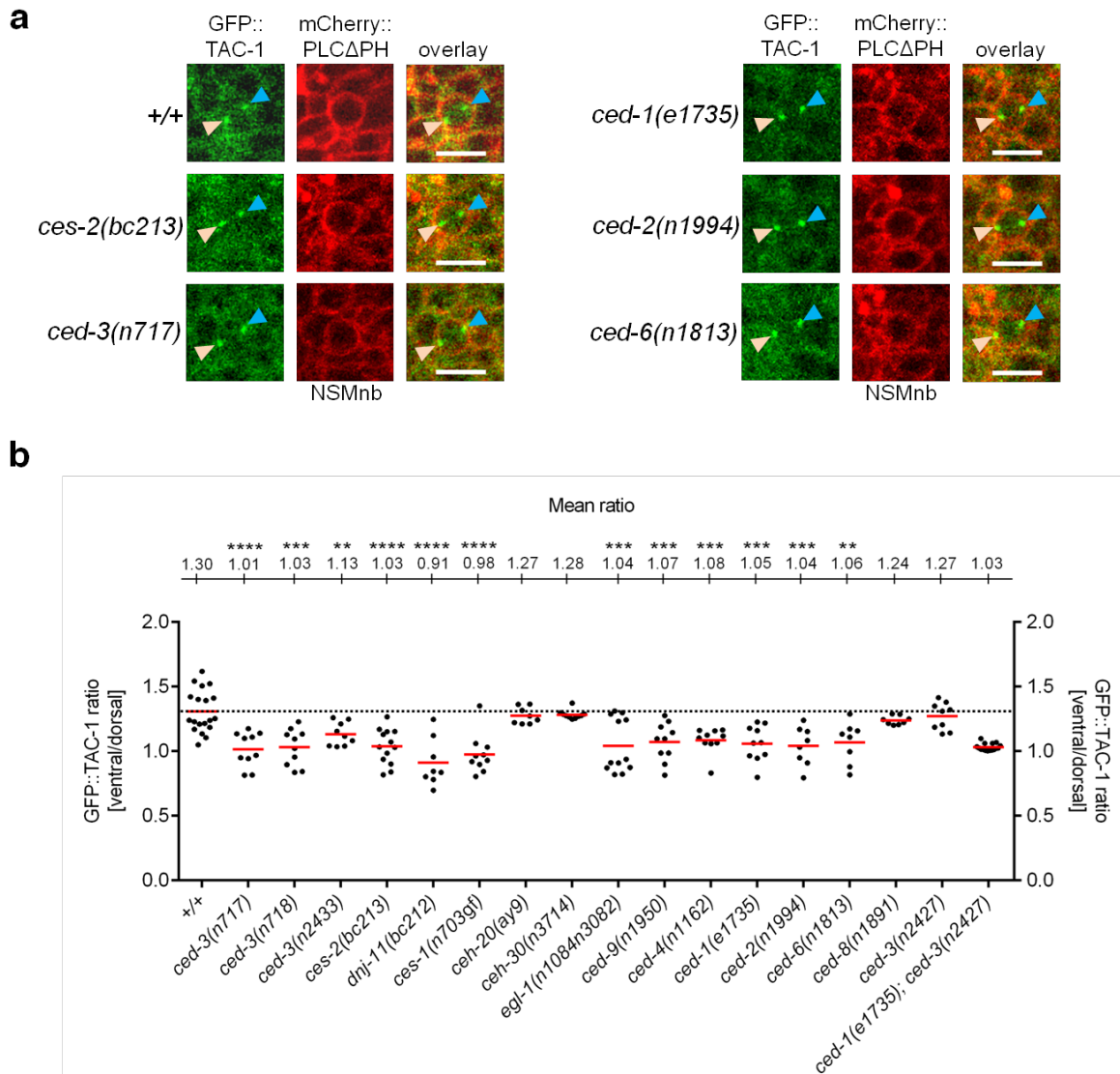
Figure 21. **A gradient of CED-3 caspase activity in the NSMnb is dependent on the components of the cell death pathway and the cell corpse engulfment pathways.**
a. Maximum intensity single channel and overlay projections of confocal images of representative NSMnb at metaphase in wild-type (+/+), *ces-2(bc213), ced-3(n717), ced-1(e1735), ced-6(n1813)* and *ced-2(n1994)* embryos expressing P*pie-1gfp::tac-1* (*bcIs104*) and P*pie-1mCherry::plcδph* (*ltIs44*) (scale bar = 5 μm). Orange arrowheads indicate the PCM in the ventral part of the NSMnb and blue arrowheads indicate the PCM in the dorsal part of the

NSMnb. **b.** Ratios of GFP::TAC-1 pixels associated with the ventral and dorsal PCM in individual NSMnb cells at metaphase in various genetic backgrounds (wild-type (+/+), *ced-3(n717)*, *ced-3(n718)*, *ced-3(n2433)*, *ces-2(bc213)*, *dnj-11(bc212)*, *ces-1(n703*gf*)*, *ceh-20(ay9)*, *ceh-30(n3714)*, *egl-1(n1084n3082)*, *ced-9(n1950)*, *ced-4(n1162)*, *ced-1(e1735)*, *ced-2(n1994)*, *ced-6(n1813)*, *ced-8(n1891)*, *ced-3(n2427)* and *ced-1(e1735); ced-3(n2427)*)) (n=8-19). The mean ratio is given (top). For comparison, the dotted line indicates mean ratio of wild-type (ratio of 1.3). Mean ratios were analyzed using the Student's t-test (**p≤0.01, ***p≤0.001 and ****p≤0.0001). All statistical analyses were done in comparisons to wild-type.
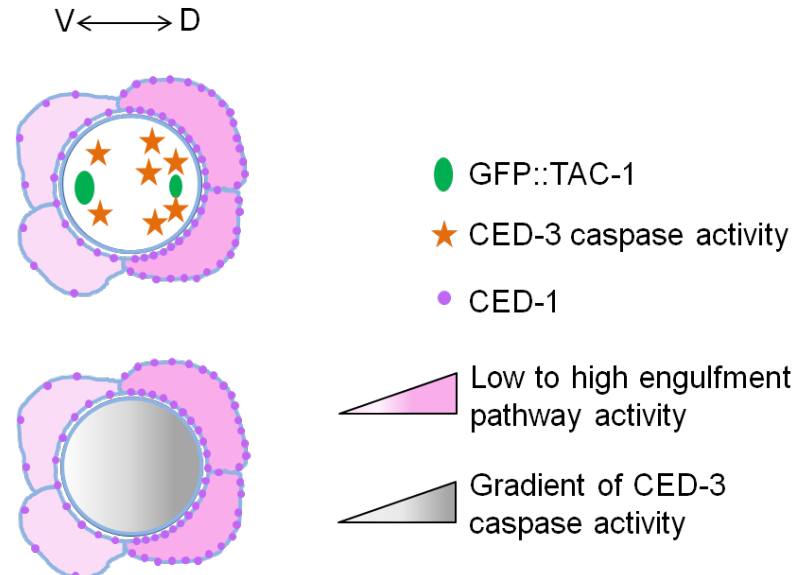
Figure 22. **A gradient of CED-3 caspase activity exists in the NSMnb.**
Comparatively less amounts of GFP::TAC-1 at the dorsal side of the NSMnb indicates the probable presence of a higher amount of CED-3 caspase activity on that side. This process is dependent on the components of the cell death pathway and cell corpse engulfment pathways. A gradient of CED-3 caspase activity is thus set up in the NSMnb at metaphase.

2. Asymmetric centrosome inheritance in asymmetric cell divisions

Centrosomes are the main microtubule organizing centers (MTOCs) of animal cells. Once a cell is born, it harbors one centrosome. A centrosome consists of a pair of centrioles which are surrounded by a proteinaceous matrix, the pericentriolar material (PCM). In *C. elegans*, ZYG-1 (ZYG, zygote lethal), SAS-4 (SAS, spindle assembly abnormal), SAS-5 and SAS-6 proteins constitute the core centriole assembly module (Figure 23a) (Rocheleau et al., 1997; Meneghini et al., 1999; Shin et al., 1999; Maduro et al., 2002; Smit et al., 2004). These molecules are indispensible for centriole duplication. SPD-2 (SPD, spindle defective) and SPD-5 play roles in centrosome maturation (Shetty et al., 2005; Rujano et al., 2006). SPD-2 is necessary for the recruitment of ZYG-1 kinase during centriolar duplication. During maturation of the PCM, TBG-1 (TBG, tubulin gamma) mediates microtubule (MT) nucleation (Green et al., 2008). TAC-1 and ZYG-9, which physically interact with each other, are important regulators of MT polymerization (Broadus and Doe, 1997; Bellanger and Gonczy, 2003; Le Bot et al., 2003; Srayko et al., 2003). KLP-7 (KLP, kinesin-like protein), a microtubule depolymerase localizes to both the PCM and the kinetochores during cell division and plays a role in the generation of astral forces (Reese et al., 2000). TPXL-1 (TPXL, targeting protein for *Xenopus* Klp2-like) physically interacts with AIR-1 (AIR, Aurora/Ipl1 related kinase) and plays an essential role in mitotic spindle assembly (Lambert and Nagy, 2002; Badrinath and White, 2003).

Since centrosomes duplicate and segregate during each cell division cycle, the two centrioles of a given centrosome differ in age. During S-phase, each centriole nucleates the formation of a new centriole. This process further leads to the generation of two centrosomes

of different ages: the 'mother' and 'daughter'. The mother centrosome consists of the former oldest centriole in the cell. Following M-phase, mother and daughter centrosomes are segregated to each of the daughter cells (Figure 23b) (Mardin and Schiebel, 2012).
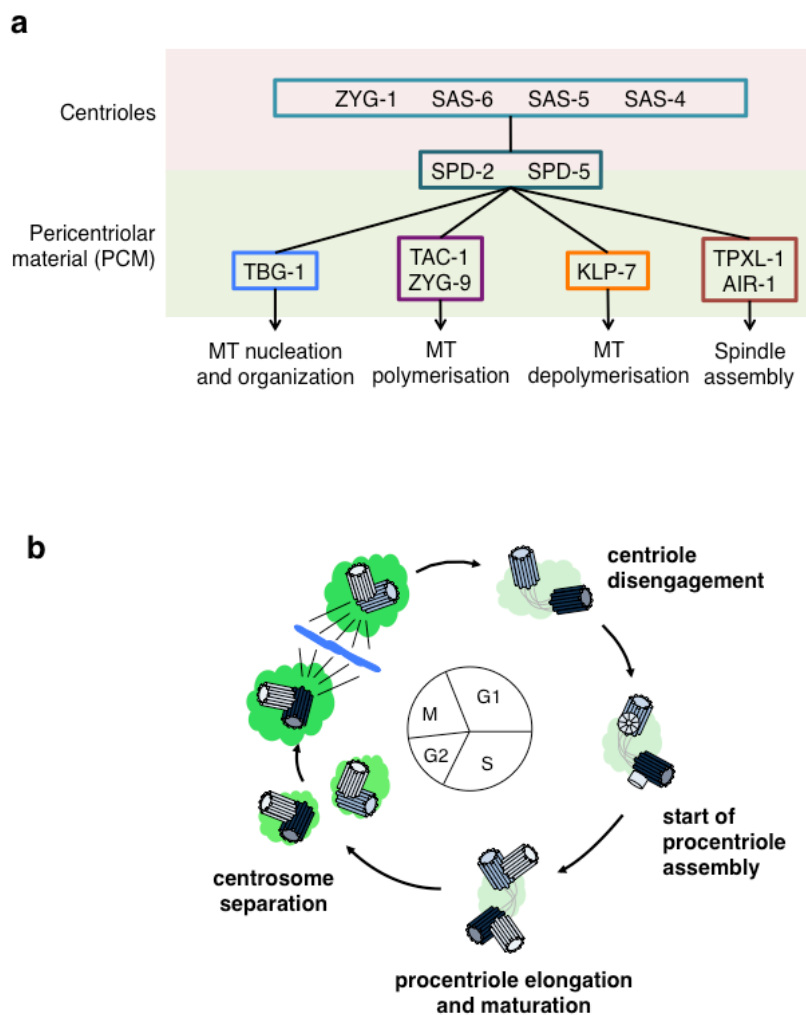
Figure 23. Components of a *C. elegans* centrosome and its duplication cycle.
a. Components of a *C. elegans* centrosome are shown according to their compartmentalization. **b.** Schematic of centrosomes progressing through a cell cycle (G1 to M). Shown are centrioles (in cylinders) of different ages (with different hues of blue), and the PCM (green). (**b.** figure courtesy of Tamara Mikeladze-Dvali)

Studies of stem cell divisions in *Drosophila melanogaster* and in mammals have shown that mother centrosome and daughter centrosome segregate in a non-random manner and that this segregation pattern correlates with the fates of the daughter cells (Reina and Gonzalez, 2014). For instance, in asymmetric germline stem cell divisions that occur during *D. melanogaster* spermatogenesis, the mother centrosome is specifically segregated into the male germline stem cell, while the daughter centrosome is segregated into the differentiating cell, the gonioblast (Figure 24a) (Pelletier and Yamashita, 2012). It has been further demonstrated that the mother centrosome remains physically attached to the stem cell niche, and therefore results in the retention of the mother centrosome in the stem cell. (Yamashita et al., 2007). The daughter centrosome is segregated to the differentiating cell. Centrosome asymmetry with respect to PCM dynamics and MTOC activity has also been observed during asymmetric divisions of neuroblasts in *D. melanogaster* (Figure 24b) (Januschke and Gonzalez, 2010). Finally, a number of factors such as the centriolar proteins Bld10/CEP135, Cnb (Centrobin) and Cnn (centrosomin) as well as POLO kinase have been shown to be critical for the regulation of PCM dynamics (Rebollo et al., 2007; Conduit et al., 2010; Conduit and Raff, 2010; Januschke et al., 2013; Lerit and Rusan, 2013; Singh et al., 2014). Whether centrosome asymmetry in terms of PCM size and non-random patterns of centrosome segregation exists in lineages other than stem cell lineages is currently unknown.

I have been able to demonstrate that asymmetry with respect to the amount of PCM associated with the centrosomes the non-random segregation of 'small' and 'large' centrosomes exists in multiple cell lineages of the developing *C. elegans* embryo. I have also found that the components of the central cell death pathway: *egl-1* BH3-only, *ced-9* Bcl-2,

ced-4 Apaf-1 and *ced-3* caspase, contribute to centrosome asymmetry and segregation during embryonic cell divisions of *C. elegans*.
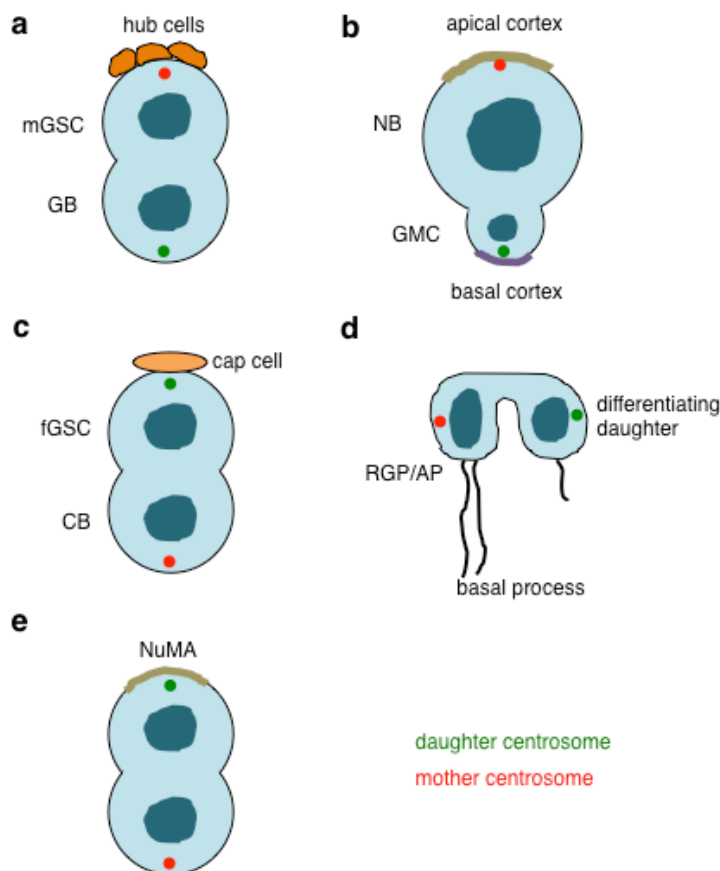
Figure 24. Asymmetric centrosome inheritance in asymmetric cell divisions.
Shown are non random inheritances of asymmetric centrosomes in various asymmetric cell divisions. Green is the daughter centrosome and red is the mother centrosome. **a.** *Drosophila* male germline stem cells (mGSC) and differentiating gonialblast (GB). **b.** *Drosophila* neuroblasts (NB) and the differentiating ganglion mother cell (GMC). **c.** *Drosophila* follicular germline stem cells (fGSC) and differentiating cytoblast (CB). **d.** Mice and rat radial glial progenitor cells/apical progenitors (RGP/AP). **e.** Neuroblastoma cell line.

2.1. Centrosomes in early *C. elegans* embryonic divisions are asymmetric with respect to amounts of proteins associated with the PCM and their segregation is non-random

In order to investigate whether centrosomes segregate asymmetrically by centriole age during *C. elegans* embryonic development, I attempted to design a tool using a photo-convertible fluorophore to observe the segregation of mother and daughter centrioles. Dendra is a monomeric dual-color photo-convertible (green to red) fluorophore derived from the coral *Dendronephthya sp*. (Gurskaya et al., 2006). Similar to EGFP and other green fluorescent proteins, non-activated Dendra possesses excitation and emission maxima at 490 and 507 nm. Photo-conversion of Dendra from green to red fluorescent state is obtained in response to intense blue light irradiation at 460-500 nm. To follow centriole segregation by age during a cell division, activation of Dendra needs to be carried out in the mother of the cell to be analyzed (Figure 25). The mother of the cell to be analyzed will contain a 'green' centriolar pair. Upon photo-conversion of Dendra by a 488 nm laser, this centriolar pair will appear 'red'. Following centriole duplication, this cell will harbor two pairs of centrioles, each containing a 'red' mother centriole and a 'green' daughter centriole. The cell of interest will then inherit a centriolar pair. Post centriole duplication, one centriolar pair will appear 'green' while the other will consist of a 'green' and a 'red' centriole. Subsequently, the centriolar pairs and the 'green' and 'red' signals can be used to visualize the segregation of mother vs. daughter centrioles during the division of the cell to be studied. SAS-4 is one of the constituents of a typical *C. elegans* centriole (Figure 23a). In order to observe centrioles, I used the ubiquitous promoters P*let-858* and P*rps-27* to drive both N-terminal and C-terminal

fusions of Dendra-SAS-4. However, due to technical complications, I could not generate a stable line expressing either of these reporters.
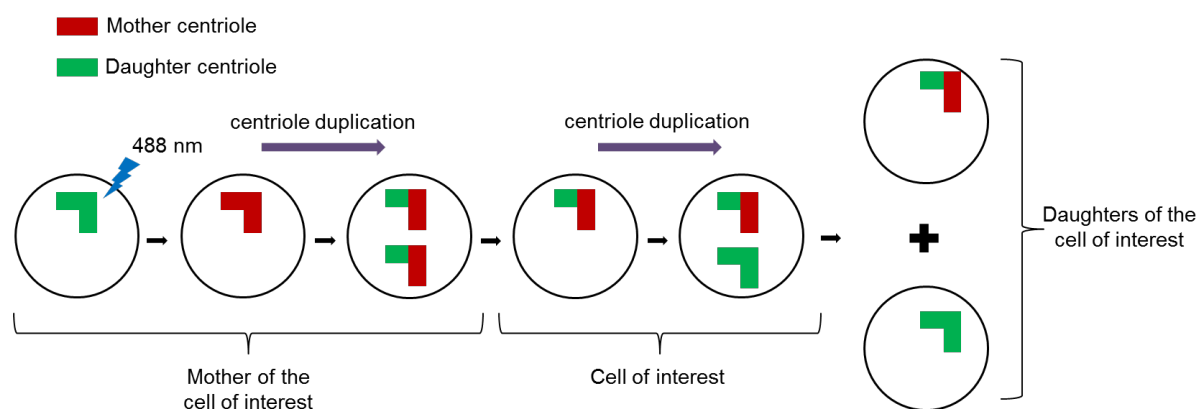
Figure 25: A schematic for using Dendra as a marker for centrosome segregation with respect to centriole age.
The green and red signals can be used to visualize the segregation of mother vs. daughter centrioles during the division of the cell to be studied.

Next, I determined whether there is centrosome asymmetry in individual cell lineages in the developing *C. elegans* embryo, with respect to the amount of proteins associated with the pericentriolar material (PCM) of a centrosome at metaphase during different cell divisions. I had previously demonstrated that the multi-copy integrated GFP::TAC-1 transgene can be used as a tool to determine the 'size' of a given centrosome with respect to proteins associated with the PCM (Figure 21). Hence, I analyzed centrosomes during the 9th round of division, which is the first round of division that generates cells fated to die (Sulston et al., 1983). In particular, I analyzed the divisions of ABprppapa, ABprppapp and ABprpppaa (referred to as divisions 1-3), all of which divide symmetrically to give rise to two daughters of similar sizes

both of which are fated to survive (Figure 26a, b). For all three divisions I found that the centrosomes at metaphase were asymmetric with respect to the amount of associated TAC-1. Within a single cell, I classified the centrosome with a higher amount of GFP::TAC-1 as the 'large' centrosome and the one with the lower amount of GFP::TAC-1 as the 'small' centrosome. The GFP::TAC-1 ratio of 'large' to 'small' centrosome was 1.32-1.41 (Figure 26b, 27 and 28). I also followed the segregation of 'large' and 'small' centrosomes and found that the 'small' centrosome always segregated into the anterior daughter (Figure 27a, 28 and 29a). Because TAC-1 dissociates from the centrosomes post-cytokinesis, I determined its 'time of dissociation' (TOD) in the daughters (mean time of GFP::TAC-1 dissociation). I found that the TOD was similar in anterior and posterior daughters (Figure 27b and 30).

Subsequently, I analyzed the divisions of ABprpppap and ABplpappa (referred to as divisions 4 and 5), both of which divide asymmetrically to give rise to a larger anterior daughter that is programmed to survive and a smaller posterior daughter that is programmed to die (Figure 26a, b). For both divisions I found that the centrosomes were less asymmetric with respect to the amount of associated TAC-1 (ratios of 1.14 and 0.89, respectively) (Figure 26b, 27 and 28). In the case of division 4, I further found that the 'large' centrosome always segregated into the larger, anterior daughter, which survives (Figure 29a). In the case of division 5, due to the lack of a statistically significant difference in the sizes of the two centrosomes, I was unable to determine the segregation pattern (Figure 27, 28 and 29a). Finally, I found that the TOD of TAC-1 in the smaller posterior daughter, which is programmed to die, was delayed compared to the TOD of TAC-1 in the larger anterior daughter, which is programmed to survive (Figure 29b and 30).
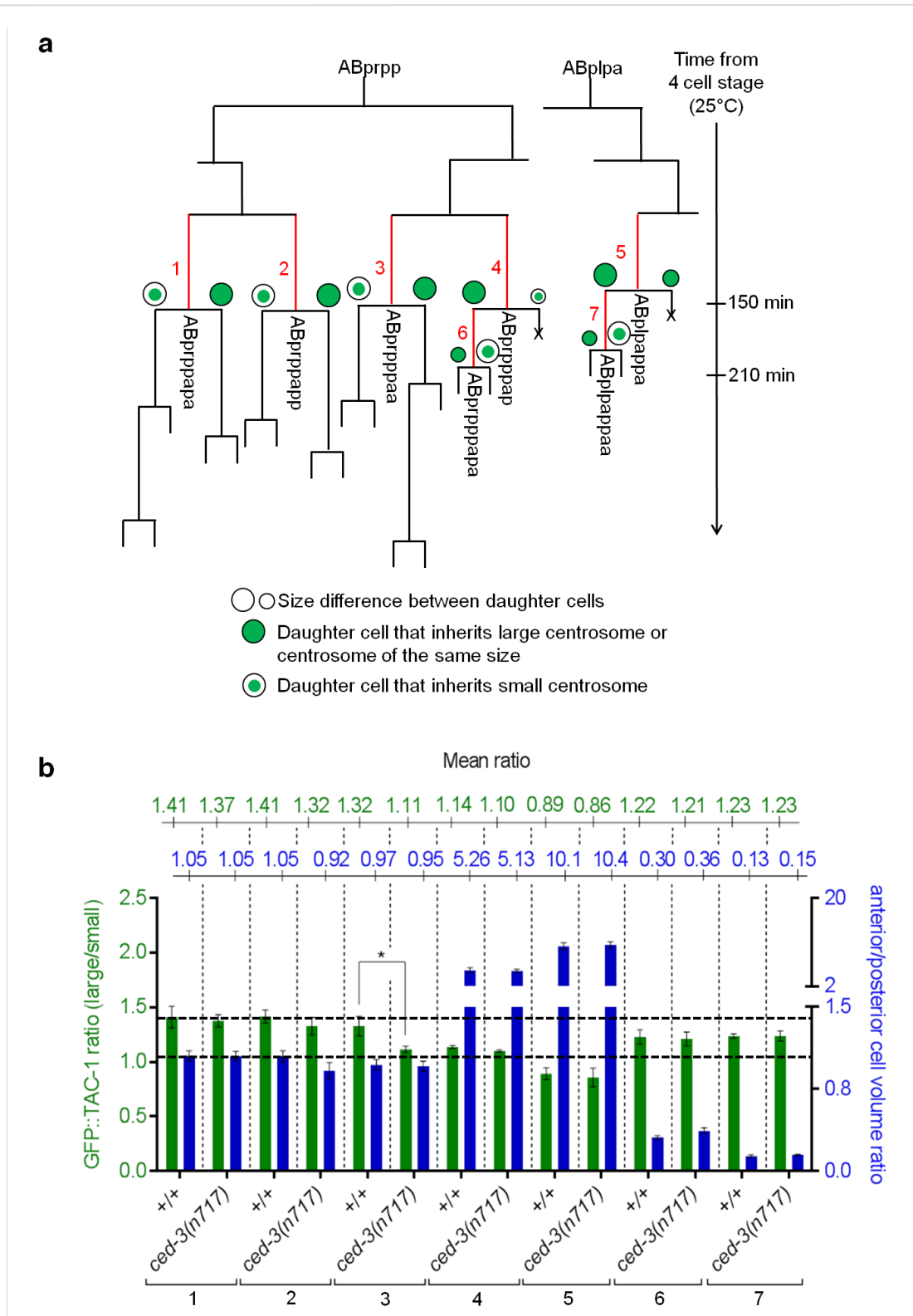
Figure 26. Centrosomal asymmetries in early *C. elegans* embryonic divisions.
a. Cell lineage of ABprppapa (1), ABprppapp (2), ABprpppaa (3), ABprpppap (4), ABplpappa (5), ABprpppapa (6) and ABplpappaa (7). Cellular asymmetries in terms of cell size,

centrosome size in terms of the amount of associated TAC-1 and centrosome segregation in the daughter cells are depicted schematically. **b.** Ratios of GFP::TAC-1 (green) of 'large' centrosome to 'small' centrosome of individual ABprppapa (1), ABprppapp (2), ABprpppaa (3), ABprpppap (4), ABplpappa (5), ABprpppapa (6) and ABplpappaa (7) cells in wild type (+/+) and *ced-3(n717)* animals expressing P*pie-1gfp::tac-1* (*bcIs104*) and P*pie-1mCherry::plcδph* (*ltIs44*) at metaphase (n=7-8). The mean ratio is given (top; green). Also shown are anterior to posterior daughter cell volume ratios (blue) from the respective divisions (n=7-8). The mean ratio is given (top; blue). For comparison, the dotted line indicates mean ratios of wild-type. The mean GFP::TAC-1 ratio was analyzed using the Student's t-test (*p≤0.05). Error bars denote the standard error of the mean.
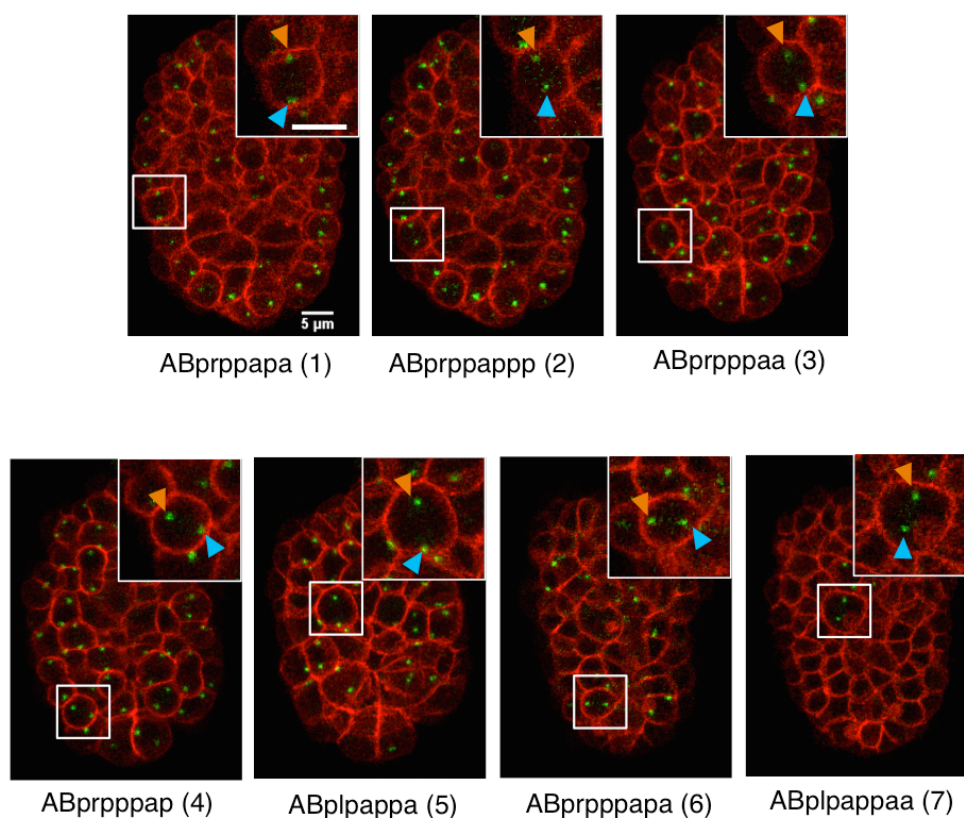
Figure 27. GFP::TAC-1 in early *C. elegans* embryonic divisions.
Maximum intensity projections of confocal images of representative wild-type embryos expressing P*pie-1gfp::tac-1* (*bcIs104*) and P*pie-1mCherry::plcδph* (*ltIs44*) during the 9th (divisions 1-5) or 10th (divisions 6 and 7) rounds of division. Dividing cells are shown at metaphase and are labeled 1-7. Insets represent enlarged maximum intensity projections of the respective cells (scale bar = 5 μm). Orange arrowheads indicate the centrosomes positioned anteriorly and blue arrowheads point to the centrosomes positioned posteriorly.
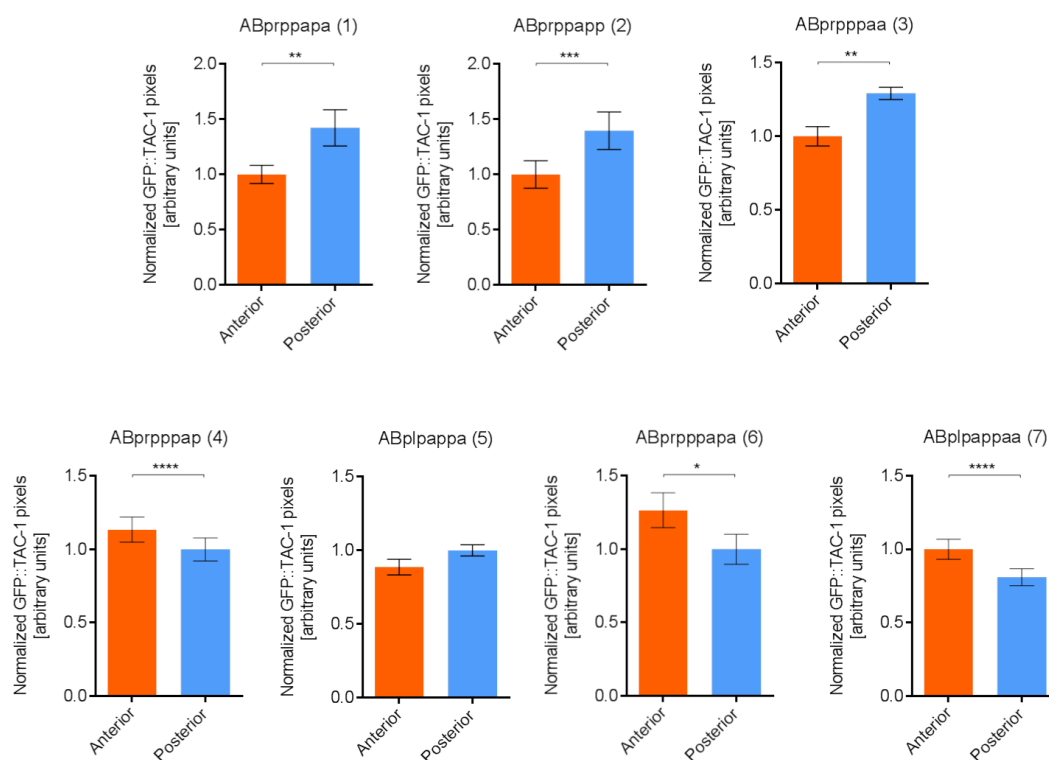
Figure 28. Centrosomal asymmetries in divisions around the first wave of cell death.
Normalized GFP::TAC-1 pixels [arbitrary units] in divisions 1-7 (n=7-8). Orange bars indicate centrosomes positioned anteriorly during metaphase and blue bars indicate centrosomes positioned posteriorly during metaphase. The normalized means were analyzed using the Student's t-test (*p≤0.05, **p≤0.01, ***p≤0.001 and ****p≤0.0001).

a

Division	Inheritance of centrosomes (GFP::TAC-1)					
	+/+		n	ced-3(n717)		n
	Anterior cell	Posterior cell		Anterior cell	Posterior cell	
1	S	L	8	L (5/8) S (3/8)	S (5/8) L (3/8)	8
2	S	L	8	L (4/8) S (4/8)	S (4/8) L (4/8)	8
3	S	L	8	L (3/8) S (5/8)	S (3/8) L (5/8)	8
4	L	S	8	S (2/8) L (6/8)	L (2/8) S (6/8)	8
5	nd	nd	8	nd	nd	8
6	L	S	7	S (4/8) S (4/8)	L (4/8) S (4/8)	8
7	L	S	7	S (3/8) L (5/8)	L (3/8) S (5/8)	8

S=small centrosome
L=large centrosome

b
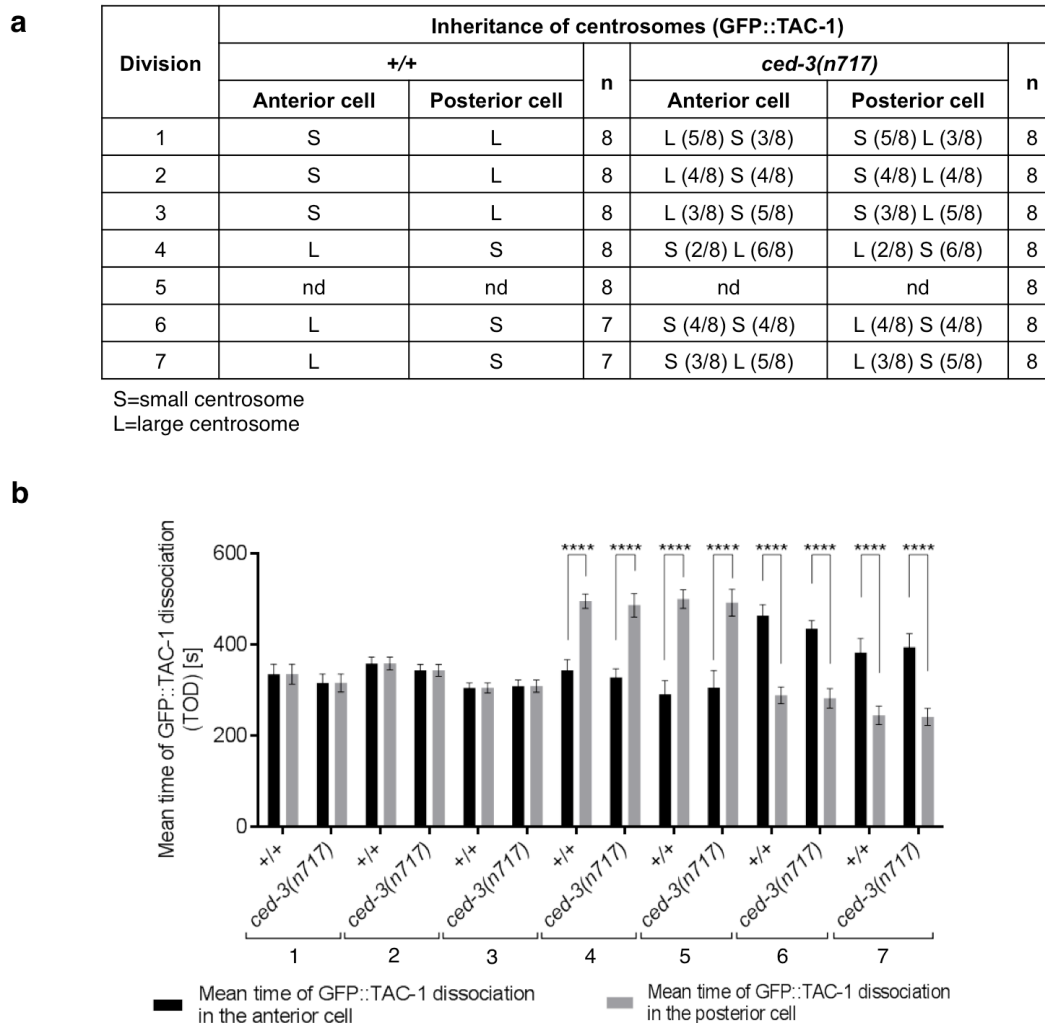
Figure 29. Centrosomal asymmetries post-cytokinesis in early *C. elegans* embryonic divisions.
a. Inheritance pattern of 'small' (S) and 'large' (L) centrosomes (GFP::TAC-1) in wild type (+/+) and *ced-3(n717)* backgrounds. n, number of respective divisions analyzed (nd=not determined). **b.** Mean time of GFP::TAC-1 dissociation (TOD) [s] post-cytokinesis of ABprppapa (1), ABprppapp (2), ABprpppaa (3), ABprpppap (4), ABplpappa (5), ABprpppapa (6) and ABplpappaa (7) in wild type (+/+) and *ced-3(n717)* animals expressing P$_{pie-1}$*gfp::tac-1* (*bcIs104*) and P$_{pie-1}$*mCherry::plcδph* (*ltIs44*) (n=7-8). The mean times of dissociation were analyzed using the Student's t-test (****p≤0.0001). Error bars denote the standard error of the mean.
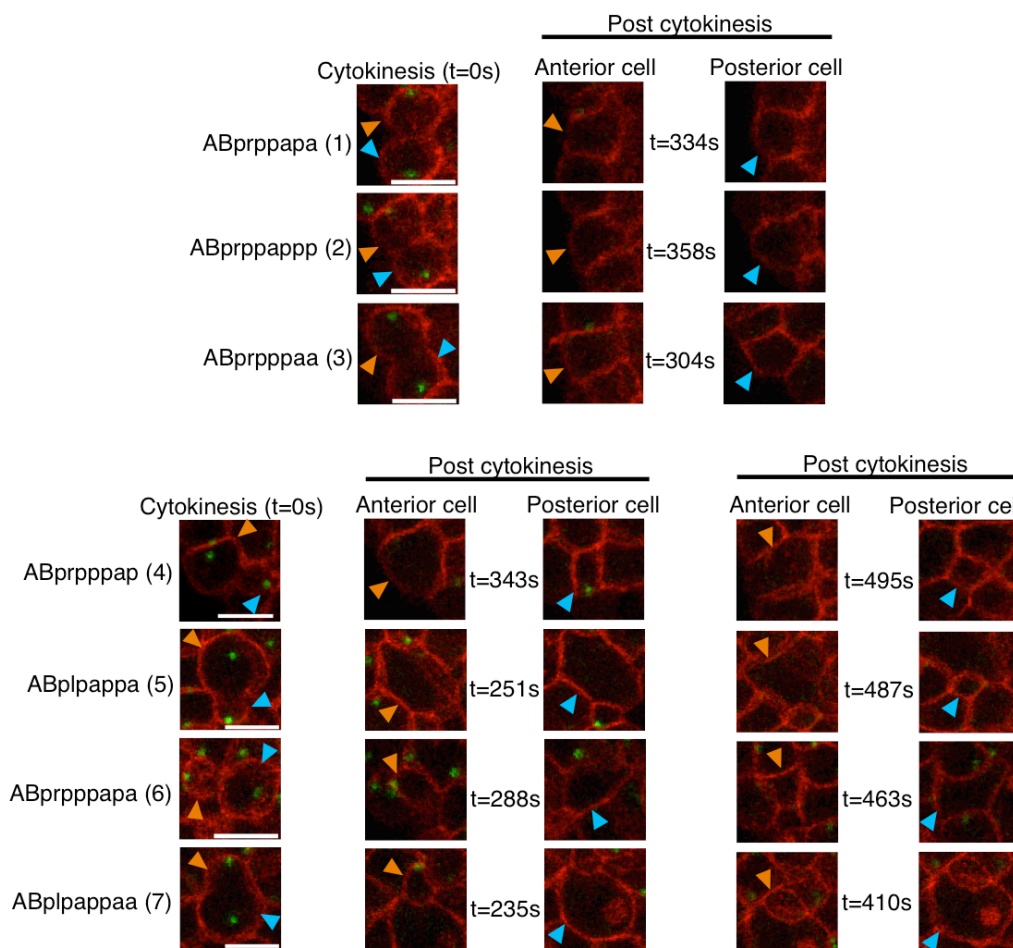
Figure 30. Time of dissociation of GFP::TAC-1 in early *C. elegans* embryonic divisions.
Maximum intensity projections of confocal images of representative wild-type embryos expressing P*pie-1gfp::tac-1* (*bcIs104*) and P*pie-1mCherry::plcδph* (*ltIs44*) during the 9th (divisions 1-5) or 10th (divisions 6 and 7) round of division (scale bars = 5 μm). Divisions are shown at cytokinesis (t=0) and at one time point after post cytokinesis. Orange arrowheads points to the anterior daughters and blue arrowheads point to the posterior daughters. The mean time of GFP::TAC-1 dissociation (TOD) [s] is indicated for each of the daughters.

The larger anterior daughters that are generated by divisions 4 and 5 divide asymmetrically ~50 min after being generated and each gives rise to a smaller anterior daughter and a larger posterior daughter, both of which are programmed to survive (ABprpppapa – division 6; ABplpappaa – division 7) (Figure 26a, b). For both divisions I found that the centrosomes were asymmetric with respect to the amount of associated GFP::TAC-1 (ratios of 1.22 and 1.23, respectively) (Figure 26b, 27 and 28), that the 'large' centrosome always segregated into the smaller, anterior daughter (Figure 29a), and that the TOD of TAC-1 in the smaller anterior daughter was delayed (Figure 29b and 30).

Based on these observations, I can draw the following conclusions about centrosome asymmetry and segregation during the 9th and 10th rounds of cell division:

1. Independent of whether a division is symmetric or asymmetric in terms of the sizes of the daughter cells, centrosomes can be asymmetric with respect to the amount of associated TAC-1.

2. 'Large' and 'small' centrosomes are segregated in a non-random pattern. However, this pattern is different for different divisions, i.e., 'small' centrosomes can be segregated into the smaller or larger daughter or into the anterior or posterior daughter.

3. In the case of divisions that are asymmetric with respect to the sizes of the daughters, there is a non-random asymmetry in the TOD of GFP::TAC-1. This non-random asymmetry is independent of the size of the centrosome in terms of the amount of associated TAC-1, and the position (anterior, posterior) or fate of the daughters, but it does appear to be

dependent on daughter cell size. Specifically, in all four divisions of this kind analyzed (divisions 4-7), the TOD of TAC-1 was always delayed in the smaller daughter.

2.2. Centrosomes are asymmetric in size with respect to different PCM proteins in *C. elegans* embryonic lineages

In order to determine whether components of the PCM other than TAC-1 are also asymmetric in terms of the amounts associated with each of the centrosomes at metaphase, I further analyzed TBG-1 and SPD-5 using the transgenes TBG-1::GFP and GFP::SPD-5 in different embryonic lineages of *C. elegans* (Strome et al., 2001; Hamill et al., 2002; van der Voet et al., 2009; Cabral et al., 2013).

Interestingly in the early lineages ABprppapa (1), ABprppapp (2), ABprpppaa (3), ABprpppap (4), ABplpappa (5), ABprpppapa (6) and ABplpappaa (7), TBG-1::GFP exhibited similar levels of asymmetry during cell divisions (ratios of 1.37, 1.43, 1.16, 1.20, 1.16, 1.27 and 1.16, respectively) (Figure 31). This observation suggests that centrosome asymmetry with respect to the associated PCM is not limited to varying amounts of one protein. Unlike TAC-1, TBG-1 persists at the centrosomes post cytokinesis. Hence I could not determine the TOD of TBG-1::GFP.
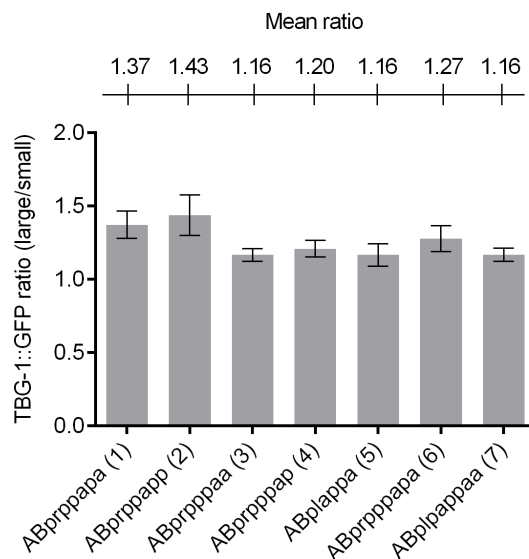
Figure 31. Centrosomes in early *C. elegans* lineages are also asymmetric with respect to PCM associated TBG-1.
Ratios of TBG-1::GFP of 'large' centrosome to 'small' centrosome of individual ABprppapa (1), ABprppapp (2), ABprpppaa (3), ABprpppap (4), ABplpappa (5), ABprpppapa (6) and ABplpappaa (7) cells in wild type (+/+) animals expressing P*pie-1tbg-1::gfp* (*ddIs6*) and P*pie-1mCherry::plcδph* (*ltIs44*) at metaphase (n=8). The mean ratio is given (top). Error bars denote the standard error of the mean.

Next, I extended my study to the NSM lineage. Concomitant with my previous observation in the NSMnb at metaphase, the 'large' centrosome in terms of PCM associated GFP::TAC-1 was positioned ventrally and 1.3 times larger than the 'small' centrosome which was positioned dorsally (Figure 32a, b; +/+). Furthermore, I found that the 'large' centrosome consistently segregated into the larger daughter, the NSM and the 'small' centrosome in the smaller daughter, the NSMsc (Figure 33a, b; +/+). Interestingly, the TOD of TAC-1 was delayed in the NSMsc compared to the NSM (407 s vs. 269 s) (Figure 33b, c; +/+). In order to assess whether these observations were limited to TAC-1, I further analyzed the amounts of PCM associated SPD-5 and TBG-1. Using the GFP::SPD-5 fusion protein, I found that at

metaphase the centrosomes were asymmetric with respect to the amount of associated SPD-5 (ratio of 1.32) (Figure 34a-c). However, depending on the division, the centrosome located either dorsal or ventral had more PCM associated SPD-5. Furthermore, I found that there was a random segregation of 'large' and 'small' centrosomes into the daughters. Since SPD-5 also dissociates from the centrosomes post-cytokinesis, I determined the TOD of GFP::SPD-5 in the NSM and the NSMsc. Like GFP::TAC-1, the TOD of GFP::SPD-5 was also delayed in the NSMsc compared to the NSM (375 s vs. 255 s) (Figure 35a-c). The TOD of GFP::SPD-5 was independent of the amount of PCM associated SPD-5 inherited by the daughter cells.

Using the TBG-1::GFP fusion protein, I found that at metaphase, the centrosomes were asymmetric in terms of the amount of PCM associated TBG-1 (ratio of 1.3) (Figure 34d, e). Specifically, I found that the centrosome located ventrally had more TBG-1 associated than the centrosome located dorsally. Furthermore, I found that the 'large' centrosome was always inherited by the NSM, whereas the 'small' centrosome by the NSMsc (Figure 35d).

Based on these results I conclude that centrosome asymmetry and non-random segregation of PCM associated TAC-1 and TBG-1 can also be observed during the last round of division during *C. elegans* embryogenesis (i.e. 11th round of division). Since the amounts of PCM associated SPD-5 at each centrosome varies across divisions, I can propose that the amounts of different proteins associated with the PCM are independent of each other. Whether this phenomenon holds any functional significance remains to be elucidated. For the remainder of my study, I used GFP::TAC-1 to analyze centrosome asymmetry and segregation.
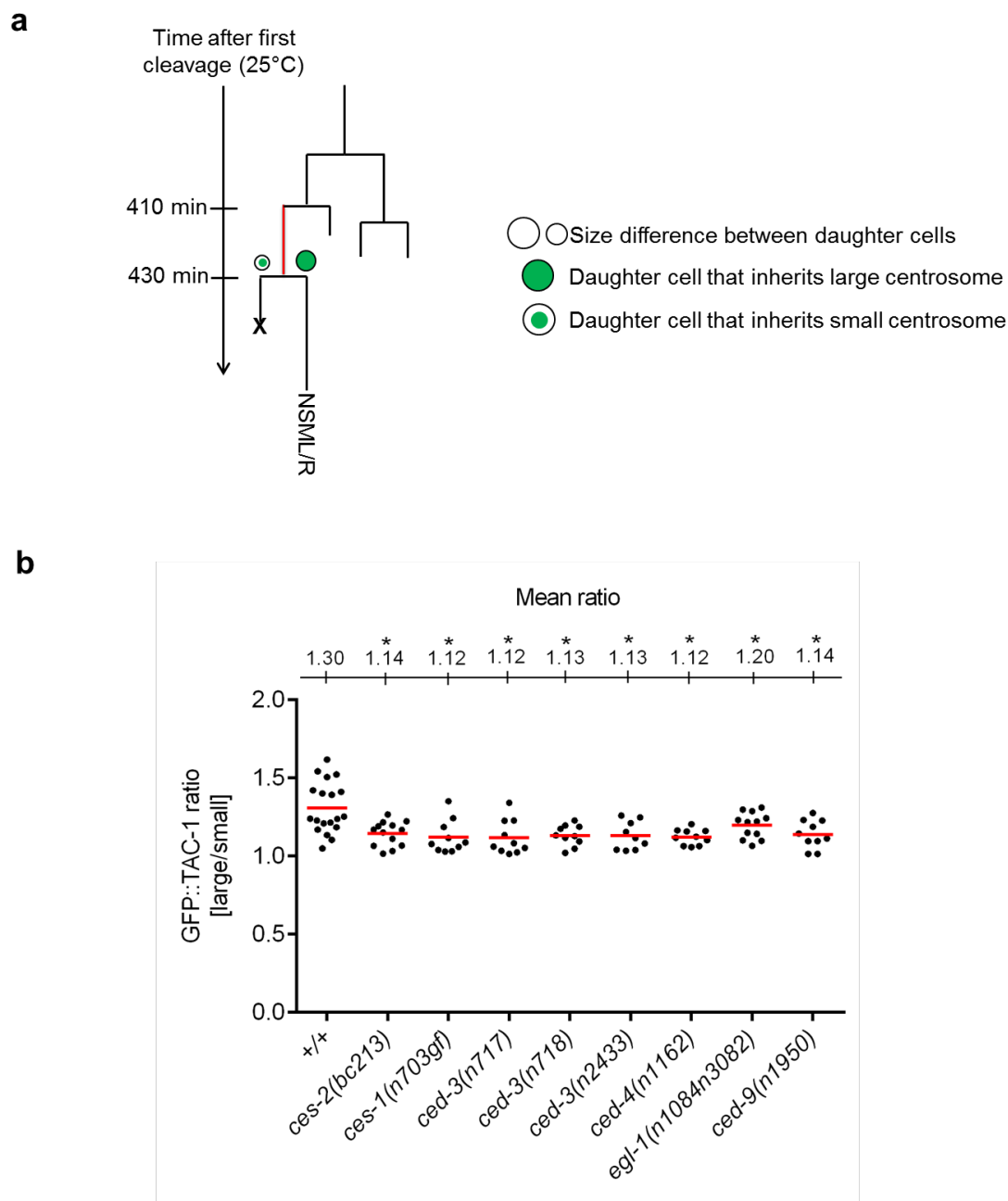
Figure 32. Centrosome asymmetry in the NSM neuroblast.
a. NSM lineage at 25°C depicting cellular asymmetries in terms of cell size, centrosome size and centrosome segregation in the daughter cells. **b.** Ratios of GFP::TAC-1 of 'large' centrosome to 'small' centrosome of individual NSMnb cells at metaphase in various genetic backgrounds [+/+, *ceh-20(ay9)*, *ceh-30(n3714)*, *ces-1(n703*gf*)*, *ces-2(bc213)*, *ced-3(n717)*, *ced-3(n718)*), *ced-3(n2433)* and *ced-4(n1162)*] (n=8-19). The mean ratio is given (top). Mean

ratios were analyzed using the Student's t-test (**p≤0.01, ***p≤0.001 and ****p≤0.0001). All statistical analyses were done in comparisons to the NSMnb in wild type (+/+).

a

| Genotype | Inheritance of centrosomes | | | | n |
| | NSM | | NSMsc | | |
	Large	Small	Large	Small	
+/+	19	0	0	19	19
ces-2(bc213)	8	5	5	8	13
ces-1(n703gf)	3	7	7	3	10
ced-3(n717)	5	5	5	5	10
ced-3(n718)	5	5	5	5	10
ced-3(n2433)	9	0	0	9	9
ced-4(n1162)	7	3	3	7	10
egl-1(n1084n3082)	5	7	7	5	12
ced-9(n1950)	6	4	4	6	10

b

c
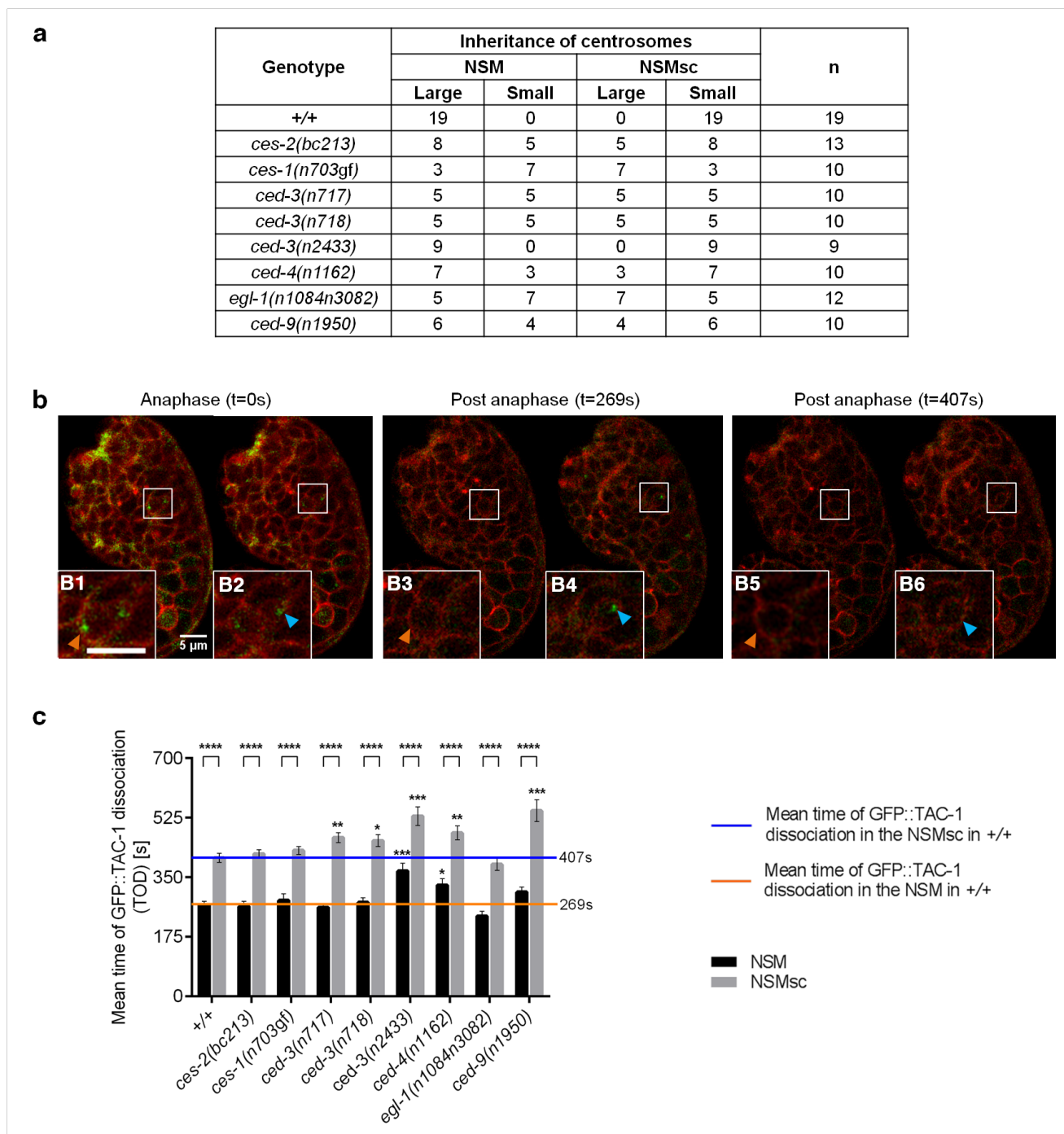
Figure 33. Centrosome segregation and dynamics in the NSM lineage.
a. Inheritance pattern of 'small' and 'large' centrosomes (GFP::TAC-1) in various genetic backgrounds. n, number of NSMnb divisions analyzed. **b.** Maximum intensity projections **(b1, b2)** and single focal planes **(b3-b6)** of confocal images of representative wild-type embryo

expressing P*pie-1gfp::tac-1* (*bcIs104*) and P*pie-1mCherry::plcδph* (*ltIs44*) at ~410 min post fertilization. Insets represent enlarged projections (scale bar = 5 μm) of NSMnb or NSMnb daughter cells at anaphase (t=0s) **(b1-B2)** and 269s **(b3-b4)** or 407s **(b5-b6)** post anaphase. Blue arrowheads point to the centrosomes inherited by the NSMsc and orange arrowheads point to the centrosomes inherited by the NSM. At anaphase, the centrosomes start moving away from their metaphase position. This time point was defined as t=0 s to determine the time it takes GFP::TAC-1 to dissociate from the centrosomes in the NSMsc and the NSM. **b1 and b2.** GFP::TAC-1 starts to dissociate from the centrosome inherited by the NSM soon after the completion of cytokinesis. **b3 and b4.** At t=269s post-anaphase, GFP::TAC-1 has completely dissociated from the centrosome inherited by the NSM; however, GFP::TAC-1 still persists on the centrosome inherited by the NSMsc. **b5 and b6.** At t=407s post-anaphase, GFP::TAC-1 has completely dissociated from the centrosome inherited by the NSMsc. **c.** Mean time of GFP::TAC-1 dissociation (TOD) [s] from centrosomes in NSM (black bars) and NSMsc (grey bars) (starting at anaphase [t=0s]) in various genetic backgrounds [+/+, *ces-1(n703*gf*)*, *ces-2(bc213)*, *ced-3(n717)*, *ced-3(n718))*, *ced-3(n2433)*, *ced-4(n1162)*, *egl-1(n1084n3082)* and *ced-9(n1950)*] (n=8-13). Also indicated are the mean time of GFP::TAC-1 dissociation from the centrosomes in the NSM (blue line) and NSMsc (orange line) in wild type (+/+). Error bars denote the standard error of the mean. The mean times of dissociation were analyzed using the Student's t-test (*$p \leq 0.05$, **$p \leq 0.01$, ***$p \leq 0.001$ and ****$p \leq 0.0001$). The statistical analyses were done in comparisons to wild type (+/+) or between NSM and NSMsc for a given genotype.
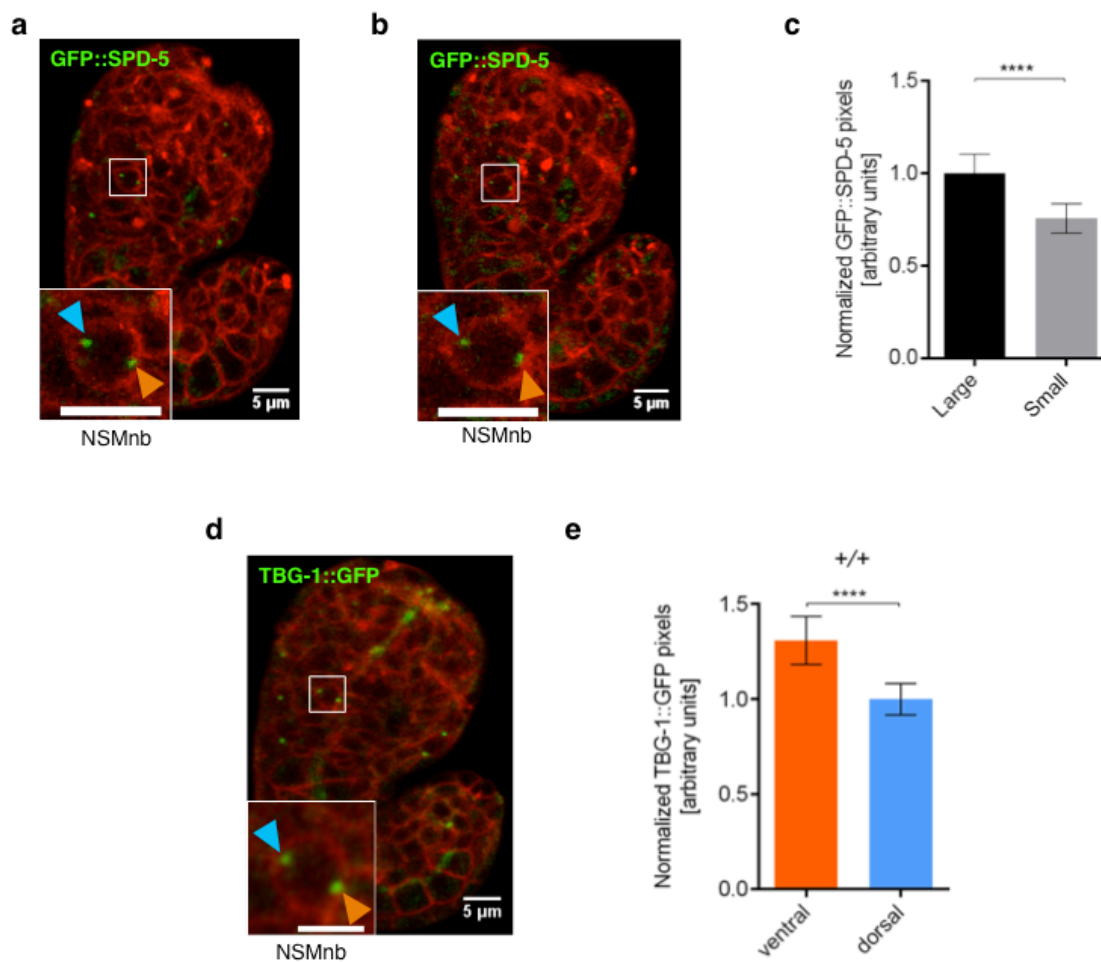
Figure 34. SPD-5 and TBG-1 asymmetry in the NSM lineage.
Maximum intensity projections of confocal images of two representative wild-type embryo ~410 min post fertilization expressing $P_{spd-5}gfp::spd-5$ (*vieSi15*) **(a and b)**, $P_{pie-1}tbg-1::gfp$ (*ddIs6*) **(d)** and $P_{pie-1}mCherry::plcδph$ (*ltIs44*). **(a)** represents an embryo where the centrosome located dorsally in the NSMnb was larger than the centrosome located ventrally and **(b)** represents an embryo where the centrosome located ventrally in the NSMnb was larger than the centrosome located dorsally. Inset represents enlarged projection of NSMnb (scale bar = 5µm) at metaphase at which stage GFP::SPD-5 and TBG-1::GFP was quantified in the NSMnb. Blue arrowhead points to the centrosome located dorsally and orange arrowhead points to the centrosome located ventrally. **c.** Normalized GFP::SPD-5 pixels [arbitrary units] based on the GFP::SPD-5 pixels in the 'large' (black bar) and 'small' (grey bar) centrosomes. **d.** Normalized TBG-1::GFP pixels [arbitrary units] of centrosomes positioned ventral (orange bar) and centrosomes positioned dorsal (blue bar) in the NSMnb at metaphase (n=8, 10). Error

bars denote the standard error of the mean. The normalized means were analyzed using the Student's t-test (****p≤0.0001).

a

Genotype	Inheritance of centrosomes (GFP::SPD-5)				n
	NSM		NSMsc		
	Large	Small	Large	Small	
+/+	4	4	4	4	8

b

Anaphase (t=0s)	Post anaphase (t=255s)	Post anaphase (t=373s)

c

Mean time of GFP::SPD-5 dissociation in the NSMsc in +/+

Mean time of GFP::SPD-5 dissociation in the NSM in +/+

NSM

NSM sister cell

d

Genotype	Inheritance of centrosomes (TBG-1::GFP)				n
	NSM		NSMsc		
	Large	Small	Large	Small	
+/+	10	0	0	10	10

Figure 35. SPD-5 and TBG-1 dynamics in the NSM lineage

Inheritance pattern of 'small' and 'large' centrosomes [GFP::SPD-5 **(a)**] and [TBG-1::GFP **(d)**] in wild-type background (+/+). n, number of NSMnb divisions analyzed. **b.** Maximum intensity projections **(b1, b2)** and single focal planes **(b3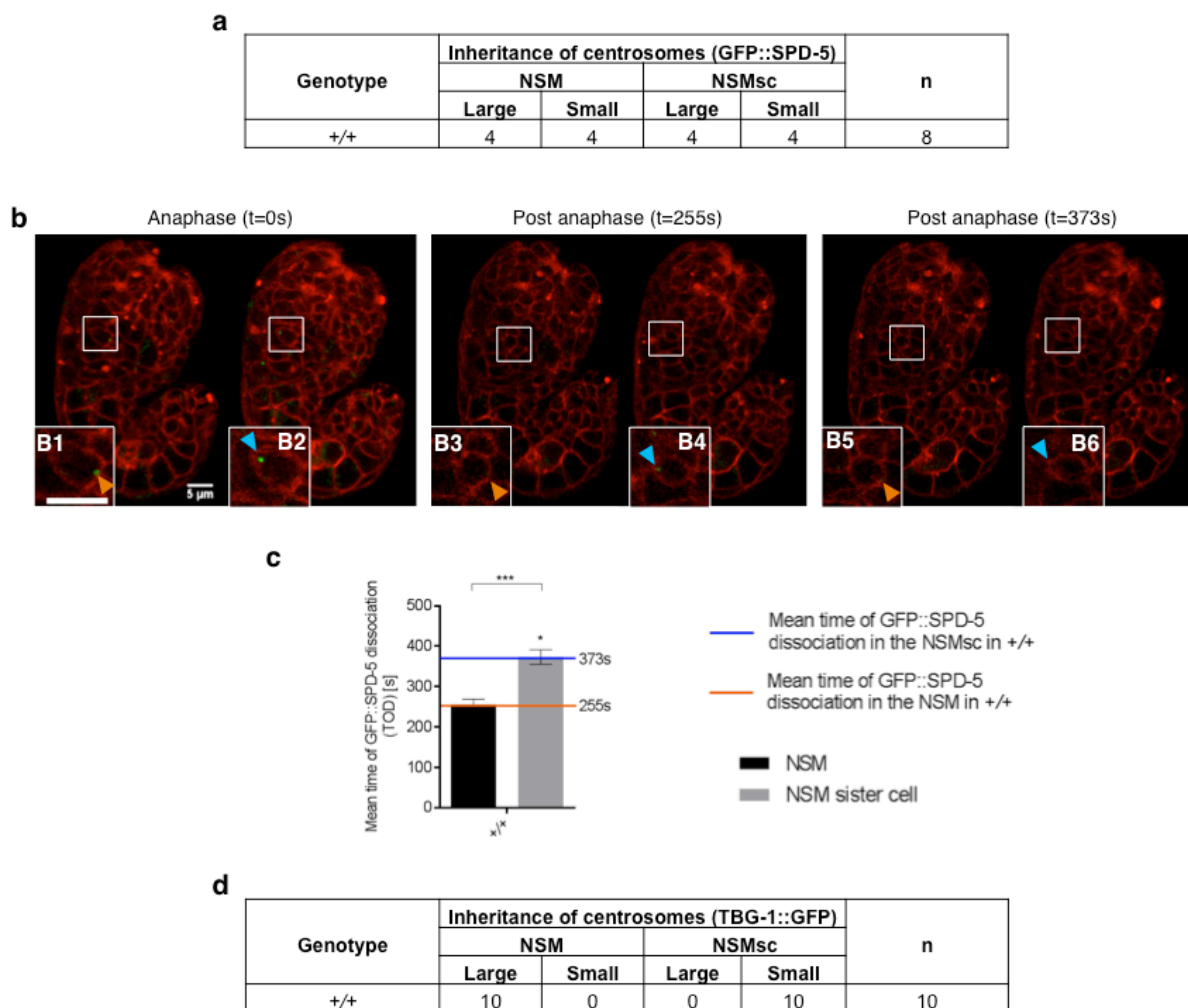-b6)** of confocal images of representative wild-type embryo at ~410 min post fertilization expressing P$_{spd-5}$*gfp::spd-5* (*vieSi15*) and P$_{pie-1}$*mCherry::plcδph* (*ltIs44*). Insets represent enlarged projections (scale bar = 5 μm) of NSMnb or NSMnb daughter cells at anaphase (t=0s) **(b1-B2)** and 255s **(b3-b4)** or 373s **(b5-b6)** post anaphase. Blue arrowheads point to the centrosomes inherited by the NSMsc and orange arrowheads point to the centrosomes inherited by the NSM. At anaphase,

the centrosomes start moving away from their metaphase position. This time point was defined as t=0 s to determine the time it takes GFP::SPD-5 to dissociate from the centrosomes in the NSMsc and the NSM. **b1 and b2.** GFP::SPD-5 starts to dissociate from the centrosome inherited by the NSM soon after the completion of cytokinesis. **b3 and b4.** At t=255s post-anaphase, GFP::SPD-5 has completely dissociated from the centrosome inherited by the NSM; however, GFP::SPD-5 still persists on the centrosome inherited by the NSMsc. **b5 and b6.** At t=373s post-anaphase, GFP::SPD-5 has completely dissociated from the centrosome inherited by the NSMsc. **c.** Mean time of GFP::SPD-5 dissociation (TOD) [s] from centrosomes in NSM (black bars) and NSMsc (grey bars) (starting at anaphase [t=0s]) (n=8). Also indicated are the mean time of GFP::SPD-5 dissociation from the centrosomes in the NSM (blue line) and NSMsc (orange line) in wild type (+/+). Error bars denote the standard error of the mean. The mean times of dissociation were analyzed using the Student's t-test ***p≤0.001).

2.3. Mutations in *ces-1* Snail and *ces-2* HLF affect centrosome asymmetry and segregation in the NSM lineage

As I previously described, the death of the NSMsc can specifically be blocked by either a gain-of-function (gf) mutation of the Snail-related gene *ces-1*, or loss-of-function mutations of the HLF-like gene *ces-2* (Ellis and Horvitz, 1991; Metzstein et al., 1996; Metzstein and Horvitz, 1999; Thellmann et al., 2003; Hatzold and Conradt, 2008). Each of these mutations presumably causes increased levels of CES-1 protein in the NSM lineage, which leads to the transcriptional repression of the pro-apoptotic BH3-only gene *egl-1* not only in the NSMnb but also in the NSM and NSMsc. As a consequence, this results in the inappropriate survival of the NSMsc (Thellmann et al., 2003; Hatzold and Conradt, 2008). Mutations in *ces-1* and *ces-2* also cause the NSMnb to divide symmetrically, giving rise to two daughters of similar sizes (Figure 12) (Hatzold and Conradt, 2008). Compared to wild type, the centrosomes in *ces-1(n703*gf*))* and *ces-2(bc213)* animals were more symmetric with a ratio

of 1.12 and 1.16, respectively (Figure 32b). Furthermore, I observed that 'small' and 'large' centrosomes were randomly segregated into the NSM and NSMsc (Figure 33a). For example, in *ces-2(bc213)* mutants, in 5 out of 13 cases, I observed that the comparatively smaller centrosome was inherited by the NSM while the comparatively 'large' centrosome was inherited by the NSMsc. Therefore, mutations of *ces-1* and *ces-2* not only affect cell cycle progression and cell polarity in the NSMnb and its ability to divide asymmetrically, but they also compromise centrosome size in terms of amounts of PCM proteins associated with the centrosomes and the segregation pattern in the NSM lineage (Thellmann et al., 2003; Hatzold and Conradt, 2008; Yan et al., 2013). Finally, I analyzed the TOD of TAC-1 from the centrosomes inherited by the NSM and the NSMsc in *ces-1(n703*gf*)* and *ces-2(bc213)* animals irrespective of their sizes. Compared to wild type, the TODs of TAC-1 in the NSM and the NSMsc were not significantly different (Figure 33c). Since, NSMsc survive in *ces-1(n703*gf*)* and *ces-2(bc213)* animals, I conclude that the relatively long TOD of TAC-1 within the NSMsc is independent of its apoptotic fate.

Neither *ceh-20(ay9)* nor *ceh-30(n3714)* had an effect on the centrosome size, segregation pattern and the TOD of TAC-1 in the NSM lineage (Figure 32b, 33a and c). Therefore, I propose that the phenotypes observed due to mutations in *ces-1* and *ces-2* are due to the specific effects of these lesions in the NSM lineage.

2.4. The novel role of *ced-3* caspase in centrosome asymmetry and segregation

The death of the NSMsc can also be blocked by loss-of-function mutations of *ced-3* caspase (such as *n717* and *n718*) (Ellis and Horvitz, 1986). Unlike in *ces-1(n703*gf*)* or *ces-*

2(bc213) animals, in *ced-3(n717)* and *ced-3(n718)* animals, the NSMnb division occurs asymmetrically along the dorsal-ventral axis as it does in wild type (Figure 12). I found that in *ced-3* mutant animals, the centrosomes were more symmetric at metaphase with a ratio of 1.12 (*ced-3(n717)*) and 1.13 (*ced-3(n718)*), respectively (Figure 32b). As previously shown, this reduction in size difference was predominantly caused by an increase in GFP::TAC-1 associated with the 'small' centrosomes (Figure 20). Furthermore, in *ced-3(n717)* and *ced-3(n718)* animals, the segregation of 'large' and 'small' centrosomes into the NSM and NSMsc was random (Figure 33a). I also observed a significant difference in the TOD of TAC-1 in *ced-3* animals. Although the TOD of TAC-1 in the NSM remained close to that of wild type (262 s or 276 s vs. 269 s, respectively), it was significantly delayed in the NSMsc (467 s or 458 s vs. 407 s, respectively) (Figure 33c). Therefore, in the NSMnb, the loss of *ced-3* function not only affects the size of the centrosome that is normally inherited by the NSMsc, but also the segregation pattern of 'small' and 'large' centrosome during NSMnb division. Furthermore, in the NSMsc, *ced-3* is not only required for NSMsc death, but it also contributes to the timing of dissociation of TAC-1 from the centrosome.

I also investigated whether the loss of *ced-3* affects centrosomal asymmetry and segregation pattern in divisions 1-7 during the 9th round of division. Using GFP::TAC-1, I found that in *ced-3*(*n717*) animals the centrosomes were more symmetric in division 3 (ratio of 1.11 compared to 1.32 in wild type) (Figure 25b). Furthermore, I found that the segregation pattern was randomized in all divisions (divisions 1-4, 6, 7) (Figure 29a). My observations suggest that during early embryonic cell divisions, *ced-3* may not influence centrosome asymmetry in terms of PCM associated TAC-1. However, the role of *ced-3* in centrosome

segregation is not restricted to the NSMnb division, i.e. it is not restricted to divisions that generate a cell that is fated to die. The TOD of TAC-1 in divisions 1-7 however, was not affected in *ced-3(n717)* animals (Figure 29b). The data obtained for centrosome asymmetry in *ced-3* mutants and the absence of an effect on the TOD of TAC-1 in the early embryonic cell divisions of these mutants indicate that the asymmetric segregation of *ced-3* activity as previously described in Part I of this thesis, may not be a universal process in *C. elegans* but, it is more likely to be a lineage specific mechanism.

2.5. The role of CED-3 protease activity in centrosome asymmetry and segregation in the NSM lineage

To determine whether the function of *ced-3* caspase in centrosome asymmetry and segregation in the NSM lineage is dependent on the protease activity of the CED-3 protein, I analyzed animals homozygous for *ced-3(n2433)*, which affects the active site of CED-3 and hence, its protease activity (Xue et al., 1996; Shaham et al., 1999). In addition, I analyzed animals homozygous for a loss-of-function mutation of *ced-4(n1162)* which prevents apoptosome formation and hence, the maturation of proCED-3 and the full induction of CED-3 protease activity (Ellis and Horvitz, 1986). Using GFP::TAC-1, I found that the centrosomes in the NSMnb were more symmetric in both these mutants, suggesting that the protease activity of CED-3 is necessary to generate centrosomal asymmetry in the NSMnb (Figure 32b). Furthermore, I found that *ced-4(n1162),* but not *ced-3(n2433),* randomized the segregation pattern of the centrosomes during NSMnb division (Figure 33a). This finding suggests that the protease activity of CED-3 is not necessary for the segregation pattern of the

centrosomes during NSMnb division. Moreover, since the presence of both CED-4 and CED-3 protein is necessary, the segregation pattern may depend on the CED-4-CED-3 complex *per se* rather than the caspase activity. Finally, I found that in *ced-3(n2433)* and *ced-4(n1162)* animals the TOD of TAC-1 was delayed in both the NSM and the NSMsc (Figure 33c). Since, both *ced-3(n2433)* and *ced-4(n1162)* presumably lead to a relative increase in the level of catalytically inactive CED-3 protein, catalytically inactive CED-3 can delay TAC-1 dissociation in the NSM. Therefore, I speculate that in the NSMsc, the protease activity of CED-3 is required to contribute to TAC-1 dissociation.

2.6. EGL-1 and CED-9 also have non-apoptotic roles in centrosome asymmetry and segregation in the NSM lineage

Since, loss of *ced-4* and *ced-3* function disrupted centrosome asymmetry, segregation and the TOD of TAC-1 in the NSM lineage, I further determined whether EGL-1 and CED-9 also play a role in establishing this cellular asymmetry in the NSM lineage. I found that in *egl-1* loss-of-function and *ced-9* gain-of-function animals, the centrosomal asymmetry with respect to PCM associated TAC-1 in the NSMnb was significantly disrupted with a ratio of 1.20 (*egl-1(1084n3082)*) and 1.14 (*ced-9(n1950)*), respectively (Figure 32b). Further, the segregation of 'large' and 'small' centrosomes was also randomized during NSMnb division in these animals (Figure 33a). Interestingly, the TOD of TAC-1 was significantly delayed only in the NSMsc of *ced-9(n1950)* animals compared to their wild-type counterparts (545s s vs. 269 s, respectively), while the TOD in the NSM remained unaffected (Figure 33c). This observation suggests that the dissociation of TAC-1 from the centrosome inherited by the

NSMsc is in part mediated by CED-9 but, independent of *egl-1* activity. Further, both EGL-1 and CED-9 perform their non-apoptotic functions in establishing asymmetric centrosomes with respect to different amounts of PCM associated TAC-1 in the NSMnb and the proper segregation of these entities into the NSMnb daughters.

DISCUSSION

1. Engulfment pathways promote apoptosis by enhancing the asymmetric segregation of apoptotic factors

Taking together all the observations I made for *ced-3* activity, CED-1 enrichment, gradient of CED-3 caspase activity and level of CED-3 caspase in the NSM lineage, I can now speculate about the mechanism by which the timely death of NSMsc is modulated in the nematode *C. elegans* (Figure 36).
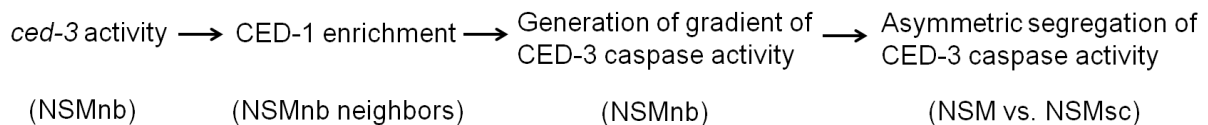
Figure 36. A flowchart of the mechanism underlying the asymmetric segregation of apoptotic potential in the NSM lineage.
A sequential model of how *ced-3* activity and CED-1 enrichment function in the generation of the gradient of CED-3 caspase activity, ultimately contributing to the asymmetric segregation of CED-3 caspase activity to the NSMsc

1. In strong loss-of-function mutants of *ced-3*, absence of any *ced-3* activity disrupts asymmetric CED-1 enrichment around the NSMnb. Further, the absence of CED-3 caspase results in 100% NSMsc survival (Figure 9).

2. In animals that harbor a weak *ced-3* mutation *n2427*, functioning of CED-3 caspase is compromised. This hindrance in CED-3 protein function may not be sufficient to cause a disruption in asymmetric CED-1 enrichment on the plasma membrane regions of the neighboring cells apposing the dorsal side of NSMnb. Hence the asymmetric segregation of CED-3 caspase activity still occurs (Figure 36). On the other hand, even though a subtle

disruption of this gradient of CED-3 caspase activity in *ced-3(n2427)* animals may occur, GFP::TAC-1 might not be a sufficiently sensitive tool to detect this subtle change. However, since the mutation *n2427* hampers CED-3 caspase activity, it leads to ~13% NSMsc survival (Figure 9).

3. *ced-3* activity is retained in *ced-1* loss-of-function mutant but, the absence of CED-1 enrichment disrupts the gradient of CED-3 caspase activity in the NSMnb (Figure 36). This results in sub-optimal segregation of CED-3 caspase activity into the NSMsc. Although the NSMsc in these animals undergo apoptosis, the level of CED-3 caspase in these cells is reduced compared to their wild-type counterparts (Figure 9, 11f, g and h). This decrease in level of CED-3 caspase can be attributed to the disruption of the gradient of CED-3 caspase activity in the NSMnb.

4. In *ced-1(e1735); ced-3(n2427)* animals, asymmetric CED-1 enrichment around the NSMnb is abolished (Figure 36). Since *ced-1* is required for the generation of the gradient of CED-3 caspase activity, in *ced-1(e1735); ced-3(n2427)* animals, this gradient is also disrupted. Therefore, the proper segregation of CED-3 caspase activity is hampered. Thus, post NSMnb cytokinesis, the impairment in CED-3 protein function together with the improper segregation of CED-3 caspase activity results in delayed programmed cell death and more than 50% NSMsc survival (Figure 9).

Hence, my findings have revealed that it is not the process of engulfment *per se* that promotes NSMsc apoptosis. In fact, it is a novel signaling mechanism mediated in a non-cell autonomous manner by the two engulfment pathways that promotes the programmed cell

death of the NSMsc. I have demonstrated that this mechanism is essential for the polarization of the NSMnb and hence results in the unequal segregation of the apoptotic potential to the daughters. Apoptotic potential denotes the factors that have pro-apoptotic functions. This can consist of *ced-3* mRNA or active CED-3 itself or a population of both. I have specifically shown that CED-3 caspase activity is already present in the NSMnb before division. Further, a gradient of CED-3 caspase activity exists in this cell. The establishment of this gradient is dependent on the components of the central cell death pathway and the cell corpse engulfment pathways (Figure 21). *ced-3* activity in the NSMnb is further required for CED-1 enrichment on the plasma membranes of the neighboring cells apposing the dorsal side of the NSMnb. Since the NSMnb does not undergo apoptosis, this enrichment is independent of *ced-8* function and PS exposure, as also suggested by the observation that CED-1 enrichment is unaffected in *ced-8* mutants (Figure 18). Hence, other molecules exposed on the NSMnb surface may be required to activate CED-1. Specifically, I propose that a higher number of such molecules are exposed on the dorsal compared to the ventral side of the NSMnb (Figure 37, 38). This is further supported by the observation that CED-1 enrichment and activation occurs preferentially in dorsal rather ventral neighbors since higher expression of *ced-1* is present in the dorsal NSMnb neighbors compared to the ventral neighbors (Figure 16). Discovering the identity of these novel CED-1 interactors and the mechanisms via which an asymmetric exposure of these proteins may occur on the surface of the NSMnb are avenues for future investigation.

My current model is consistent with the previous findings wherein it has been shown that the engulfment pathways act cell non-autonomously to promote apoptosis (Reddien et al.,

2001). Upon activation of the engulfment pathways in the dorsal NSMnb neighbors, a signaling event mediated by these pathways results in the generation of a dorsal-ventral gradient of apoptotic potential in the NSMnb. It will be of key importance to determine the components in the NSMnb neighbors that act downstream of the engulfment pathways and promote the generation of the gradient of CED-3 caspase activity in the NSMnb (Figure 37). Further, it remains to be elucidated how CED-1 signaling feeds into the NSMnb and how the gradient of CED-3 caspase activity is set up in the NSMnb. Once the NSMnb undergoes division, this gradient results in the asymmetric segregation of the apoptotic potential (Figure 38). For instance, higher CED-3 caspase activity may be segregated into the NSMsc. This notion is supported by my observation that the loss of *ced-3* affects GFP::TAC-1 dissociation specifically from the PCM of the centrosome inherited by the NSMsc (Figure 39). I also propose that gradients of factors other than the CED-3 caspase activity are set up in the NSMnb. Since centrosomes have been demonstrated to play a role in asymmetric segregation of cell fate determinants (Pelletier and Yamashita, 2012), it is likely that elements responsible for the increase in CED-3::GFP concentration in the NSMsc and/or decrease in the NSM may be oppositely polarized in the NSMnb with the help of centrosomes thus, leading to their proper segregation. Further, *ced-3* mRNA and/or regulators of *ced-3* mRNA translation such as miR-60 may as well be asymmetrically segregated by a similar process (Lau et al., 2001; Lee and Ambros, 2001).

It has previously been proposed that *ced-3* caspase is active only in cells that are programmed to die (Horvitz, 2003; Lettre and Hengartner, 2006; Conradt, 2009). My results demonstrate that not only *ced-3* caspase is active to a certain degree in the mother of a dying

cell, but that, CED-3 caspase plays a non-apoptotic role in predetermining the fate of the NSMsc. I have also found that *egl-1* BH3-only, *ced-4* Apaf-1 and *ced-9* Bcl-2 in addition have non-apoptotic funtions in the NSMnb (Figure 21). My observations further increase the list of non-apoptotic functions of EGL-1, CED-9, CED-4 and CED-3 () (Pinan-Lucarre et al., 2012; Weaver et al., 2014; Yee et al., 2014). Since, I observed CED-3 caspase in the NSMnb, it remains to be elucidated whether all of the CED-3 caspase that exists in the NSMnb is active CED-3 or whether it is a population of both pro- and active CED-3. Determining the levels and localizations of pro- and active CED-3 will help us determine the spatiotemporal non-apoptotic functions of these separate CED-3 caspase populations in the NSM lineage. Because the NSMnb does not undergo programmed cell death despite the presence of CED-3 caspase, it is likely that the factors which inhibit caspase activity are also present in the NSMnb. Inhibitors of apoptotic proteins (IAPs) in *D. melanogaster* and mammals have been implicated in controlling caspase activity and also the mechanisms that activate caspases (Deveraux and Reed, 1999). It remains to be investigated whether *C. elegans* homologs of these proteins, BIR-1 and BIR-2, play a similar role in regulation of NSMsc apoptosis (Speliotes et al., 2000). It is also plausible that other inhibitory factors apart from BIR-1 and BIR-2 perform a similar function in *C. elegans*. Upon NSMnb cytokinesis, these inhibitory factors may be preferentially segregated to the NSM which is programmed to survive. Absence of these inhibitory factors in the NSMsc may result in the generation of a higher CED-3 caspase activity thereby causing apoptosis. Concomitant with the previous observation that asymmetric segregation of the *egl-1* transcriptional repressor CES-1 leads to NSM survival and NSMsc apoptosis (Figure 6) (Hatzold and Conradt, 2008), my observations further strenghten the concept of asymmetric segregation of pro- and anti-apoptotic factors in

the NSM lineage. I have found that *egl-1* BH3-only, *ced-9* Bcl-2, *ced-4* Apaf-1 and *ced-3* caspase are active in the NSMnb yet, the cell does not undergo apoptosis. This suggests that the levels of EGL-1, CED-4 and CED-3 are tightly regulated in the NSMnb. Such a regulation is important to stop the protein levels crossing the threshold wherein they can induce cell death. MicroRNAs, known for regulation of mRNA translation, may have a key role in regulating EGL-1 and CED-3 levels in the NSM lineage (Lee et al., 1993; Wightman et al., 1993; Lagos-Quintana et al., 2001; Lau et al., 2001; Lee and Ambros, 2001; Ambros et al., 2003; Lim et al., 2003). Since, it has also been demonstraed that activation of *egl-1* transcription in the NSMsc is mediated by HLH-2/HLH-3 complex (Figure 6), it will be interesting to determine whether HLH-2/HLH-3 complex is asymmetrically segregated to the NSMsc. Insights into the asymmetric segregation of HLH-2/HLH-3 complex will help strenghten the observation that CES-1 antoagonizes HLH-2/HLH-3 function in the NSM lineage.

Asymmetric cell divisions are also inherent to stem cells (Roubinet and Cabernard, 2014). Stem cells divide asymmetrically to give rise to a self-renewing stem cell and a differentiating daughter cell. In a broader perspective, my findings raise the question whether the process of asymmetric segregation of apoptotic potential described in this study holds true in stem cell divisions of other organisms. It also remains to be determined whether the novel signaling function mediated by the engulfment pahtways is evolutionarily conserved. Macrophages are a type of white blood cells which perform phagocytic functions in mammals. Previous reports suggest that macrophage-mediated cell killing is an important aspect of mammalian development. For instance, inappropriate vascular endothelial cell survival can be

observed upon elimination of macrophages in rats and this process of cell killing may be dependent on the canonical WNT-pathway (Lobov et al., 2005; Rao et al., 2007). Further, microglia, which are the resident macrophages of the brain, also promote the killing of developing neurons (Marin-Teva et al., 2004). Detailed molecular mechanisms underlying these processes in mammals however remain to be elucidated. Hence, it will be of prime importance to determine whether mammalian homologs of the components of the two *C. elegans* engulfment pathways also perform the novel functions described in this study.
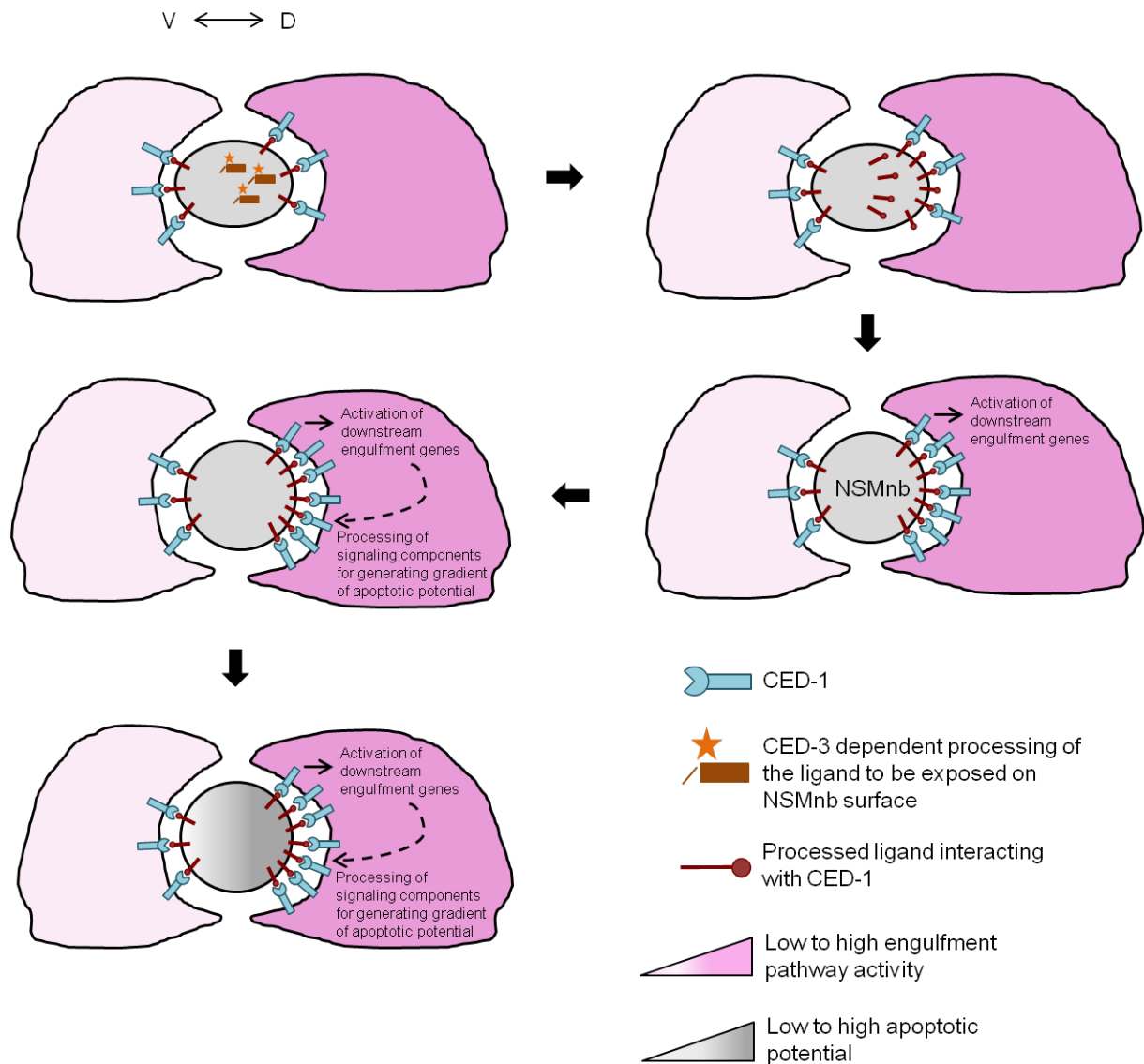
Figure 37. Asymmetric CED-1 enrichment is probably dependent on asymmetric exposure of CED-1 interacting ligands on the NSMnb.
Molecular model depicting the probable mechanism via which asymmetric clustering occurs on the plasma membranes of neighboring cells apposing the dorsal 'd' side of the NSMnb. The neighboring cells shown here do not represent the actual number of NSMnb neighbors. CED-3 dependent processing of these ligands might be necessary to allow them to be exposed on the NSMnb surface. Once exposed, they stimulate CED-1 enrichment which further activates the downstream components of the engulfment pathways. This results in activation of other genes which might play a role in the generation of the gradient of apoptotic potential in the NSMnb.
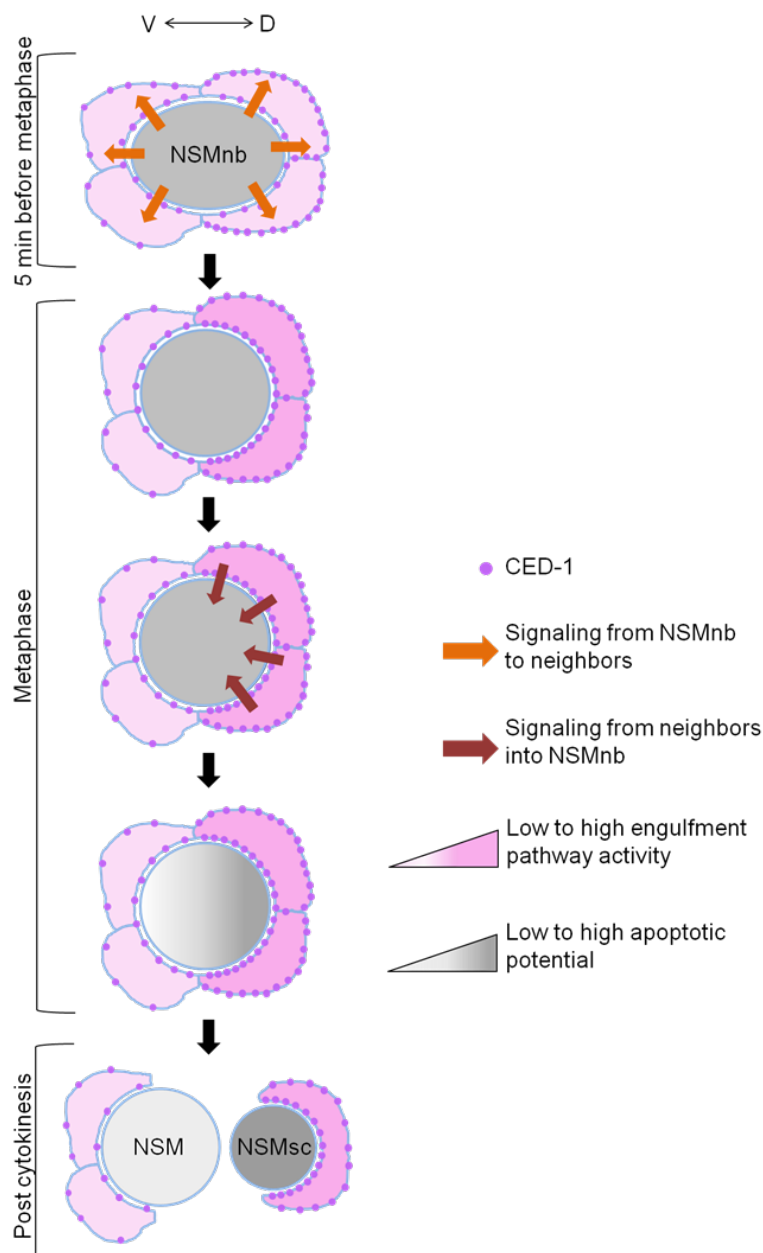
Figure 38. Components of engulfment pathways promote the apoptotic death of the NSMsc.

A simplified molecular model for how components of the engulfment pathways promote NSMsc apoptosis. CED-3 caspase activity present in the mother of the NSMsc, the NSMnb, produces a signal (orange arrow) that results in the enrichment of CED-1 on plasma membranes of neighboring cells apposing the dorsal side of the NSMnb. CED-1 enrichment on the plasma membranes of the dorsal neighbors leads to the activation of components of the two engulfment pathways in these cells. A signal from these neighbors (brown arrow), which

92

is dependent on the functions of components of the two engulfment pathways, subsequently promotes the generation of a gradient of 'apoptotic potential' (including a gradient of CED-3 caspase activity) along the dorsal-ventral axis of the NSMnb. During NSMnb division, this gradient causes the unequal segregation of apoptotic potential. As a result, the small dorsal daughter cell, the NSMsc, inherits a higher concentration of this potential. This higher concentration is reflected in a higher level of CED-3 caspase activity and an increase in CED-3 concentration in the NSMsc, both of which contribute to the apoptotic death of the NSMsc within ~20 min post cytokinesis, the time point at which the NSMsc corpse is engulfed by a neighboring cell.
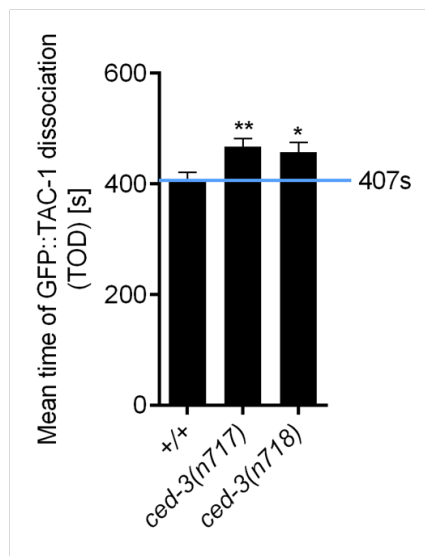
Figure 39. CED-3 promotes the dissociation of GFP::TAC-1 from the PCM inherited by the NSMsc.

Mean time of GFP::TAC-1 dissociation from the PCM (TOD) [s] segregated into the NSMsc in wild-type (+/+), *ced-3(n717)* and *ced-3(n718)*) embryos expressing P*pie-1gfp::tac-1* (*bcIs104*) and P*pie-1mCherry::plcδph* (*ltIs44*) (n=8-13). For comparison, the TOD in wild-type (+/+) is indicated by the blue line. Error bars denote the standard error of the mean. The mean times of dissociation were analyzed using the Student's t-test (*p≤0.05 and **p≤0.01). The statistical analyses were done in comparisons to wild-type (+/+).

2. Novel functions of *C. elegans* central cell death pathway in centrosome asymmetry and segregation

Centrosome asymmetry and non-random segregation of centrosomes by age have so far only been described for stem cell lineages in *D. melanogaster* and mammals. This study demonstrates that centrosome asymmetry (in terms of the amount of proteins associated with the PCM) and non-random segregation of centrosomes are a widespread phenomenon during *C. elegans* embryogenesis. These events occur during both symmetric and asymmetric cell divisions. Centrosomes can also function as vehicles to facilitate the differential segregation of cell fate determinants, organelles and protein aggregates (Lerit et al., 2013). For instance, during the division of sensory organ precursors in *D. melanogaster,* Rab11 exclusively associates with one of the two centrosomes and thereby segregates specifically into the neuronal precursor (Emery et al., 2005). Therefore, I speculate that centrosome asymmetry (in terms of the amount of associated PCM) and non-random segregation of centrosomes during *C. elegans* embryogenesis might also provide a means to differentially segregate cellular components. I have hence uncovered a previously undescribed layer of complexity within the highly reproducible, essentially invariant *C. elegans* somatic cell lineage.

A number of factors have been described that act in stem cell lineages to contribute to centrosome asymmetry in terms of the amount of associated PCM. Most of these factors represent centrosomal proteins or proteins that have been implicated in various aspects of cell polarity (Rebollo et al., 2007; Conduit et al., 2010; Conduit and Raff, 2010; Januschke et al., 2013; Lerit and Rusan, 2013; Singh et al., 2014). My analysis of *ced-3* activity demonstrates that CED-3 caspase may not play a role in establishing centrosome asymmetry in all *C.*

elegans embryonic divisions but, it has a lineage specific function. Nonetheless, *C. elegans* *ced-3* caspase does play a global role in the non-random segregation of PCM associated centrosomal proteins. Since many of the lineages in which centrosome asymmetry and segregation are affected by the loss of *ced-3* function do not generate cells that are fated to die, these novel *ced-3* functions are most likely unrelated to the function of *ced-3* in apoptosis. Therefore, the list of non-apoptotic functions of the components of the central cell death pathway including CED-3 caspase continues to grow. It has been reported that CED-3 caspase dependent cleavage regulates *C. elegans* developmental events by the proteolytic inactivation of the known miRNA targets LIN-14 (LIN, abnormal cell <u>lin</u>eage), LIN-28 and DISL-2 (DISL, <u>DIS</u>3-<u>l</u>ike exonuclease-2 homolog) (Weaver et al., 2014). miRNAs regulate post-transcriptional protein synthesis by acting in conjunction with miRNA-induced-silencing complex (miRISC). AIN-1 is a part of the *C. elegans* miRISC (Ding et al., 2005). Loss of *ain-1* results in a number of developmental defects. It has been demonstrated that loss of *egl-1*, *ced-4* or *ced-3* function significantly enhances the developmental defects of *ain-1(*lf*)* animals. These observations suggest that the components of the cell death pathway are involved in the normal development of an animal (Weaver et al., 2014). A novel CED-9, CED-4 and CED-3 mediated mitochondrial ROS (mtROS) signal has also been described (Yee et al., 2014). Specifically, mtROS activates the central cell death pathway downstream of *ced-9*. Although this activation does not cause apoptosis, CED-9, CED-4 and CED-3 perform a protective function by inducing specific gene expression that further modulate stress response. CED-3 caspase also has a regenerative role in *C. elegans* (Pinan-Lucarre et al., 2012). Following

nerve axotomy, CED-4 dependent CED-3 caspase activity is required for outgrowth dynamics and axon repair. However, this process is independent of EGL-1 and CED-9.

My analyses of centrosome asymmetry (in terms of the amount of PCM associated proteins) and non-random segregation of centrosomes during the division of the NSMnb reveal that the role of *ced-3* caspase in these processes is complex and that it involves protease-dependent as well as protease-independent functions of CED-3 protein. Specifically, the contribution of *ced-3* to centrosome asymmetry *per se* (i.e. the generation of a 'small' and 'large' centrosome) is dependent on CED-3 protease activity and may, at least in part, be mediated by CED-3-dependent cleavage of the PCM component TAC-1. In contrast, the contribution of *ced-3* to the non-random segregation of 'small' and 'large' centrosomes into the NSMsc and NSM, respectively, is independent of CED-3 protease activity. Since *ced-4* Apaf-1 is also required for the proper segregation of 'small' and 'large' centrosome in this lineage, I propose that I have uncovered a function of the CED-4-CED-3 complex (and therefore the apoptosome) that is independent of CED-3 protease activity. Alternatively, the functions of *ced-4* and *ced-3* in centrosome segregation may be independent of each other. Based on my analyses of the time of dissociation (TOD) of TAC-1 post-cytokinesis, a catalytically inactive CED-4-CED-3 complex may also delay TAC-1 dissociation in the NSM, which is fated to survive. My results also suggest that in the NSMsc, which is fated to die, CED-3 protease activity contributes to TAC-1 dissociation potentially through CED-3-dependent cleavage of TAC-1. Since TAC-1 eventually dissociates from the centrosome in the NSMsc in the absence of *ced-3*, *ced-3*-independent mechanisms must contribute to TAC-1 dissociation in this cell as well. Interestingly, the human TAC-1 homologs TACC1, TACC2

and TACC3 are also predicted to be caspase substrates (Song et al., 2010). Therefore, I speculate that the function of *ced-3* caspase in centrosome asymmetry at metaphase and in TAC-1 dissociation from the centrosome post-cytokinesis is conserved from *C. elegans* to humans. It remains to be determined, whether the role of *ced-3* in centrosome asymmetry and segregation in the NSM lineage described in this study is functionally related to its role in apoptosis in the NSM lineage. Yeast two-hybrid studies have identified that SPD-5, which is an essential component of the *C. elegans* centrosome, can bind CED-9 (Dreze et al., 2009). It remains to be determined whether this interaction holds any functional significance *in vivo*.

Centrosomes have been shown to play a role in the asymmetric segregation of cell fate determinants during mitosis. It has been demonstrated that mRNAs of patterning genes are targeted to the PCM in a microtubule-dependent manner, and are then asymmetrically segregated (Lambert and Nagy, 2002). It has also been reported that during cell divisions in *D. melanogaster* and mammals, protein aggregates are transported to the PCM and preferentially to one of the daughters (Rujano et al., 2006). This evidence strongly suggests that the centrosomes by themselves act as carriers of intra-cellular molecules. In *S. cerevisiae*, reports of asymmetric segregation of oxidatively damaged proteins have been made (Aguilaniu et al., 2003). Asymmetric inheritance of damaged proteins has also been observed in prokaryotes. In *E. coli*, asymmetric inheritance of cellular damage has been related to ageing. The cell that inherits the old pole grows slowly and has an increased frequency of death, suggesting that asymmetric distribution of damage is a prevalent process (Stewart et al., 2005; Lindner et al., 2008). Mitochondria have been shown to segregate asymmetrically in human mammary stem-like cells (Katajisto et al., 2015). Specifically, daughter cells that received relatively few old-

mitochondria maintain stemness, suggesting that age-dependent mitochondrial segregation have a functional significance in asymmetric cell divisions. Unequal distribution of mitochondria and inheritance of cell fate determinants have also been identified in early *C. elegans* embryo (Reese et al., 2000; Badrinath and White, 2003). Therefore, such events are likely to occur during the asymmetric division of the NSMnb, wherein damaged and unwanted protein or mitochondria are preferentially segregated to the smaller NSMsc. The transport of these molecules may be dependent on non-random centrosome segregation. Such events however, remain to be ascertained in the NSM lineage. Since, I have now discovered that the engulfment pathways polarize the NSMnb, it will be interesting to determine whether they also play a role in the generation of a gradient of such molecules that need to be specifically discarded to the NSMsc. It is likely that in *C. elegans*, the dying cells act as a 'dustbin' of unwanted cellular components, proteins and organelles alike (Singhvi and Garriga, 2009). Further, whether the induction of NSMsc apoptosis is directly linked with inheritance of nonessential and undesirable molecules or organelles is an avenue for future investigation.

CONCLUSION

My studies of the evolutionarily conserved central cell death pathway and the two engulfment pathways in the NSM lineage of *C. elegans* have led to a number of discoveries regarding the functions of these pathways during normal embryonic development. Both the cell death pathways and the engulfment pathways were previously thought to act only in dying and engulfing cells, respectively (reviewed in: Lettre and Hengartner, 2006; Conradt, 2009). I have now been able to demonstrate that these pathways act a generation earlier, in the mother of the dying cells and its neighbors, respectively, and therefore have functions during development which had not yet been discovered. CED-3 caspase already active in the mother of the dying cell (NSMnb) signals to its neighbors, thereby inducing CED-1 mEGF-10 enrichment on the plasma membrane regions of the neighboring cells apposing the dorsal side of the NSMnb that gives rise to the NSMsc which is programmed to die. CED-1 mEGF10 enrichment activates the engulfment pathways and the polarization of the mother cell takes place. This polarization further facilitates the biased segregation of apoptotic factors to the dying cell. Components of the engulfment pathways thus play a role in predetermining the fate of the NSMnb daughters in the mother cell itself. These novel functions of the evolutionarily conserved pathways may therefore help in maintaining the invariant nature of programmed cell death during *C. elegans* development.

In the invariant cell lineage of a developing *C. elegans* embryo, I have further discovered an invariant intra-cellular asymmetry. I found that centrosome asymmetry and non-random patterns of centrosome segregation are widespread phenomena during *C. elegans* embryonic divisions. Furthermore, I have shown that components of the conserved apoptotic

pathway, *egl-1* BH3-only, *ced-9* Bcl-2, *ced-4* Apaf-1 and *ced-3* caspase, contribute to centrosome asymmetry and segregation.

REFERENCES

1.   Aguilaniu, H., Gustafsson, L., Rigoulet, M. and Nystrom, T. (2003) 'Asymmetric inheritance of oxidatively damaged proteins during cytokinesis', *Science* 299(5613): 1751-3.

2.   Akakura, S., Kar, B., Singh, S., Cho, L., Tibrewal, N., Sanokawa-Akakura, R., Reichman, C., Ravichandran, K. S. and Birge, R. B. (2005) 'C-terminal SH3 domain of CrkII regulates the assembly and function of the DOCK180/ELMO Rac-GEF', *J Cell Physiol* 204(1): 344-51.

3.   Allen, J. W., Eldadah, B. A., Huang, X., Knoblach, S. M. and Faden, A. I. (2001) 'Multiple caspases are involved in beta-amyloid-induced neuronal apoptosis', *Journal of neuroscience research* 65(1): 45-53.

4.   Ambros, V., Lee, R. C., Lavanway, A., Williams, P. T. and Jewell, D. (2003) 'MicroRNAs and other tiny endogenous RNAs in *C. elegans*', *Current biology : CB* 13(10): 807-18.

5.   Andree, H. A., Reutelingsperger, C. P., Hauptmann, R., Hemker, H. C., Hermens, W. T. and Willems, G. M. (1990) 'Binding of vascular anticoagulant alpha (VAC alpha) to planar phospholipid bilayers', *The Journal of biological chemistry* 265(9): 4923-8.

6.   Audhya, A., Hyndman, F., McLeod, I. X., Maddox, A. S., Yates, J. R., 3rd, Desai, A. and Oegema, K. (2005) 'A complex containing the Sm protein CAR-1 and the RNA helicase CGH-1 is required for embryonic cytokinesis in *Caenorhabditis elegans*', *The Journal of cell biology* 171(2): 267-79.

7.   Avery-Kiejda, K. A., Bowden, N. A., Croft, A. J., Scurr, L. L., Kairupan, C. F., Ashton, K. A., Talseth-Palmer, B. A., Rizos, H., Zhang, X. D., Scott, R. J. et al. (2011) 'P53 in

human melanoma fails to regulate target genes associated with apoptosis and the cell cycle and may contribute to proliferation', *BMC cancer* 11: 203.

8. Ayala-Grosso, C., Tam, J., Roy, S., Xanthoudakis, S., Da Costa, D., Nicholson, D. W. and Robertson, G. S. (2006) 'Caspase-3 cleaved spectrin colocalizes with neurofilament-immunoreactive neurons in Alzheimer's disease', *Neuroscience* 141(2): 863-74.

9. Badrinath, A. S. and White, J. G. (2003) 'Contrasting patterns of mitochondrial redistribution in the early lineages of *Caenorhabditis elegans* and Acrobeloides sp. PS1146', *Developmental biology* 258(1): 70-5.

10. Bellanger, J. M. and Gonczy, P. (2003) 'TAC-1 and ZYG-9 form a complex that promotes microtubule assembly in *C. elegans* embryos', *Current biology : CB* 13(17): 1488-98.

11. Brenner, S. (1974) 'The genetics of *Caenorhabditis elegans*', *Genetics* 77(1): 71-94.

12. Broadus, J. and Doe, C. Q. (1997) 'Extrinsic cues, intrinsic cues and microfilaments regulate asymmetric protein localization in *Drosophila* neuroblasts', *Current biology : CB* 7(11): 827-35.

13. Cabral, G., Sans, S. S., Cowan, C. R. and Dammermann, A. (2013) 'Multiple mechanisms contribute to centriole separation in *C. elegans*', *Current biology : CB* 23(14): 1380-7.

14. Chan, S. L., Griffin, W. S. and Mattson, M. P. (1999) 'Evidence for caspase-mediated cleavage of AMPA receptor subunits in neuronal apoptosis and Alzheimer's disease', *Journal of neuroscience research* 57(3): 315-23.

15. Chen, F., Hersh, B. M., Conradt, B., Zhou, Z., Riemer, D., Gruenbaum, Y. and Horvitz, H. R. (2000) 'Translocation of *C. elegans* CED-4 to nuclear membranes during programmed cell death', *Science* 287(5457): 1485-9.

16. Chen, Y. Z., Mapes, J., Lee, E. S., Skeen-Gaar, R. R. and Xue, D. (2013) 'Caspase-mediated activation of *Caenorhabditis elegans* CED-8 promotes apoptosis and phosphatidylserine externalization', *Nature communications* 4: 2726.

17. Chinnaiyan, A. M., O'Rourke, K., Lane, B. R. and Dixit, V. M. (1997) 'Interaction of CED-4 with CED-3 and CED-9: a molecular framework for cell death', *Science* 275(5303): 1122-6.

18. Conduit, P. T., Brunk, K., Dobbelaere, J., Dix, C. I., Lucas, E. P. and Raff, J. W. (2010) 'Centrioles regulate centrosome size by controlling the rate of Cnn incorporation into the PCM', *Current biology : CB* 20(24): 2178-86.

19. Conduit, P. T. and Raff, J. W. (2010) 'Cnn dynamics drive centrosome size asymmetry to ensure daughter centriole retention in Drosophila neuroblasts', *Current biology : CB* 20(24): 2187-92.

20. Conradt, B. (2009) 'Genetic control of programmed cell death during animal development', *Annual review of genetics* 43: 493-523.

21. Conradt, B. and Horvitz, H. R. (1998) 'The *C. elegans* protein EGL-1 is required for programmed cell death and interacts with the Bcl-2-like protein CED-9', *Cell* 93(4): 519-29.

22. Consortium, T. C. e. S. (1998) 'Genome sequence of the nematode *C. elegans*: a platform for investigating biology', *Science* 282(5396): 2012-8.

23.   Cotman, C. W., Poon, W. W., Rissman, R. A. and Blurton-Jones, M. (2005) 'The role of caspase cleavage of tau in Alzheimer disease neuropathology', *Journal of neuropathology and experimental neurology* 64(2): 104-12.

24.   Cribbs, D. H., Poon, W. W., Rissman, R. A. and Blurton-Jones, M. (2004) 'Caspase-mediated degeneration in Alzheimer's disease', *The American journal of pathology* 165(2): 353-5.

25.   de Herreros, A. G., Peiro, S., Nassour, M. and Savagner, P. (2010) 'Snail family regulation and epithelial mesenchymal transitions in breast cancer progression', *J Mammary Gland Biol Neoplasia* 15(2): 135-47.

26.   deBakker, C. D., Haney, L. B., Kinchen, J. M., Grimsley, C., Lu, M., Klingele, D., Hsu, P. K., Chou, B. K., Cheng, L. C., Blangy, A. et al. (2004) 'Phagocytosis of apoptotic cells is regulated by a UNC-73/TRIO-MIG-2/RhoG signaling module and armadillo repeats of CED-12/ELMO', *Current biology : CB* 14(24): 2208-16.

27.   del Peso, L., Gonzalez, V. M., Inohara, N., Ellis, R. E. and Nunez, G. (2000) 'Disruption of the CED-9.CED-4 complex by EGL-1 is a critical step for programmed cell death in *Caenorhabditis elegans*', *The Journal of biological chemistry* 275(35): 27205-11.

28.   del Peso, L., Gonzalez, V. M. and Nunez, G. (1998) '*Caenorhabditis elegans* EGL-1 disrupts the interaction of CED-9 with CED-4 and promotes CED-3 activation', *The Journal of biological chemistry* 273(50): 33495-500.

29.   Deveraux, Q. L. and Reed, J. C. (1999) 'IAP family proteins--suppressors of apoptosis', *Genes & development* 13(3): 239-52.

30. Ding, L., Spencer, A., Morita, K. and Han, M. (2005) 'The developmental timing regulator AIN-1 interacts with miRISCs and may target the argonaute protein ALG-1 to cytoplasmic P bodies in *C. elegans*', *Molecular cell* 19(4): 437-47.

31. Dreze, M., Charloteaux, B., Milstein, S., Vidalain, P. O., Yildirim, M. A., Zhong, Q., Svrzikapa, N., Romero, V., Laloux, G., Brasseur, R. et al. (2009) ''Edgetic' perturbation of a *C. elegans* BCL2 ortholog', *Nature methods* 6(11): 843-9.

32. Ellis, H. M. and Horvitz, H. R. (1986) 'Genetic control of programmed cell death in the nematode *C. elegans*', *Cell* 44(6): 817-29.

33. Ellis, R. E. and Horvitz, H. R. (1991) 'Two *C. elegans* genes control the programmed deaths of specific cells in the pharynx', *Development* 112(2): 591-603.

34. Ellis, R. E., Jacobson, D. M. and Horvitz, H. R. (1991) 'Genes required for the engulfment of cell corpses during programmed cell death in *Caenorhabditis elegans*', *Genetics* 129(1): 79-94.

35. Emery, G., Hutterer, A., Berdnik, D., Mayer, B., Wirtz-Peitz, F., Gaitan, M. G. and Knoblich, J. A. (2005) 'Asymmetric Rab 11 endosomes regulate delta recycling and specify cell fate in the *Drosophila* nervous system', *Cell* 122(5): 763-73.

36. Felix, M. A. and Duveau, F. (2012) 'Population dynamics and habitat sharing of natural populations of *Caenorhabditis elegans* and *C. briggsae*', *BMC biology* 10: 59.

37. Frokjaer-Jensen, C., Davis, M. W., Ailion, M. and Jorgensen, E. M. (2012) 'Improved Mos1-mediated transgenesis in *C. elegans*', *Nature methods* 9(2): 117-8.

38. Fuchs, Y. and Steller, H. (2011) 'Programmed cell death in animal development and disease', *Cell* 147(4): 742-58.

39.   Fulda, S., Meyer, E. and Debatin, K. M. (2002) 'Inhibition of TRAIL-induced apoptosis by Bcl-2 overexpression', *Oncogene* 21(15): 2283-94.

40.   Gastard, M. C., Troncoso, J. C. and Koliatsos, V. E. (2003) 'Caspase activation in the limbic cortex of subjects with early Alzheimer's disease', *Annals of neurology* 54(3): 393-8.

41.   Goolsby, C., Paniagua, M., Tallman, M. and Gartenhaus, R. B. (2005) 'Bcl-2 regulatory pathway is functional in chronic lymphocytic leukemia', *Cytometry. Part B, Clinical cytometry* 63(1): 36-46.

42.   Green, J. L., Inoue, T. and Sternberg, P. W. (2008) 'Opposing Wnt pathways orient cell polarity during organogenesis', *Cell* 134(4): 646-56.

43.   Gurskaya, N. G., Verkhusha, V. V., Shcheglov, A. S., Staroverov, D. B., Chepurnykh, T. V., Fradkov, A. F., Lukyanov, S. and Lukyanov, K. A. (2006) 'Engineering of a monomeric green-to-red photoactivatable fluorescent protein induced by blue light', *Nat Biotechnol* 24(4): 461-5.

44.   Hadwiger, G., Dour, S., Arur, S., Fox, P. and Nonet, M. L. (2010) 'A monoclonal antibody toolkit for *C. elegans*', *PloS one* 5(4): e10161.

45.   Hamill, D. R., Severson, A. F., Carter, J. C. and Bowerman, B. (2002) 'Centrosome maturation and mitotic spindle assembly in *C. elegans* require SPD-5, a protein with multiple coiled-coil domains', *Developmental cell* 3(5): 673-84.

46.   Hatzold, J. and Conradt, B. (2008) 'Control of apoptosis by asymmetric cell division', *PLoS biology* 6(4): e84.

47. Hedgecock, E. M., Sulston, J. E. and Thomson, J. N. (1983) 'Mutations affecting programmed cell deaths in the nematode *Caenorhabditis elegans*', *Science* 220(4603): 1277-9.

48. Hengartner, M. O., Ellis, R. E. and Horvitz, H. R. (1992) '*Caenorhabditis elegans* gene *ced-9* protects cells from programmed cell death', *Nature* 356(6369): 494-9.

49. Hengartner, M. O. and Horvitz, H. R. (1994) '*C. elegans* cell survival gene *ced-9* encodes a functional homolog of the mammalian proto-oncogene *bcl-2*', *Cell* 76(4): 665-76.

50. Hochreiter-Hufford, A. and Ravichandran, K. S. (2013) 'Clearing the dead: apoptotic cell sensing, recognition, engulfment, and digestion', *Cold Spring Harbor perspectives in biology* 5(1): a008748.

51. Hoeppner, D. J., Hengartner, M. O. and Schnabel, R. (2001) 'Engulfment genes cooperate with *ced-3* to promote cell death in *Caenorhabditis elegans*', *Nature* 412(6843): 202-6.

52. Horvitz, H. R. (2003) 'Worms, life, and death (Nobel lecture)', *Chembiochem : a European journal of chemical biology* 4(8): 697-711.

53. Huang, W., Jiang, T., Choi, W., Qi, S., Pang, Y., Hu, Q., Xu, Y., Gong, X., Jeffrey, P. D., Wang, J. et al. (2013) 'Mechanistic insights into CED-4-mediated activation of CED-3', *Genes & development* 27(18): 2039-48.

54. Irmler, M., Hofmann, K., Vaux, D. and Tschopp, J. (1997) 'Direct physical interaction between the *Caenorhabditis elegans* 'death proteins' CED-3 and CED-4', *FEBS letters* 406(1-2): 189-90.

55. Jacobson, M. D., Weil, M. and Raff, M. C. (1997) 'Programmed cell death in animal development', *Cell* 88(3): 347-54.

56. James, C., Gschmeissner, S., Fraser, A. and Evan, G. I. (1997) 'CED-4 induces chromatin condensation in *Schizosaccharomyces pombe* and is inhibited by direct physical association with CED-9', *Current biology : CB* 7(4): 246-52.

57. Januschke, J. and Gonzalez, C. (2010) 'The interphase microtubule aster is a determinant of asymmetric division orientation in *Drosophila* neuroblasts', *The Journal of cell biology* 188(5): 693-706.

58. Januschke, J., Reina, J., Llamazares, S., Bertran, T., Rossi, F., Roig, J. and Gonzalez, C. (2013) 'Centrobin controls mother-daughter centriole asymmetry in Drosophila neuroblasts', *Nature cell biology* 15(3): 241-8.

59. Katajisto, P., Dohla, J., Chaffer, C. L., Pentinmikko, N., Marjanovic, N., Iqbal, S., Zoncu, R., Chen, W., Weinberg, R. A. and Sabatini, D. M. (2015) 'Stem cells. Asymmetric apportioning of aged mitochondria between daughter cells is required for stemness', *Science* 348(6232): 340-3.

60. Kerr, J. F., Wyllie, A. H. and Currie, A. R. (1972) 'Apoptosis: a basic biological phenomenon with wide-ranging implications in tissue kinetics', *British journal of cancer* 26(4): 239-57.

61. Kimble, J. and Hirsh, D. (1979) 'The postembryonic cell lineages of the hermaphrodite and male gonads in *Caenorhabditis elegans*', *Developmental biology* 70(2): 396-417.

62. Kinchen, J. M., Cabello, J., Klingele, D., Wong, K., Feichtinger, R., Schnabel, H., Schnabel, R. and Hengartner, M. O. (2005) 'Two pathways converge at CED-10 to mediate actin rearrangement and corpse removal in *C. elegans*', *Nature* 434(7029): 93-9.

63. Kramer, J. M., French, R. P., Park, E. C. and Johnson, J. J. (1990) 'The *Caenorhabditis elegans rol-6* gene, which interacts with the *sqt-1* collagen gene to determine organismal morphology, encodes a collagen', *Molecular and cellular biology* 10(5): 2081-9.

64. Lagos-Quintana, M., Rauhut, R., Lendeckel, W. and Tuschl, T. (2001) 'Identification of novel genes coding for small expressed RNAs', *Science* 294(5543): 853-8.

65. Lambert, J. D. and Nagy, L. M. (2002) 'Asymmetric inheritance of centrosomally localized mRNAs during embryonic cleavages', *Nature* 420(6916): 682-6.

66. Lau, N. C., Lim, L. P., Weinstein, E. G. and Bartel, D. P. (2001) 'An abundant class of tiny RNAs with probable regulatory roles in *Caenorhabditis elegans*', *Science* 294(5543): 858-62.

67. Le Bot, N., Tsai, M. C., Andrews, R. K. and Ahringer, J. (2003) 'TAC-1, a regulator of microtubule length in the *C. elegans* embryo', *Current biology : CB* 13(17): 1499-505.

68. Lee, R. C. and Ambros, V. (2001) 'An extensive class of small RNAs in *Caenorhabditis elegans*', *Science* 294(5543): 862-4.

69. Lee, R. C., Feinbaum, R. L. and Ambros, V. (1993) 'The *C. elegans* heterochronic gene *lin-4* encodes small RNAs with antisense complementarity to lin-14', *Cell* 75(5): 843-54.

70. Lerit, D. A. and Rusan, N. M. (2013) 'PLP inhibits the activity of interphase centrosomes to ensure their proper segregation in stem cells', *The Journal of cell biology* 202(7): 1013-22.

71. Lerit, D. A., Smyth, J. T. and Rusan, N. M. (2013) 'Organelle asymmetry for proper fitness, function, and fate', *Chromosome research : an international journal on the molecular, supramolecular and evolutionary aspects of chromosome biology* 21(3): 271-86.

72. Lettre, G. and Hengartner, M. O. (2006) 'Developmental apoptosis in *C. elegans*: a complex CEDnario', *Nature reviews. Molecular cell biology* 7(2): 97-108.

73. Li, Z., Venegas, V., Nagaoka, Y., Morino, E., Raghavan, P., Audhya, A., Nakanishi, Y. and Zhou, Z. (2015) 'Necrotic Cells Actively Attract Phagocytes through the Collaborative Action of Two Distinct PS-Exposure Mechanisms', *PLoS genetics* 11(6): e1005285.

74. Lim, L. P., Lau, N. C., Weinstein, E. G., Abdelhakim, A., Yekta, S., Rhoades, M. W., Burge, C. B. and Bartel, D. P. (2003) 'The microRNAs of *Caenorhabditis elegans*', *Genes & development* 17(8): 991-1008.

75. Lindner, A. B., Madden, R., Demarez, A., Stewart, E. J. and Taddei, F. (2008) 'Asymmetric segregation of protein aggregates is associated with cellular aging and rejuvenation', *Proceedings of the National Academy of Sciences of the United States of America* 105(8): 3076-81.

76. Liu, H., Strauss, T. J., Potts, M. B. and Cameron, S. (2006) 'Direct regulation of *egl-1* and of programmed cell death by the Hox protein MAB-5 and by CEH-20, a *C. elegans* homolog of Pbx1', *Development* 133(4): 641-50.

77. Liu, Q. A. and Hengartner, M. O. (1998) 'Candidate adaptor protein CED-6 promotes the engulfment of apoptotic cells in *C. elegans*', *Cell* 93(6): 961-72.

78. Lobov, I. B., Rao, S., Carroll, T. J., Vallance, J. E., Ito, M., Ondr, J. K., Kurup, S., Glass, D. A., Patel, M. S., Shu, W. et al. (2005) 'WNT7b mediates macrophage-induced programmed cell death in patterning of the vasculature', *Nature* 437(7057): 417-21.

79. Lu, N. and Zhou, Z. (2012) 'Membrane trafficking and phagosome maturation during the clearance of apoptotic cells', *International review of cell and molecular biology* 293: 269-309.

80. Maduro, M. F., Lin, R. and Rothman, J. H. (2002) 'Dynamics of a developmental switch: recursive intracellular and intranuclear redistribution of *Caenorhabditis elegans* POP-1 parallels Wnt-inhibited transcriptional repression', *Developmental biology* 248(1): 128-42.

81. Mapes, J., Chen, Y. Z., Kim, A., Mitani, S., Kang, B. H. and Xue, D. (2012) 'CED-1, CED-7, and TTR-52 regulate surface phosphatidylserine expression on apoptotic and phagocytic cells', *Current biology : CB* 22(14): 1267-75.

82. Mardin, B. R. and Schiebel, E. (2012) 'Breaking the ties that bind: new advances in centrosome biology', *The Journal of cell biology* 197(1): 11-8.

83. Marin-Teva, J. L., Dusart, I., Colin, C., Gervais, A., van Rooijen, N. and Mallat, M. (2004) 'Microglia promote the death of developing Purkinje cells', *Neuron* 41(4): 535-47.

84. Maurer, C. W., Chiorazzi, M. and Shaham, S. (2007) 'Timing of the onset of a developmental cell death is controlled by transcriptional induction of the *C. elegans ced-3* caspase-encoding gene', *Development* 134(7): 1357-68.

85. Mello, C. C., Kramer, J. M., Stinchcomb, D. and Ambros, V. (1991) 'Efficient gene transfer in C.elegans: extrachromosomal maintenance and integration of transforming sequences', *The EMBO journal* 10(12): 3959-70.

86. Meneghini, M. D., Ishitani, T., Carter, J. C., Hisamoto, N., Ninomiya-Tsuji, J., Thorpe, C. J., Hamill, D. R., Matsumoto, K. and Bowerman, B. (1999) 'MAP kinase and Wnt

pathways converge to downregulate an HMG-domain repressor in *Caenorhabditis elegans*', *Nature* 399(6738): 793-7.

87. Metzstein, M. M., Hengartner, M. O., Tsung, N., Ellis, R. E. and Horvitz, H. R. (1996) 'Transcriptional regulator of programmed cell death encoded by *Caenorhabditis elegans* gene ces-2', *Nature* 382(6591): 545-7.

88. Metzstein, M. M. and Horvitz, H. R. (1999) 'The *C. elegans* cell death specification gene *ces-1* encodes a snail family zinc finger protein', *Molecular cell* 4(3): 309-19.

89. Minn, A. J., Rudin, C. M., Boise, L. H. and Thompson, C. B. (1995) 'Expression of *bcl-xL* can confer a multidrug resistance phenotype', *Blood* 86(5): 1903-10.

90. Miquel, C., Borrini, F., Grandjouan, S., Auperin, A., Viguier, J., Velasco, V., Duvillard, P., Praz, F. and Sabourin, J. C. (2005) 'Role of *bax* mutations in apoptosis in colorectal cancers with microsatellite instability', *American journal of clinical pathology* 123(4): 562-70.

91. Neukomm, L. J., Nicot, A. S., Kinchen, J. M., Almendinger, J., Pinto, S. M., Zeng, S., Doukoumetzidis, K., Tronchere, H., Payrastre, B., Laporte, J. F. et al. (2011) 'The phosphoinositide phosphatase MTM-1 regulates apoptotic cell corpse clearance through CED-5-CED-12 in *C. elegans*', *Development* 138(10): 2003-14.

92. Peden, E., Kimberly, E., Gengyo-Ando, K., Mitani, S. and Xue, D. (2007) 'Control of sex-specific apoptosis in *C. elegans* by the BarH homeodomain protein CEH-30 and the transcriptional repressor UNC-37/Groucho', *Genes & development* 21(23): 3195-207.

93. Pelletier, L. and Yamashita, Y. M. (2012) 'Centrosome asymmetry and inheritance during animal development', *Current opinion in cell biology* 24(4): 541-546.

94. Pinan-Lucarre, B., Gabel, C. V., Reina, C. P., Hulme, S. E., Shevkoplyas, S. S., Slone, R. D., Xue, J., Qiao, Y., Weisberg, S., Roodhouse, K. et al. (2012) 'The core apoptotic executioner proteins CED-3 and CED-4 promote initiation of neuronal regeneration in *Caenorhabditis elegans*', *PLoS biology* 10(5): e1001331.

95. Raffo, A. J., Perlman, H., Chen, M. W., Day, M. L., Streitman, J. S. and Buttyan, R. (1995) 'Overexpression of *bcl-2* protects prostate cancer cells from apoptosis in vitro and confers resistance to androgen depletion *in vivo*', *Cancer research* 55(19): 4438-45.

96. Rao, S., Lobov, I. B., Vallance, J. E., Tsujikawa, K., Shiojima, I., Akunuru, S., Walsh, K., Benjamin, L. E. and Lang, R. A. (2007) 'Obligatory participation of macrophages in an angiopoietin 2-mediated cell death switch', *Development* 134(24): 4449-58.

97. Raynal, P. and Pollard, H. B. (1994) 'Annexins: the problem of assessing the biological role for a gene family of multifunctional calcium- and phospholipid-binding proteins', *Biochimica et biophysica acta* 1197(1): 63-93.

98. Rebollo, E., Sampaio, P., Januschke, J., Llamazares, S., Varmark, H. and Gonzalez, C. (2007) 'Functionally unequal centrosomes drive spindle orientation in asymmetrically dividing *Drosophila* neural stem cells', *Developmental cell* 12(3): 467-74.

99. Reddien, P. W., Cameron, S. and Horvitz, H. R. (2001) 'Phagocytosis promotes programmed cell death in *C. elegans*', *Nature* 412(6843): 198-202.

100. Reddien, P. W. and Horvitz, H. R. (2000) 'CED-2/CrkII and CED-10/Rac control phagocytosis and cell migration in *Caenorhabditis elegans*', *Nature cell biology* 2(3): 131-6.

101. Reese, K. J., Dunn, M. A., Waddle, J. A. and Seydoux, G. (2000) 'Asymmetric segregation of PIE-1 in *C. elegans* is mediated by two complementary mechanisms that act through separate PIE-1 protein domains', *Molecular cell* 6(2): 445-55.

102. Reina, J. and Gonzalez, C. (2014) 'When fate follows age: unequal centrosomes in asymmetric cell division', *Philosophical transactions of the Royal Society of London. Series B, Biological sciences* 369(1650).

103. Reutelingsperger, C. P., Hornstra, G. and Hemker, H. C. (1985) 'Isolation and partial purification of a novel anticoagulant from arteries of human umbilical cord', *European journal of biochemistry / FEBS* 151(3): 625-9.

104. Riddle, D. L., Blumenthal, T., Meyer, B. J. and Priess, J. R. (1997) Introduction to *C. elegans*. in D. L. Riddle T. Blumenthal B. J. Meyer and J. R. Priess (eds.) *C. elegans II*. Cold Spring Harbor (NY).

105. Robertson, A. M. and Thomson, J. (1982) 'Morphology of programmed cell death in the ventral nerve cord of *Caenorhabditis elegans* larvae', *Journal of Embryology and experimental Morphology* 67(1): 89-100.

106. Rocheleau, C. E., Downs, W. D., Lin, R., Wittmann, C., Bei, Y., Cha, Y. H., Ali, M., Priess, J. R. and Mello, C. C. (1997) 'Wnt signaling and an APC-related gene specify endoderm in early *C. elegans* embryos', *Cell* 90(4): 707-16.

107. Rolland, S. G., Lu, Y., David, C. N. and Conradt, B. (2009) 'The BCL-2-like protein CED-9 of *C. elegans* promotes FZO-1/Mfn1,2- and EAT-3/Opa1-dependent mitochondrial fusion', *The Journal of cell biology* 186(4): 525-40.

108. Roubinet, C. and Cabernard, C. (2014) 'Control of asymmetric cell division', *Current opinion in cell biology* 31: 84-91.

109. Rujano, M. A., Bosveld, F., Salomons, F. A., Dijk, F., van Waarde, M. A., van der Want, J. J., de Vos, R. A., Brunt, E. R., Sibon, O. C. and Kampinga, H. H. (2006) 'Polarised asymmetric inheritance of accumulated protein damage in higher eukaryotes', *PLoS biology* 4(12): e417.

110. Schnabel, R., Hutter, H., Moerman, D. and Schnabel, H. (1997) 'Assessing normal embryogenesis in *Caenorhabditis elegans* using a 4D microscope: variability of development and regional specification', *Developmental biology* 184(2): 234-65.

111. Schwartz, H. T. (2007) 'A protocol describing pharynx counts and a review of other assays of apoptotic cell death in the nematode worm *Caenorhabditis elegans*', *Nature protocols* 2(3): 705-14.

112. Schwartz, H. T. and Horvitz, H. R. (2007) 'The *C. elegans* protein CEH-30 protects male-specific neurons from apoptosis independently of the Bcl-2 homolog CED-9', *Genes & development* 21(23): 3181-94.

113. Seshagiri, S. and Miller, L. K. (1997) '*Caenorhabditis elegans* CED-4 stimulates CED-3 processing and CED-3-induced apoptosis', *Current biology : CB* 7(7): 455-60.

114. Shaham, S., Reddien, P. W., Davies, B. and Horvitz, H. R. (1999) 'Mutational analysis of the *Caenorhabditis elegans* cell-death gene *ced-3*', *Genetics* 153(4): 1655-71.

115. Shaye, D. D. and Greenwald, I. (2011) 'OrthoList: a compendium of *C. elegans* genes with human orthologs', *PloS one* 6(5): e20085.

116. Shetty, P., Lo, M. C., Robertson, S. M. and Lin, R. (2005) '*C. elegans* TCF protein, POP-1, converts from repressor to activator as a result of Wnt-induced lowering of nuclear levels', *Developmental biology* 285(2): 584-92.

117. Shin, T. H., Yasuda, J., Rocheleau, C. E., Lin, R., Soto, M., Bei, Y., Davis, R. J. and Mello, C. C. (1999) 'MOM-4, a MAP kinase kinase kinase-related protein, activates WRM-1/LIT-1 kinase to transduce anterior/posterior polarity signals in *C. elegans*', *Molecular cell* 4(2): 275-80.

118. Singh, P., Ramdas Nair, A. and Cabernard, C. (2014) 'The centriolar protein bld10/cep135 is required to establish centrosome asymmetry in *Drosophila* neuroblasts', *Current biology : CB* 24(13): 1548-55.

119. Singhvi, A. and Garriga, G. (2009) 'Asymmetric divisions, aggresomes and apoptosis', *Trends in cell biology* 19(1): 1-7.

120. Smit, L., Baas, A., Kuipers, J., Korswagen, H., van de Wetering, M. and Clevers, H. (2004) 'Wnt activates the Tak1/Nemo-like kinase pathway', *The Journal of biological chemistry* 279(17): 17232-40.

121. Song, J., Tan, H., Shen, H., Mahmood, K., Boyd, S. E., Webb, G. I., Akutsu, T. and Whisstock, J. C. (2010) 'Cascleave: towards more accurate prediction of caspase substrate cleavage sites', *Bioinformatics* 26(6): 752-60.

122. Spector, M. S., Desnoyers, S., Hoeppner, D. J. and Hengartner, M. O. (1997) 'Interaction between the *C. elegans* cell-death regulators CED-9 and CED-4', *Nature* 385(6617): 653-6.

123. Speliotes, E. K., Uren, A., Vaux, D. and Horvitz, H. R. (2000) 'The survivin-like *C. elegans* BIR-1 protein acts with the Aurora-like kinase AIR-2 to affect chromosomes and the spindle midzone', *Molecular cell* 6(2): 211-23.

124. Srayko, M., Quintin, S., Schwager, A. and Hyman, A. A. (2003) '*Caenorhabditis elegans* TAC-1 and ZYG-9 form a complex that is essential for long astral and spindle microtubules', *Current biology : CB* 13(17): 1506-11.

125. Stanfield, G. M. and Horvitz, H. R. (2000) 'The *ced-8* gene controls the timing of programmed cell deaths in *C. elegans*', *Molecular cell* 5(3): 423-33.

126. Stewart, E. J., Madden, R., Paul, G. and Taddei, F. (2005) 'Aging and death in an organism that reproduces by morphologically symmetric division', *PLoS biology* 3(2): e45.

127. Strome, S., Powers, J., Dunn, M., Reese, K., Malone, C. J., White, J., Seydoux, G. and Saxton, W. (2001) 'Spindle dynamics and the role of gamma-tubulin in early *Caenorhabditis elegans* embryos', *Molecular biology of the cell* 12(6): 1751-64.

128. Sulston, J. E. (1976) 'Post-embryonic development in the ventral cord of *Caenorhabditis elegans*', *Philosophical transactions of the Royal Society of London. Series B, Biological sciences* 275(938): 287-97.

129. Sulston, J. E. and Horvitz, H. R. (1977) 'Post-embryonic cell lineages of the nematode, *Caenorhabditis elegans*', *Developmental biology* 56(1): 110-56.

130. Sulston, J. E., Schierenberg, E., White, J. G. and Thomson, J. N. (1983) 'The embryonic cell lineage of the nematode *Caenorhabditis elegans*', *Developmental biology* 100(1): 64-119.

131. Suzuki, J., Denning, D. P., Imanishi, E., Horvitz, H. R. and Nagata, S. (2013) 'Xk-related protein 8 and CED-8 promote phosphatidylserine exposure in apoptotic cells', *Science* 341(6144): 403-6.

132. Suzuki, J., Imanishi, E. and Nagata, S. (2014) 'Exposure of phosphatidylserine by Xk-related protein family members during apoptosis', *The Journal of biological chemistry* 289(44): 30257-67.

133. Sze, J. Y., Victor, M., Loer, C., Shi, Y. and Ruvkun, G. (2000) 'Food and metabolic signalling defects in a *Caenorhabditis elegans* serotonin-synthesis mutant', *Nature* 403(6769): 560-4.

134. Tait, J. F., Gibson, D. and Fujikawa, K. (1989) 'Phospholipid binding properties of human placental anticoagulant protein-I, a member of the lipocortin family', *The Journal of biological chemistry* 264(14): 7944-9.

135. Takacs-Vellai, K., Vellai, T., Chen, E. B., Zhang, Y., Guerry, F., Stern, M. J. and Muller, F. (2007) 'Transcriptional control of Notch signaling by a HOX and a PBX/EXD protein during vulval development in *C. elegans*', *Developmental biology* 302(2): 661-9.

136. Thellmann, M., Hatzold, J. and Conradt, B. (2003) 'The Snail-like CES-1 protein of *C. elegans* can block the expression of the BH3-only cell-death activator gene *egl-1* by antagonizing the function of bHLH proteins', *Development* 130(17): 4057-71.

137. Tursun, B., Cochella, L., Carrera, I. and Hobert, O. (2009) 'A toolkit and robust pipeline for the generation of fosmid-based reporter genes in *C. elegans*', *PloS one* 4(3): e4625.

138. van der Voet, M., Berends, C. W., Perreault, A., Nguyen-Ngoc, T., Gonczy, P., Vidal, M., Boxem, M. and van den Heuvel, S. (2009) 'NuMA-related LIN-5, ASPM-1, calmodulin and dynein promote meiotic spindle rotation independently of cortical LIN-5/GPR/Galpha', *Nature cell biology* 11(3): 269-77.

139. Venegas, V. and Zhou, Z. (2007) 'Two alternative mechanisms that regulate the presentation of apoptotic cell engulfment signal in *Caenorhabditis elegans*', *Molecular biology of the cell* 18(8): 3180-92.

140. Vermes, I., Haanen, C., Steffens-Nakken, H. and Reutelingsperger, C. (1995) 'A novel assay for apoptosis. Flow cytometric detection of phosphatidylserine expression on early apoptotic cells using fluorescein labelled Annexin V', *Journal of immunological methods* 184(1): 39-51.

141. Vogt, C. I. (1842) *Untersuchungen über die Entwicklungsgeschichte der Geburtshelferkröte (Alytes obstetricans).*

142. Wang, X., Tsai, J. W., Imai, J. H., Lian, W. N., Vallee, R. B. and Shi, S. H. (2009) 'Asymmetric centrosome inheritance maintains neural progenitors in the neocortex', *Nature* 461(7266): 947-55.

143. Weaver, B. P., Zabinsky, R., Weaver, Y. M., Lee, E. S., Xue, D. and Han, M. (2014) 'CED-3 caspase acts with miRNAs to regulate non-apoptotic gene expression dynamics for robust development in *C. elegans*', *eLife* 3: e04265.

144. Wightman, B., Ha, I. and Ruvkun, G. (1993) 'Posttranscriptional regulation of the heterochronic gene *lin-14* by *lin-4* mediates temporal pattern formation in *C. elegans*', *Cell* 75(5): 855-62.

145. Wu, D., Wallen, H. D. and Nunez, G. (1997) 'Interaction and regulation of subcellular localization of CED-4 by CED-9', *Science* 275(5303): 1126-9.

146. Wu, Y. C. and Horvitz, H. R. (1998) '*C. elegans* phagocytosis and cell-migration protein CED-5 is similar to human DOCK180', *Nature* 392(6675): 501-4.

147. Xue, D., Shaham, S. and Horvitz, H. R. (1996) 'The *Caenorhabditis elegans* cell-death protein CED-3 is a cysteine protease with substrate specificities similar to those of the human CPP32 protease', *Genes & development* 10(9): 1073-83.

148. Yamashita, Y. M., Mahowald, A. P., Perlin, J. R. and Fuller, M. T. (2007) 'Asymmetric inheritance of mother versus daughter centrosome in stem cell division', *Science* 315(5811): 518-21.

149. Yan, B., Memar, N., Gallinger, J. and Conradt, B. (2013) 'Coordination of cell proliferation and cell fate determination by CES-1 snail', *PLoS genetics* 9(10): e1003884.

150. Yan, N., Chai, J., Lee, E. S., Gu, L., Liu, Q., He, J., Wu, J. W., Kokel, D., Li, H., Hao, Q. et al. (2005) 'Structure of the CED-4-CED-9 complex provides insights into programmed cell death in *Caenorhabditis elegans*', *Nature* 437(7060): 831-7.

151. Yan, N., Gu, L., Kokel, D., Chai, J., Li, W., Han, A., Chen, L., Xue, D. and Shi, Y. (2004) 'Structural, biochemical, and functional analyses of CED-9 recognition by the proapoptotic proteins EGL-1 and CED-4', *Molecular cell* 15(6): 999-1006.

152. Yang, X., Chang, H. Y. and Baltimore, D. (1998) 'Essential role of CED-4 oligomerization in CED-3 activation and apoptosis', *Science* 281(5381): 1355-7.

153. Yee, C., Yang, W. and Hekimi, S. (2014) 'The Intrinsic Apoptosis Pathway Mediates the Pro-Longevity Response to Mitochondrial ROS in *C. elegans*', *Cell* 157(4): 897-909.

154. Yu, X., Odera, S., Chuang, C. H., Lu, N. and Zhou, Z. (2006) '*C. elegans* Dynamin mediates the signaling of phagocytic receptor CED-1 for the engulfment and degradation of apoptotic cells', *Developmental cell* 10(6): 743-57.

155. Yuan, J. and Horvitz, H. R. (1992) 'The *Caenorhabditis elegans* cell death gene ced-4 encodes a novel protein and is expressed during the period of extensive programmed cell death', *Development* 116(2): 309-20.

156. Yuan, J., Shaham, S., Ledoux, S., Ellis, H. M. and Horvitz, H. R. (1993) 'The *C. elegans* cell death gene *ced-3* encodes a protein similar to mammalian interleukin-1 beta-converting enzyme', *Cell* 75(4): 641-52.

157. Zarkower, D. (2006) 'Somatic sex determination', *WormBook : the online review of C. elegans biology*: 1-12.

158. Zhou, Z., Hartwieg, E. and Horvitz, H. R. (2001) 'CED-1 is a transmembrane receptor that mediates cell corpse engulfment in *C. elegans*', *Cell* 104(1): 43-56.

159. Zhou, Z. and Yu, X. (2008) 'Phagosome maturation during the removal of apoptotic cells: receptors lead the way', *Trends in cell biology* 18(10): 474-85.

CURRICULUM VITAE

SAYANTAN CHAKRABORTY

Ludwig-Maximilians-University Munich - Biozentrum,
Department of Cell and Developmental biology,
Großhaderner Str. 2, 82152 Planegg-Martinsried
sayantan_chakraborty@outlook.com
https://de.linkedin.com/in/chakrabortysayantan

Education

Since 2011   Doctoral student in Cell and Developmental Biology
                    Ludwig-Maximilians-University, Munich, Germany

2011   Master studies in Marine Biotechnology
                    Goa University, India

2009   Bachelor studies in Microbiology
                    University of Calcutta, India

Research experience

Ludwig-Maximilians-University, Munich, Germany   September 2011 – present
Doctoral student with Prof. Dr. Barbara Conradt
Genetic and cell biological studies of the role of central cell death pathway during *C. elegans* embryonic development using quantitative *in vivo* single cell analysis.

Goa University, India   June 2010 – April 2011
Master's dissertation with Prof. Dr. U.M.X. Sangodkar
Studies related to the co-mineralization of Sodium benzoate and Dibenzothiophene in *Alcaligenes sp.* strain GU110.

Banaras Hindu University, India   May – June 2010
Internship with Prof. Dr. J.K. Roy
Analysis of a novel mutation $l(3)tb^e$ in *Drosophila melanogaster*.

Open Source Drug Discovery, India   December 2009 – April 2010
Annotator in Connect to Decode Programme'10.

Publications

- **Sayantan Chakraborty**, Eric J. Lambie, Samik Bindu, Tamara Mikeladze-Dvali and Barbara Conradt (2015). Engulfment pathways promote programmed cell death by enhancing the unequal segregation of apoptotic potential. (Accepted in *Nature Communications*).

- **Sayantan Chakraborty**, Tamara Mikeladze-Dvali and Barbara Conradt. Novel functions of *C. elegans ced-3* caspase in centrosome asymmetry and segregation. (*In preparation*).

Conferences/Workshops attended

Speaker
- 2nd LMU-NTU workshop – Molecular biology 2015.
- EMBO Conference on centrosomes and spindle pole bodies 2014, Portugal.
- CIPSM Wilbad Kreuth Conference 2014, Germany.

Poster presentation
- Cell death meeting 2015 – Cold Spring Harbor Laboratories, USA.
- Gordon Research Conference on Cell Death 2014 - Cell Death Mechanisms at the Interface of Health and Disease, USA.

Others
- "Synthetic Building Blocks and Modules-2013": a part of the CAS research focus "Synthetic Biology II - Single Cells within the Focus of Synthetic Biology.
- <Interact> 2012, Munich, Germany.

Achievements

Fellowships
- EMBO travel fellowship for attending the EMBO Conference on centrosomes and spindle pole bodies 2014.
- Summer Research Fellowship-2010 sponsored by the Indian Academy of Sciences, The National Academy of Sciences, India and the Indian National Science Academy to pursue summer research at the Banaras Hindu University, India from May-June 2010.
- Department of Biotechnology (DBT) Scholarship (2009-2011) for pursuing M.Sc. Marine Biotechnology at Goa University, India.

Academics and others
- 2nd position in M.Sc. Marine Biotechnology, 2009-2011 at Goa University, India.
- Certificate of Credit in The International Competition of Schools-1998 conducted by the University of New South Wales, Australia.